Precision big bang nucleosynthesis with improved Helium-4 predictions

Cyril Pitrou,[1,*] Alain Coc,[2,†] Jean-Philippe Uzan,[1,‡] and Elisabeth Vangioni[1,§]
[1] *Institut d'Astrophysique de Paris, CNRS UMR 7095, 98 bis Bd Arago, 75014 Paris, France*
Sorbonne Université, Institut Lagrange de Paris, 98 bis Bd Arago, 75014 Paris, France
[2] *Centre de Sciences Nucléaires et de Sciences de la Matière (CSNSM), CNRS IN2P3,*
Univ. Paris-Sud, Université Paris-Saclay, Bâtiment 104, F-91405 Orsay Campus France

(Dated: June 25, 2018)

Primordial nucleosynthesis is one of the three historical evidences for the big bang model, together with the expansion of the universe and the cosmic microwave background. There is a good global agreement between the computed primordial abundances of helium-4, deuterium, helium-3 and their values deduced from observations. Now that the number of neutrino families and the baryonic densities have been fixed by laboratory measurements or CMB observations, the model has no free parameter and its predictions are rigid. Since this is the earliest cosmic process for which we *a priori* know all the physics involved, departure from its predictions could provide hints or constraints on new physics or astrophysics in the early universe. Precision on primordial abundances deduced from observations has recently been drastically improved and reach the percent level for both deuterium and helium-4. Accordingly, the BBN predictions should reach the same level of precision. For most isotopes, the dominant sources of uncertainty come from those on the laboratory thermonuclear reactions. This article focuses on helium-4 whose predicted primordial abundance depends essentially on weak interactions which control the neutron-proton ratio. The rates of the various weak interaction processes depend on the experimentally measured neutron lifetime, but also includes numerous corrections that we thoroughly investigate here. They are the radiative, zero–temperature, corrections, finite nucleon mass corrections, finite temperature radiative corrections, weak-magnetism, and QED plasma effects, which are for the first time all included and calculated in a self consistent way, allowing to take into account the correlations between them, and verifying that all satisfy detailed balance. Finally, we include the incomplete neutrino decoupling and claim to reach a 10^{-4} accuracy on the helium-4 predicted mass fraction of 0.24709 ± 0.00017 (when including the uncertainty on the neutron lifetime). In addition, we provide a *Mathematica* primordial nucleosynthesis code that incorporates, not only these corrections but also a full network of reactions, using the best available thermonuclear reaction rates, allowing the predictions of primordial abundances of helium-4, deuterium, helium-3 and lithium-7 but also of heavier isotopes up to the CNO region.

Contents

*Electronic address: pitrou@iap.fr
†Electronic address: coc@csnsm.in2p3.fr
‡Electronic address: uzan@iap.fr
§Electronic address: vangioni@iap.fr

I. INTRODUCTION

Besides the universal spatial expansion and the cosmic microwave background (CMB) radiation, the third historical evidence for the hot big bang model comes from primordial, or big bang nucleosynthesis (BBN). During the first ≈20 minutes of the Universe, when it was dense and hot enough for nuclear reactions to take place, BBN describes the production of the so called "light elements", ^{4}He, D, ^{3}He and ^{7}Li, together with only minute traces of heavier nuclei (see e.g. Coc and Vangioni (2017); Cyburt *et al.* (2016); Olive (2010); Patrignani and Particle Data Group (2016 and 2017 update); Steigman (2007) for recent reviews). The number of free parameters that entered in standard BBN has now been reduced to zero. Indeed, the number of light neutrino families is now known from the measurement of the Z^0 width by LEP experiments at CERN: $N_\nu = 2.984 \pm 0.008$ (Patrignani and Particle Data Group, 2016 and 2017 update). The lifetime of the neutron entering in weak reaction rate calculations and many nuclear reaction rates have been measured in nuclear physics laboratories (Coc *et al.*, 2015; Cyburt *et al.*, 2016; Descouvemont *et al.*, 2004; Serpico *et al.*, 2004). The last parameter to have been independently determined is the baryonic density of the Universe which is now deduced from the analysis of the anisotropies of the CMB radiation from the *Planck* satellite data (Ade *et al.*, 2016). Hence, there is no more free parameter in standard BBN and the calculated primordial abundances are in principle only affected by the moderate uncertainties in nuclear cross sections. Keeping in mind that abundances span a range of nine orders of magnitude, the agreement between primordial abundances, either deduced from observations, or from primordial nucleosynthesis calculations, is an outstanding support to the hot big bang model (Cyburt *et al.*, 2016). Hence, BBN is an invaluable tool for probing the physics of the early Universe, and it has been very efficient to constrain physics beyond the standard model. When we look back in time, it is the ultimate process for which we *a priori* know all the physics involved, given that it is very well tested in laboratories, so that departures from its predictions provide hints for new physics or astrophysics (Iocco *et al.*, 2009; Mathews *et al.*, 2017; Nakamura *et al.*, 2017; Pospelov and Pradler, 2010).

Great progresses have been made in the precision of both observations and laboratory measurements. The precision on deuterium observations have now reached the percent level (Cooke *et al.*, 2018), a precision hardly reached in nuclear physics measurements. The determination of the primordial abundance of ^{4}He has been reduced to less than 2% by the inclusion of an additional atomic infrared line (Aver *et al.*, 2015). However, there is still a significant discrepancy on lithium, for which predictions are a factor of ≈3 higher than observations. The previous paper Coc *et al.* (2015) investigated the uncertainties on D/H predictions which directly reflects the experimental uncertainties on few reaction rates that have all been re-evaluated (Gómez Iñesta *et al.*, 2017; Iliadis *et al.*, 2016), leading to a small but significant decrease of the predicted deuterium abundance with reduced uncertainty. This review aims at reducing the uncertainties, this time on the ^{4}He abundance prediction which are dominated by theoretical uncertainties on the weak reactions that interconvert neutrons and protons.

To that goal, we implemented the BBN equations into a *Mathematica* code[1], in addition to the Fortran code, that has been used recently, e.g. in Coc *et al.* (2009); Coc *et al.* (2015); Coc and Vangioni (2010). This Fortran code originates from the model created at IAP by Elisabeth Vangioni (Vangioni-Flam *et al.*, 2000) and further developed by Alain Coc (Coc *et al.*, 2002). Hence, it was possible to cross–check the implementations and after tuning the parameters to reach similar precisions, verify that the results were virtually identical, and next to focus on nuclear reaction rate uncertainties. Leaving aside, the "lithium problem" that has not yet found a fully satisfactory solution (Fields, 2011), it has become essential to improve the precision on deuterium and ^{4}He primordial abundances (^{3}He is not pertinent here). As nuclear uncertainties affecting deuterium BBN have already been investigated recently (Coc *et al.*, 2015; Gómez Iñesta *et al.*, 2017; Iliadis *et al.*, 2016), we will just summarize the situation. On the contrary the uncertainties impacting the ^{4}He abundance predictions are limited by the experimental value of the neutron lifetime (Patrignani and Particle Data Group, 2016 and 2017 update; Wietfeldt and Greene, 2011) but also by the numerous corrections that have to be introduced in the theoretical weak–interaction reaction rates. The main aim of this article is to calculate in details all these corrections. In our previous works, either only a fraction of them was taken into account (Coc *et al.*, 2009; Coc and Vangioni, 2010) or were also supplemented by a final correction to

[1] `PRIMAT` : PRImordial MATter, freely available at `http://www2.iap.fr/users/pitrou/primat.htm`

the ^{4}He abundance (Coc *et al.*, 2014), based on other works (Dicus *et al.*, 1982; Lopez and Turner, 1999).

With the now precise theoretical and observational determinations of both the deuterium and ^{4}He primordial abundances, it is now possible to better constrain the standard models of particle physics and cosmology and eventually provide hints of physics beyond the standard model.

We define n_i as *volume* density of isotope i, and $n_{\rm b}$, the baryon or nucleon *volume* density. The (pseudo-)mass fraction of isotope i is defined as

$$X_i \equiv A_i \frac{n_i}{n_{\rm b}}\,, \tag{1}$$

where A_i is the *dimensionless* mass integer *number* of nuclear physics, or baryon number of particle physics, (i.e. not the atomic mass). Baryon number conservation requires that $\sum_i A_i n_i = n_{\rm b}$ or $\sum_i X_i = 1$. For ^{4}He it is customary to define

$$Y_{\rm P} \equiv X_{^4{\rm He}}\,, \tag{2}$$

and to introduce for convenience

$$Y_{\rm P}^{(4)} \equiv 10^4 Y_{\rm P}\,. \tag{3}$$

For other elements, it is customary to use the density ratio with ^{1}H, that is $n_i/n_{^1{\rm H}}$, abbreviated as i/H.

A. Observed abundances

During the galactic evolution, massive stars are the main source of enrichment of the interstellar medium, when they explode as supernovae, out of which next generations of stars are born. In this process, they release matter, enriched in heavy elements that they have synthesized during the various phases of their evolution. Accordingly, the abundance of *metals* (elements heavier than helium) in star forming gas increases with time. The observed *metallicity* is therefore an indication of age: the older, the lower the *metallicity*. Hence, primordial abundances are extracted from observations of objects with low metallicity, but depending on their galactic chemical evolution, pristine abundances have to be derived from different classes of objects as detailed below.

1. ^{4}He observations

After BBN, stars produce also ^{4}He and its primordial abundance can be measured thanks to observations in HII (ionized hydrogen) regions inside compact blue galaxies. It is thought that galaxies are formed by the merging of such dwarf galaxies, in a hierarchical structure formation paradigm, hence these are considered to be more primitive. First, for each HII region, the ^{4}He abundance has to be determined within a model aiming at reproducing the observed ^{4}He emission lines, that also depends on parameters like e.g. the electron density. Then, to account for stellar production, the ^{4}He deduced abundances should be extrapolated to zero metallicity. Recently, the observation (Izotov *et al.*, 2014) of an additional atomic infrared line (λ10830) in 45 low–metallicity HII regions have allowed to better constrain the thermodynamic conditions that prevail in the emission regions. After selecting 28 object, Izotov *et al.* (2014) obtained $Y_{\rm P} = 0.2551 \pm 0.0022$ for the ^{4}He mass fraction. However, Aver *et al.* (2015) (see also Cyburt *et al.* (2016)), starting from the same observational data made a stricter selection, based, in particular on goodness of fit for the emission model of each object. For the selected 16 objects, the uncertainties were so reduced that a slope in the Y_p versus metallicity data could be considered. After extrapolation to zero metallicity, Aver *et al.* (2015) obtained,

$$Y_{\rm P} = 0.2449 \pm 0.0040\,, \tag{4}$$

that we use here.

2. Deuterium observations

Deuterium is a very fragile isotope. It can only be destroyed after BBN thanks to stellar evolution. The deuterium abundance closest to primordial abundance is determined from the observation of a few cosmological clouds (absorbers) at high redshift on the line of sight of distant quasars (emitters). Figure 1 shows the observed D/H values as a function of the redshift of the absorber. Until recently, the distribution of D/H observations showed a significant scatter (see e.g. Pettini and Cooke (2012)). It allowed Olive *et al.* (2012) to adopt a weighted mean of D/H $= (3.02 \pm 0.23) \times 10^{-5}$ without excluding an upper limit of D/H $= 4 \times 10^{-5}$. This is not possible anymore thanks to the recent new observations or reanalyses of existing data (Balashev *et al.*, 2016; Cooke *et al.*, 2014, 2016, 2018; Riemer-Sørensen *et al.*, 2017) that now display a plateau as a function of redshift (and metallicity) with a very small scatter (Fig. 1). Moreover, in Dvorkin *et al.* (2016), the comparison with the available measurements is consistent with the cosmic merger tree model of structure formation. It is shown that at redshift higher than 2 (see their Fig. 2), the dispersion in the cosmic deuterium abundance is very tiny leading to think that at these redshifts the observation of the D abundance is probably primordial. Hence, we adopt the new recommended value provided by Cooke *et al.* (2018):

$$\mathrm{D/H} = (2.527 \pm 0.030) \times 10^{-5}\,, \tag{5}$$

lower and with smaller uncertainties than in previous determinations [2]. If such a precision of $\sim$1% in observations

[2] A recent reanalysis and new D/H observations towards the Q1009+2956 quasar (Zavarygin *et al.*, 2017, 2018) provided a

is confirmed, great care should be paid to nuclear cross sections affecting deuterium nucleosynthesis.

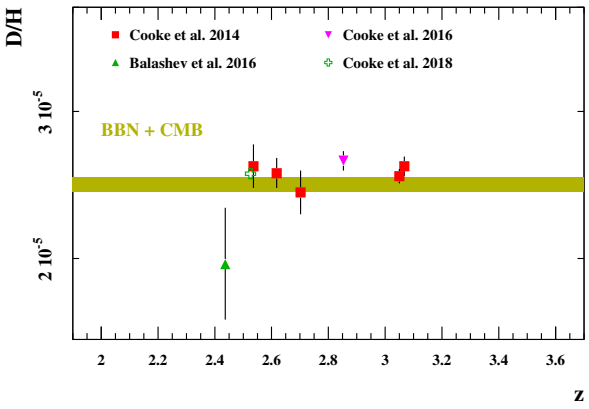

FIG. 1 D/H observations, as a function of the redshift of the absorber. These most recent observations (Cooke *et al.*, 2014, 2016, 2018) have very small error bars and show very few dispersion compared to previous determinations (except Balashev *et al.* (2016)), and are in fair agreement with our BBN calculations when using *Planck* (Ade *et al.*, 2016) baryonic density.

3. ^{3}He observations

Contrary to the case of ^{4}He, stars can both produce and destroy ^{3}He, so that the evolution of its abundance in time is not known precisely (Vangioni-Flam *et al.*, 2003). Since observing helium is difficult, and given the small ^{3}He/^{4}He ratio, ^{3}He was only observed in our Galaxy and the bounds obtained are $^3\mathrm{He/H} = (0.9 - 1.3) \times 10^{-5}$, keeping in mind that this is an upper limit extracted from a single object (Bania *et al.*, 2002). However, the next generation of 30+ m telescope facilities may allow to extract the ^{3}He/^{4}He ratio from observations of extragalactic metal poor HII regions (Cooke, 2015).

4. ^{7}Li observations

^{7}Li is peculiar because it has three distinct sources: BBN but also spallative nuclear reactions between galactic cosmic rays and the interstellar medium, and a stellar source (Asymptotic giant branch stars and novae) (Fu *et al.*, 2018). For instance, recent observations (Izzo *et al.*, 2015; Tajitsu *et al.*, 2016) have confirmed Li production by novae, at a level even higher than model predictions (Hernanz *et al.*, 1996). Hence, after BBN, ^{7}Li can be produced but can also easily be destroyed in the interior of stars by proton capture at temperatures as low as 2.5 MK.

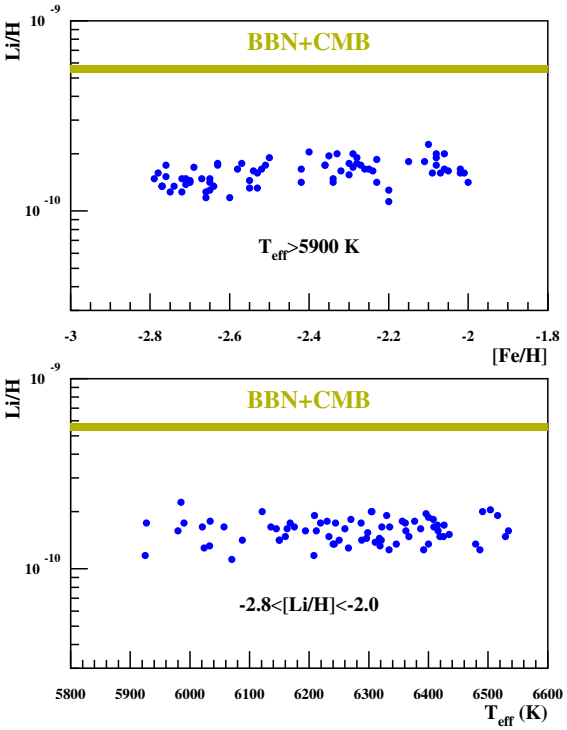

FIG. 2 Li/H observations, as a function of metallicity[3] and effective temperature. Data (Aoki *et al.*, 2009; Asplund *et al.*, 2006; Bonifacio *et al.*, 2007; Charbonnel and Primas, 2005; Hosford *et al.*, 2009; Meléndez *et al.*, 2010; Sbordone *et al.*, 2010; Schaeuble and King, 2012; Scholz *et al.*, 2015) come from a compilation by Spite *et al.* (2012, 2015).

The life expectancy of stars with masses lower than our Sun is larger than the age of the Universe so that very old such stars can still be observed in the halo of our Galaxy. In this context, lithium can be observed at the surface of these stars and its abundance was found to be independent of metallicity and effective temperature in the ranges -2.4≤[Fe/H]≤-1.4[3] (i.e. between $\approx 4 \times 10^{-3}$ and 4×10^{-1} of the solar metallicity) and $5700 \leq T_{\rm eff} \leq 6800$ K (Fu *et al.*, 2018). This *plateau* was discovered by François

new value of D/H = $(2.48^{+0.41}_{-0.35}) \times 10^{-5}$ with a limited precision (17%). If included, it shifts the abundance downward to D/H= $(2.545 \pm 0.025) \times 10^{-5}$

[3] Logarithm of the ratio, relative to its solar value: $[X/Y] \equiv \log((X/Y)/(X_\odot/Y_\odot))$.

and Monique Spite (Spite and Spite, 1982) and this constant Li abundance is interpreted as corresponding to the BBN ^{7}Li production. The thinness of the "Spite plateau" has generally been considered as an indication that surface Li depletion may not have been very effective so that it should reflect the primordial value. However, as shown in Fig. 2, there is a discrepancy of a factor $\approx$3 between the BBN predicted value and the lithium abundance derived in metal-poor main-sequence (MS) stars. This discrepancy could be alleviated if the stars observed today had undergone photospheric depletion of lithium. Different observations in globular clusters (see Gruyters *et al.* (2016)) and stellar scenarios concerning the formation of the early metal poor stars have been developed, (Fu *et al.*, 2015) trying to follow lithium evolution in metal-poor stars, from pre-main sequence to the Spite plateau. Li evolution could affect its abundance by introducing the effects of convective overshooting, atomic diffusion and mixing (Richard *et al.*, 2005). In this context, ^{7}Li could be depleted and it could be possible to move closer to the observed Li Spite plateau. Indeed, several globular clusters (NGC 6397, 6752, M30) show that the discrepancy could be reduced by atomic diffusion leading to a factor of 1.6 instead 3 (Michaud *et al.*, 1984). Finally the pre-MS depletion can be efficient and this is presently an open question. Note that recent lithium observations (Howk *et al.*, 2012) have been done in the Small Magellanic Cloud which has a quarter of the sun's metallicity and a Li abundance nearly equal to the BBN predictions.

Recently, Reggiani *et al.* (2017) have constrained cosmic scatter in the galactic halo using a differential analysis of metal poor for several elements. Regarding lithium, they find a very low scatter (0.04 dex) and a mean value 1.86×10^{-10} which is compatible with other studies. We adopt here the analysis of Sbordone *et al.* (2010), namely [4]

$$^7\mathrm{Li/H} = (1.58 \pm 0.3) \times 10^{-10}\,. \tag{6}$$

B. Outlook on weak-rates corrections

Given the observational precision on ^{4}He, we aim at predictions with a precision better than 0.1%. This amounts to considering all effects which affect $Y_{\rm P}^{(4)}$ by units, and to treat carefully all effects which modify the abundance by an order 10^{-4}. $Y_{\rm P}$ is almost exclusively controlled by weak reactions, because nearly all neutrons end up in ^{4}He. By varying artificially the weak rates (Γ) we find the relation[5]

$$\frac{\delta Y_{\rm P}}{Y_{\rm P}} \simeq -0.73 \frac{\delta\Gamma}{\Gamma}\,. \tag{7}$$

[4] All uncertainties are given with one standard deviation.
[5] Using Eq. (146a) and $\Gamma \propto \tau_{\rm n}^{-1}$ from Eq. (91).

Hence we need to focus on all corrections which affect the weak rates by 10^{-4} or more, on top of the experimental uncertainty on the neutron lifetime.

As for ^{2}H and ^{3}He, we aim at predictions of order 10^{-3} if we leave aside the uncertainty in nuclear rates, and of order of a few 10^{-2} when including uncertainties in nuclear rates. In all our computations, we must also make sure to maintain numerical errors much below 10^{-3}.

There are many effects to take into account for the weak rates and we must also consider their possible couplings since they cannot always be summed linearly. These effects have several origins, namely

1. radiative corrections,
2. finite nucleon mass corrections,
3. finite temperature radiative corrections,
4. weak-magnetism,
5. QED plasma effects,
6. incomplete neutrino decoupling.

Radiative corrections correspond to the contribution of virtual photons in weak reactions, together with the emission of photons in the final state (bremsstrahlung) from the electron line. They are typically order 10^{-2} effects (see § V.C) because of the value of the fine-structure constant $\alpha_{\rm FS} \simeq 1/137$. They are well established in the context of neutron beta decay (Czarnecki *et al.*, 2004), and even with some resummed effects which are higher orders in $\alpha_{\rm FS}$ for increased precision (Ivanov *et al.*, 2013). In the context of BBN, these effects were originally estimated by Dicus *et al.* (1982).

Finite nucleon mass correction correspond to the effect of nucleon recoil and nucleon thermal distribution of velocity in the theoretical computation of the weak rates. These corrections are also of order 10^{-2} (see § V.C) even if smaller than radiative corrections. Wilkinson (1982) provided a comprehensive list of these effects in the context of neutron beta decay, and Seckel (1993) reviewed these corrections in the context of BBN. These were later estimated numerically by Lopez *et al.* (1997) using a Monte-Carlo estimation of multidimensional integrals. We introduce a new efficient method which relies on a Fokker-Planck expansion in the energy transfer, and which relies only on one-dimensional integrals.

Finite temperature radiative corrections correspond to the interactions with the bath of electrons and positrons during weak reactions. They lead to a long subject of controversy in the literature. They were initially computed in Dicus *et al.* (1982) and Cambier *et al.* (1982). Discrepancies between these approaches were analyzed by Kernan (1993) and a numerical estimation was provided by Lopez and Turner (1999). However, Brown and Sawyer (2001) pointed incoherences and the lack of detailed balance, and they proposed to set the

finite temperature radiative correction on firm ground by providing a comprehensive theoretical computation from finite-temperature quantum field theory. We find, and this is new, that to be complete and satisfy detailed balance, one must also consider corrections to the bremsstrahlung effects and add them to finite temperature corrections. Overall, when finite-temperature corrections and bremsstrahlung corrections are added, they almost perfectly cancel, leaving $Y_{\rm P}^{(4)}$ nearly unchanged (see § V.C).

Weak-magnetism which arises from the internal structure of nucleons is part of finite mass corrections and is order 10^{-3} (see § V.C).

Quantum Electrodynamics (QED) is responsible for two effects. First the interaction with the plasma modifies the electron mass. However this effect is strictly speaking part of finite temperature radiative corrections in our computations. Second, QED effects modify the thermodynamics of the plasma, that is it modifies the pressure and energy density. We find that this effect, taken alone, results in a negligible modification of $Y_{\rm P}^{(4)}$ which is of order 10^{-5} (see § V.C). However it affects the number of effective neutrinos for subsequent cosmology such as the physics of cosmic microwave background (CMB).

Incomplete neutrino decoupling corrections occur when electrons and positrons annihilate, because neutrinos are not fully decoupled from the plasma and some annihilations end up heating the neutrino bath. This effect increases the neutrino temperature and produces distortions in their spectrum. In order to track the neutrinos spectral distortions, it is necessary to use the full machinery of coupled Boltzmann equations, especially when considering neutrino oscillations. Since this effect also modifies the effective number of neutrinos for the subsequent cosmology, several authors among which Dolgov *et al.* (1997); Grohs *et al.* (2016); Mangano *et al.* (2005); de Salas and Pastor (2016) focused on it. We shall use a fit taken from Pisanti *et al.* (2008) for the heating rate of neutrinos. Eventually we find that this correction is of order 10^{-3} (see § V.C).

All these effects are detailed in § III.

C. Main eras of BBN

During BBN, one can distinguish different eras depending on the dominant physical processes.

1. For plasma temperatures T in the range $2\,\mathrm{MeV} \lesssim T \lesssim \mathrm{GeV}$, nucleons are formed and their density is only affected by expansion. Neutrinos are still in thermal equilibrium with the plasma (electron-positrons and protons), that is $T_\gamma = T_\nu$ and the neutron to proton ratio X_n/X_p is enforced to be the thermodynamical equilibrium value since weak interactions interconvert efficiently neutrons in protons and vice-versa, through the reactions (68).

2. In the range, $0.8\,\mathrm{MeV} \lesssim T \lesssim 2\,\mathrm{MeV}$ neutrinos have essentially decoupled but weak interactions maintain neutrons and proton in thermodynamical equilibrium. However at weak-interactions freeze-out temperature $T_F \simeq 0.8\mathrm{MeV}$, defined by the equality between weak interaction rates and the cosmological expansion rate, the abundance of neutrons are mostly affected by neutron beta decay. In practice, freeze-out is not instantaneous and the neutron abundance is subject only to neutron beta decay around $T_F \simeq 0.28\,\mathrm{MeV}$. The abundance of neutrons is then about $X_n \simeq 0.17$ and it is eventually reduced to $X_n^{\rm Nuc} \simeq 0.125$ by beta decay when nucleosynthesis starts (see Fig. 3).

3. Around 0.5MeV, electrons and positrons annihilate and heat up the photon bath, resulting in a different temperature between photons and neutrinos ($T_\gamma > T_\nu$). This affects directly the expansion history of the Universe since the energy content of massive particles (electrons and positrons) is replaced by massless particles (photons), but it also affects weak-interaction rates since this is concomitant with the freeze-out period.

4. As long as $T \gtrsim 0.078\mathrm{MeV}$, deuterium dissociation is too efficient to allow for deuterium synthesis. Even though the binding energy of deuterium is about 2.2MeV, deuterium is efficiently destroyed by the high-energy tail of the Bose-Einstein distribution of photons, because the ratio between baryon number density and photon number density η is smaller than 10^{-9}.

5. Below $T \lesssim T_{\rm Nuc} = 0.078\mathrm{MeV}$, deuterium can be formed. Then since the binding energy per nucleon of ^{4}He is much larger than for deuterium, a network of reactions ends up in producing nearly only ^{4}He and very tiny amounts of other light elements. Since ^{4}He is made of two neutrons and two protons, the (pseudo-)mass abundance satisfies $Y_{\rm P} \simeq 2X_n^{\rm Nuc}$, hence leading to a final value $Y_{\rm P} \simeq 0.25$. Nucleosynthesis is completely over for all elements when $T \lesssim 0.01\mathrm{MeV}$ or $T \lesssim 10^8\mathrm{K}$ but for prediction with 10^{-3} precision on deuterium, we found that we must wait until $T \lesssim 6 \times 10^7\mathrm{K}$.

D. Resolution strategy and outline

This outline of nucleosynthesis implies that we do not need to solve jointly the abundance of all species at all times. Indeed, given that the matter-radiation equivalence occurs around $T \simeq 3000\mathrm{K}$, this means that baryonic matter accounts for less than 10^{-4} of the total energy

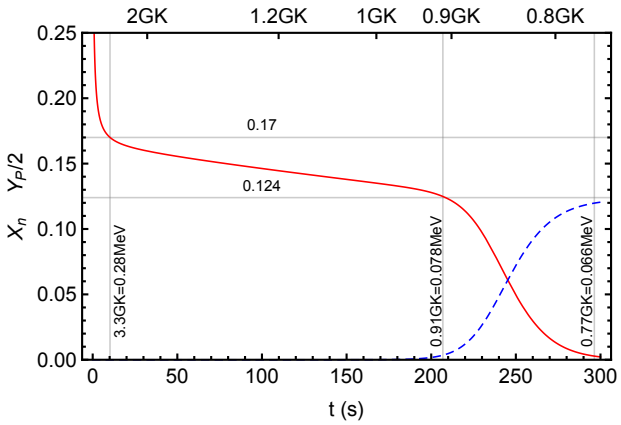

FIG. 3 Evolution of X_n (red continuous line with nuclear reactions and red dotted line without nuclear reactions) and $Y_{\rm P}/2$ (blue dashed line).

density at the end of BBN and even less during freeze-out. In principle, one should account for the fact that neutron abundance evolves even though the nucleonic density (protons and baryons) is only affected by cosmic expansion. Since the mass difference between neutrons and protons is of order 10^{-3} of their rest mass energy, we can ignore this effect when evaluating the total energy density of the Universe. Similarly, given that the binding energy in nuclei is around or less than 10^{-2} of the rest mass energy, we can also consider to a very good approximation that nuclear reactions do not affect the baryon energy density. Hence it is possible to compute the evolution of the cosmological background, without having to compute in details the abundance of neutrons nor the details of nuclear reactions. In § II we study the thermodynamics of all species and the dynamics of the cosmic expansion. Then in § III we focus on weak interactions and detail all corrections. Since the weak interaction rates depend on the plasma of electrons, positrons and neutrinos only, they can be studied ignoring nuclear reactions. Finally in § IV we focus on nuclear reactions and we present the results obtained when coupling the background dynamics, the weak interactions and the nuclear reactions. Most technical details can be found in the appendices for ease of reading. We use natural units in all expressions, that is we work in units in which

$$k_B = \hbar = c = 1\,, \tag{8}$$

except when we judge instructive to write them explicitly.

II. BACKGROUND THERMODYNAMICS

We consider a homogeneous and isotropic cosmology, more precisely a flat Friedmann-Lemaître (FL) spacetime characterized by the scale factor $a(t)$ where t is the cosmic time. The Hubble expansion rate is $H = \dot{a}/a$, where a dot indicates a derivative with respect to t. Since cosmological perturbations are of order 10^{-5}, it is fully justified to ignore their effect and consider an homogeneous cosmology given our precision goal.

A. Thermodynamics in a FL spacetime

1. Distribution function and Boltzmann equation

Relativistic species, which encompass neutrinos, photons and electrons with positrons during the relevant BBN era, are best described with a distribution function $f(t,p)$ for each species, and where the dependence is only on the magnitude of momenta $p = \sqrt{E^2 - m^2}$ given the symmetries of the FL spacetime. This description is valid even out of thermodynamical equilibrium. The distribution function satisfies the general Boltzmann equation in a FL spacetime

$$L[f] \equiv \frac{\partial f}{\partial t} + \dot{p}\frac{\partial f}{\partial p} = C[f]\,, \qquad \dot{p} = -Hp\,. \tag{9}$$

We have used that $p \propto 1/a$ because of cosmic expansion and $C[f]$ is the collision term of the species under scrutiny. In order to relate this description to the fluid description, thermodynamical quantities such as number density n, energy density ρ and pressure P, can be formed from the distribution function as summarized in App. A.

2. Number density evolution

From the definition of thermodynamic quantities (Eqs. A1), considering $\int L[f] 4\pi p^2 {\rm d}p/(2\pi)^3$ with the Boltzmann equation (9) leads after integration by parts to the number conservation equation

$$\dot{n} + 3Hn = \mathcal{J}\,, \qquad \mathcal{J} \equiv \int C[f]\frac{4\pi p^2 {\rm d}p}{(2\pi)^3}\,. \tag{10}$$

$\mathcal{J}$ is the net creation rate of particles per unit of physical volume. When the collision term vanishes or when it conserves the number of particles because it describes elastic scattering,

$$\dot{n} + 3Hn = 0 \quad \Rightarrow \quad \frac{{\rm d}(na^3)}{{\rm d}t} = 0\,. \tag{11}$$

In that case, for a comoving volume a^3, the total number of particles $N \equiv na^3$ remains constant.

3. Energy density evolution

Similarly, starting from the definition of thermodynamic quantities (Eqs. A1), and considering $\int L[f] E 4\pi p^2 {\rm d}p/(2\pi)^3$ with the Boltzmann equation (9), leads after integration by parts (and using $E{\rm d}E = p{\rm d}p$) to the energy conservation equation

$$\dot{\rho} + 3H(\rho + P) = \dot{q}\,, \qquad \dot{q} \equiv \int C[f]\frac{4\pi E p^2 {\rm d}p}{(2\pi)^3}\,. \tag{12}$$

$\dot{q}$ is the volume heating rate. For massless particles, such as photons or neutrinos (which can be considered massless during the BBN), $E = p$ and $P = \rho/3$, implying that when the collision term is vanishing

$$\dot{\rho} + 4H\rho = 0 \quad \Rightarrow \quad \frac{\mathrm{d}(\rho a^4)}{\mathrm{d}t} = 0\,. \tag{13}$$

Eqs. (12) and (13) are general and do not rely on a specific distribution function.

4. Entropy evolution

Volume entropy is defined (see e.g. Grohs *et al.* (2016)) from the distribution function by

$$s = -\int S_{\rm B}(f)\frac{4\pi p^2 \mathrm{d}p}{(2\pi)^3}\,, \tag{14}$$

where the Boltzmann entropy is defined as

$$S_{\rm B}(f) \equiv [f\ln f \pm (1\mp f)\ln(1\mp f)] \tag{15}$$

with upper (lower) sign for fermions (bosons). Using the identity

$$\partial_p[S_{\rm B}(f)] = \ln\left(\frac{f}{1\mp f}\right)\partial_p f \tag{16}$$

and multiplying Eq. (9) by $S_{\rm B}(f)$ we get after integration by parts

$$\dot{s} + 3Hs = -\int C[f]\ln\left(\frac{f}{1\mp f}\right)\frac{4\pi p^2 \mathrm{d}p}{(2\pi)^3}\,, \tag{17}$$

which dictates the evolution of volume entropy. If there are no collisions, it is only affected by dilution as $s \propto 1/a^3$ such that the total entropy in a given comoving volume, $S \equiv sa^3$, is conserved ($\dot{S} = 0$).

5. Local thermodynamical equilibrium

In case of local thermodynamical equilibrium (LTE), fermions (bosons) follow a Fermi-Dirac (Bose-Einstein) distribution (A3) and

$$\ln\left(\frac{f}{1\mp f}\right) = \frac{\mu - E}{T}\,, \tag{18}$$

where μ is the chemical potential. Hence the evolution of volume entropy for a given species satisfies, using Eqs. (10) and (17),

$$\dot{s} + 3Hs = \frac{\dot{q}}{T} - \frac{\mu}{T}(\dot{n} + 3Hn)\,, \tag{19}$$

with $\dot{q}$ defined in Eq. (12). From Eq. (19) multiplied by a^3, we recover the usual thermodynamical identity

$$T\dot{S} = \dot{Q} - \mu\dot{N} \tag{20}$$

with $\dot{Q} \equiv \dot{q}a^3$. Hence, the entropy for a given species is conserved if there is no heat exchange, that is no interactions, and either a vanishing chemical potential (in practice $\mu \ll T$) or conservation of the number of particles (i.e. $\dot{N} = 0$). From the conservation of the total stress-energy tensor, we must have $\sum_i \dot{q}_i = 0$, that is there can be no global production of heat. Hence, in case of local thermodynamical equilibrium, the total entropy is conserved whenever for all species either the chemical potential is negligible $\mu_i \ll T$ or the number of particles is conserved.

If there is LTE, entropy for a given species i can then be linked to other thermodynamical quantities thanks to

$$s_i = \frac{P_i + \rho_i - \mu_i n_i}{T_i}\,. \tag{21}$$

The total entropy is obtained from the extensivity of ρ and n, given that pressure and temperature of all species are equal at equilibrium

$$s = \sum_i \frac{P_i + \rho_i}{T} + \sum_i \frac{\mu_i n_i}{T} = \frac{\rho + P}{T} + \sum_i \frac{\mu_i n_i}{T}\,. \tag{22}$$

During nucleosynthesis, given the very low value of the baryon-to-photon ratio η (see § II.C below), we can totally ignore the entropy of protons and neutrons. This amounts to neglecting the electrons, positrons and neutrinos created and destroyed in weak interactions, and any energy exchange with these particles and the photons. Hence we can focus only on the thermodynamics of electrons, positrons, photons and neutrinos. During nucleosynthesis, neutrinos are nearly fully decoupled from other species and their entropy is separately conserved if we can assume that they are totally decoupled. See §II.F for the small modifications induced by incomplete decoupling (ID).

Conversely, electrons, positrons and photons are tightly coupled by electromagnetic interactions and they behave collectively as a plasma whose common temperature is defined as T. Photons decouple from electrons only around recombination much later when the CMB is formed and $T \lesssim$ eV. Due to electron-positron annihilations, the number of particles in the plasma is not conserved, and it is crucial that we can neglect the chemical potential of plasma particles to claim that the plasma entropy is conserved. The chemical potential of photons is always vanishing due to processes which do not conserve the number of photons so we need only to make sure that the chemical potential of electrons and positrons can be neglected. In App. A.2, we evaluate these chemical potentials and show they are completely negligible, implying that we can use entropy conservation.

For convenience we define dimensionless reduced energy density, pressure, number density and entropy as

$$\bar{n}_i \equiv \frac{n_i}{T_i^3} \quad \bar{P}_i \equiv \frac{P_i}{T_i^4} \quad \bar{\rho}_i \equiv \frac{\rho_i}{T_i^4} \quad \bar{s}_i \equiv \frac{s_i}{T_i^3} \tag{23}$$

such that the relation (21) reads simply in case of vanishing chemical potential

$$\bar{s}_i = \bar{\rho}_i + \bar{P}_i \,. \tag{24}$$

For photons the reduced thermodynamic variables do not depend on temperature and are constants when there is LTE. We find

$$\bar{n}_\gamma = \frac{2}{2\pi^2} I_-^{(1,1)} = \frac{2\zeta(3)}{\pi^2} \tag{25a}$$

$$\bar{\rho}_\gamma = \frac{2}{2\pi^2} I_-^{(2,1)} = \frac{\pi^2}{15} \tag{25b}$$

$$\bar{P}_\gamma = \frac{2}{6\pi^2} I_-^{(0,3)} = \frac{\pi^2}{45} \tag{25c}$$

$$\bar{s}_\gamma = \bar{\rho}_\gamma + \bar{P}_\gamma = \frac{4\pi^2}{45} \,. \tag{25d}$$

where the definitions for the $I_\pm^{(p,q)}$ are given in App. A.1. Similarly for neutrinos, and assuming that they have a negligible chemical potential, the reduced variables defined in case of LTE, take the constant values

$$\bar{n}_\nu = \frac{2}{2\pi^2} I_+^{(1,1)} = \frac{3}{4}\bar{n}_\gamma \tag{26a}$$

$$\bar{\rho}_\nu = \frac{2}{2\pi^2} I_+^{(2,1)} = \frac{7}{8}\bar{\rho}_\gamma \tag{26b}$$

$$\bar{P}_\nu = \frac{2}{6\pi^2} I_+^{(0,3)} = \frac{7}{8}\bar{P}_\gamma \tag{26c}$$

$$\bar{s}_\nu = \bar{\rho}_\nu + \bar{P}_\nu = \frac{7}{8}\bar{s}_\gamma \,, \tag{26d}$$

where we used $g_\nu = 1$ since only left-handed neutrinos contribute to the relativistic species, but we have multiplied by a factor 2 since conventionally we add together the contributions of neutrinos and antineutrinos[6]. In particular we deduce from Eq. (13) that for photons or (massless) neutrinos in thermodynamical equilibrium

$$\frac{\mathrm{d}(aT)}{\mathrm{d}t} = \frac{\mathrm{d}(aT_\nu)}{\mathrm{d}t} = 0 \,, \tag{27}$$

if they are completely decoupled from other species. During BBN, aT varies because of electron-positron annihilations. It is customary to define (Mangano *et al.*, 2005; de Salas and Pastor, 2016)

$$z \equiv a(T)T \qquad z_\nu \equiv a(T_\nu)T_\nu \tag{28}$$

to characterize this total variation of aT and aT_ν, with the convention that long before decoupling when all species were coupled together and at the same temperature, that is when $T = T_\nu \gg m_e$, we had $a(T)T = a(T_\nu)T_\nu = 1$, that is $z = z_\nu = 1$ at early times.

[6] If neutrinos were Majorana particles, neutrinos would be their own antiparticle but they would possess both helicities and one would take $g = 2$, resulting in the same final result

Additionally, in a first approximation, one can also assume that during BBN neutrinos are fully decoupled, implying that aT_ν is constant and $z_\nu = 1$ remains always true. The tiny effect of incomplete decoupling induces in fact a small variation of z_ν that we shall take into account in § II.F. Ignoring it, the neutrino temperature scales simply as

$$T_\nu = \frac{a_0 T_0}{a\, z_0} \qquad z_0 \equiv z(T \ll m_e) \,, \tag{29}$$

where T_0 is the photons temperature today and z_0 is the value of z long after BBN is finished.

B. Plasma temperature

Since for the plasma $S = sa^3$ is conserved, we can obtain the relation between temperature and scale factor. From Eq. (24) and expressions in App. A, we find that the ratio between plasma entropy at a given time of BBN and photons entropy today is given by

$$\frac{s}{s_0} = \frac{T^3}{T_0^3}\mathcal{S}(T) \tag{30a}$$

$$\mathcal{S}(T) \equiv \frac{\bar{s}_{\rm pl}}{\bar{s}_\gamma} = \frac{\bar{s}_\gamma + \bar{s}_{e^+}(T) + \bar{s}_{e^-}(T)}{\bar{s}_\gamma} = 1 + \frac{2}{\pi^2 \bar{s}_\gamma}\left[\frac{1}{3} I_+^{(0,3)}(x) + I_+^{(2,1)}(x)\right] \tag{30b}$$

where $x \equiv m_e/T$. The function $\mathcal{S}$ is plotted in Fig. 4. For $T \gg m_e$, $\mathcal{S} \to 11/4$ whereas for $T \ll m_e$, $\mathcal{S} \to 1$. Entropy conservation ($sa^3 = s_0 a_0^3$) allows then to relate the scale factor to the plasma temperature as

$$\frac{z_0^{\rm stand}}{z^{\rm stand}} = \frac{a_0 T_0}{aT} = \mathcal{S}^{1/3} \quad \Rightarrow \quad a(T) = \frac{a_0 T_0}{T\mathcal{S}(T)^{1/3}} \,. \tag{31}$$

Here $z^{\rm stand}$ denotes z in the case where we can ignored incomplete neutrino decoupling and QED plasma effects which we analyze in § II.E and II.F respectively. The inverse relation $T(a)$ is obtained by numerical inversion. $z_0^{\rm stand}$ takes the value

$$z_0^{\rm stand} = S^{1/3}(T \gg m_e) = \left(\frac{11}{4}\right)^{1/3} \simeq 1.40102 \,. \tag{32}$$

From Eqs. (31) and (29) the ratio between neutrino and plasma temperatures is given by

$$\frac{T_\nu}{T} = \frac{\mathcal{S}^{1/3}(T)}{z_0^{\rm stand}} \,, \tag{33}$$

and tends to $1/z_0^{\rm stand} = (4/11)^{1/3}$ at low temperatures, which is the celebrated result of instantaneous decoupling.

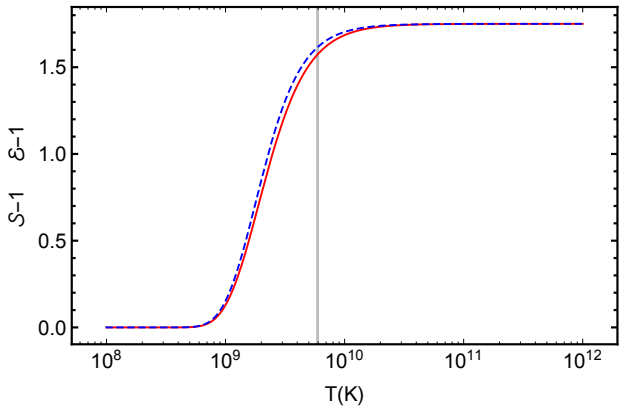

FIG. 4 *Red continuous line* : $\mathcal{S}(T) - 1$. *Blue dashed line* : $\mathcal{E}(T) - 1$. The vertical bar corresponds to $T = m_e \simeq 0.511\,\mathrm{MeV}$.

C. Baryon density

In order to obtain the energy density of baryons, it is sufficient to use that for non-relativistic and cold species $\rho \propto 1/a^3$. Hence

$$\rho_\mathrm{b} = \left(\frac{a_0}{a}\right)^3 \rho_0^\mathrm{crit}\Omega_\mathrm{b} = \left(\frac{a_0}{a}\right)^3 \rho_{100}^\mathrm{crit} \times \left(\Omega_\mathrm{b} h^2\right) \tag{34}$$

where we defined the critical densities $\rho_0^\mathrm{crit} \equiv 3H_0^2/(8\pi G)$ and $\rho_{100}^\mathrm{crit} \equiv 3H_{100}^2/(8\pi G)$, with the reduced Hubble rate $h \equiv H_0/H_{100}$ (with the standard definition $H_{100} \equiv 100\,\mathrm{km/s/Mpc}$). The numerical value of ρ_{100}^crit can be found in appendix D. The baryon energy density can be converted into a number density by estimating the average mass of nucleons

$$n_\mathrm{b} = \frac{\rho_\mathrm{b}}{m_\mathrm{b}}\,. \tag{35}$$

More details about the definition of m_b are given in App. C. We define the ratio between baryons and photons by

$$\eta \equiv \frac{n_\mathrm{b}}{n_\gamma}\,. \tag{36}$$

Since $n_\mathrm{b} \propto 1/a^3$ and $n_\gamma \propto T^3$ it can be rewritten in the form

$$\eta = \eta_0 \left(\frac{z_0}{z}\right)^3\,. \tag{37}$$

Using Eq. (C6), the value today is approximately found to be

$$\begin{aligned}\eta_0 \;\simeq\; & 6.0913 \times 10^{-10} \left(\frac{\Omega_\mathrm{b} h^2}{0.02225}\right) \left(\frac{2.7255}{T_0}\right)^3 \\ & \times \left(\frac{1 - 1.759 \times 10^{-3}}{1 - 1.759 \times 10^{-3}\frac{Y_\mathrm{P}}{0.24709}}\right)\,.\end{aligned} \tag{38}$$

Finally, note that we can safely ignore the thermal energy of baryons since its ratio with the energy density of photons is of order

$$\frac{n_\mathrm{b} T}{\rho_\gamma} = \frac{\bar{n}_\mathrm{b}}{\bar{\rho}_\gamma} \propto \eta \ll 1\,, \tag{39}$$

thus justifying the use of the scaling (34) which is the one of cold particles.

D. Cosmology and scale factor

The evolution of the scale factor is dictated by the Friedmann equation

$$H^2 = \frac{8\pi G}{3}\rho\,. \tag{40}$$

It determines the evolution of the scale factor $a(t)$, and to solve it we need the expressions of the total energy density as a function of a. Since we already have found the relations $a(T)$, it is sufficient to express the energy density in terms of temperature. This is fortunate, because the energy density of the plasma depends only on temperature as it is always in local thermodynamical equilibrium. From App. A, we find that for the plasma

$$\rho_\mathrm{pl} \;=\; \mathcal{E}(T)\bar{\rho}_\gamma T^4\,, \tag{41a}$$

$$\mathcal{E}(T) \;\equiv\; \frac{\bar{\rho}_\gamma + \bar{\rho}_{e^+} + \bar{\rho}_{e^-}}{\bar{\rho}_\gamma} = 1 + \frac{30}{\pi^4} I_+^{(2,1)}(x)\,, \tag{41b}$$

where we use the definitions (A5)-(A7). The function $\mathcal{E}$ is plotted in Fig. 4 and in the limit $T \gg m_e$ it also tends to 11/4. The energy density of the N_ν generations of (massless) neutrinos is

$$\rho_\nu = N_\nu \bar{\rho}_\nu T_\nu^4\,. \tag{42}$$

As for the energy density of baryons, we use the simple dilution relation (34) which amounts to neglecting their thermal energy. Hence a similar scaling can be used for cold dark matter.

Using that[7]

$$\rho = \rho_\nu + \rho_\mathrm{pl} + \rho_\mathrm{b} + \rho_\mathrm{cdm}, \tag{43}$$

we obtain $\rho(T)$ that we combine with the relation $T(a)$ obtained in section II.B to get $\rho(a)$, such that the Friedmann equation (40) is in the form of an ordinary differential equation for the function $a(t)$ that we can solve numerically. The relation $t(a)$ is then deduced by numerical inversion.

[7] The effect of the cosmological constant is also totally negligible as it accounts for less than 10^{-30} of the energy content during BBN even if it dominates today.

E. QED corrections for the plasma thermodynamics

The thermal bath of electrons and positrons has electromagnetic interactions with the bath of photons. Using QED, this leads to a modification of the plasma thermodynamics which depend on its temperature. First this leads to an effective modification of the electron and photon masses, which come from the diagrams 5 and 6.

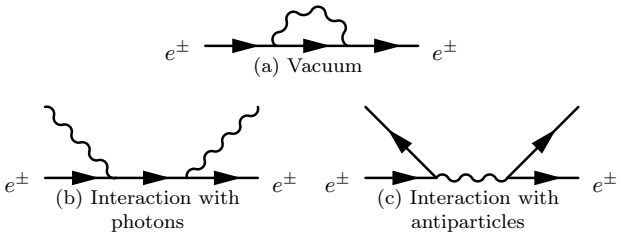

FIG. 5 *Top :* electron/positron self-energy. *Bottom :* electron/positron mass shift from interaction with plasma.

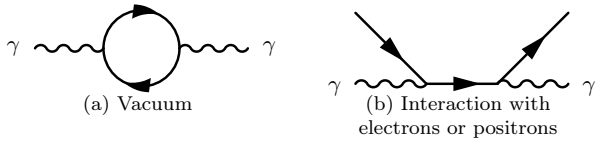

FIG. 6 *Left :* photon self-energy. *Right :* photon mass shift from interaction with electron/positron plasma.

The electron mass is shifted by (see Mangano *et al.* (2002, Eq. 12), Lopez and Turner (1999, Eq. 35) or Fornengo *et al.* (1997); Heckler (1994) for further details on its derivation)

$$\frac{\delta m_e^2(p,T)}{T^2} = \frac{4\alpha}{\pi}\left[I_-^{(0,1)} + I_+^{(0,1)}(x)\right] - \frac{2\bar{m}_e^2\alpha}{\pi\bar{p}}\int_0^\infty \mathrm{d}\bar{q}\,\frac{\bar{q}}{\mathcal{E}_{\bar{q}}}\ln\left|\frac{\bar{p}+\bar{q}}{\bar{p}-\bar{q}}\right| g^+\left(\mathcal{E}_{\bar{q}}\right) \tag{44}$$

where we used the definitions (A5)-(A7). In this expression, $\mathcal{E}_{\bar{q}} \equiv \sqrt{\bar{q}^2+x^2}$, $\bar{m}_e = x = m_e/T$ $\bar{p} \equiv p/T$ and $g^\pm(\mathcal{E}_{\bar{q}}) \equiv 1/(\mathrm{e}^{\mathcal{E}_{\bar{q}}} \pm 1)$. The second contribution, which depends explicitly on the $e^\pm$ momentum, accounts for less than 10% to the total mass shift (see Lopez and Turner (1999); Mangano *et al.* (2002)). The mass shift (44) can be further simplified using

$$I_-^{(0,1)} \equiv \int_0^\infty g^-\left(\bar{k}\right)\bar{k}\mathrm{d}\bar{k} = \frac{\pi^2}{6}\,. \tag{45}$$

The photon mass shift is instead given by

$$\frac{\delta m_\gamma^2}{T^2} = \frac{8\alpha}{\pi} I_+^{(0,1)}(x)\,. \tag{46}$$

These mass shifts induce a change in the pressure of the plasma whose expression is given by Heckler (1994, Eq. 13) or Mangano *et al.* (2002, Eq. 16). The pressure shift reads

$$\overline{\delta P} \equiv \frac{\delta P}{T^4} = -\int_0^\infty \frac{\mathrm{d}\bar{p}}{2\pi^2}\frac{\bar{p}^2}{\mathcal{E}_{\bar{p}}}\frac{\delta m_e^2(p,T)}{T^2} g^+\left(\mathcal{E}_{\bar{p}}\right) - \int_0^\infty \frac{\mathrm{d}\bar{k}}{2\pi^2}\frac{\bar{k}}{2}\frac{\delta m_\gamma^2(T)}{T^2} g^-\left(\bar{k}\right)\,. \tag{47}$$

Hence from the expressions of the mass shifts we get

$$\overline{\delta P} = \overline{\delta P}_\mathrm{d} + \overline{\delta P}_\mathrm{s}\,, \tag{48}$$

where the dominant and subdominant terms are respectively

$$\overline{\delta P}_\mathrm{d} \equiv \frac{\alpha_\mathrm{FS}}{\pi}\left[-\frac{2}{3}I_+^{(0,1)}(x) - \frac{2}{\pi^2}\left(I_+^{(0,1)}(x)\right)^2\right] \tag{49}$$

$$\overline{\delta P}_\mathrm{s} \equiv \frac{\alpha_\mathrm{FS}}{\pi^3}\frac{\bar{m}_e^2}{\bar{p}\bar{q}}\int\frac{\bar{p}^2\mathrm{d}\bar{p}}{\mathcal{E}_{\bar{p}}}\frac{\bar{q}^2\mathrm{d}\bar{q}}{\mathcal{E}_{\bar{q}}}\ln\left|\frac{\bar{p}+\bar{q}}{\bar{p}-\bar{q}}\right| g^+\left(\mathcal{E}_{\bar{p}}\right) g^+\left(\mathcal{E}_{\bar{q}}\right)\,.$$

These pressure modifications are plotted in Fig. 7. We can check that the subdominant contribution is indeed negligible since QED plasma corrections are already very small (see § V.C), but we include it anyway for completeness.

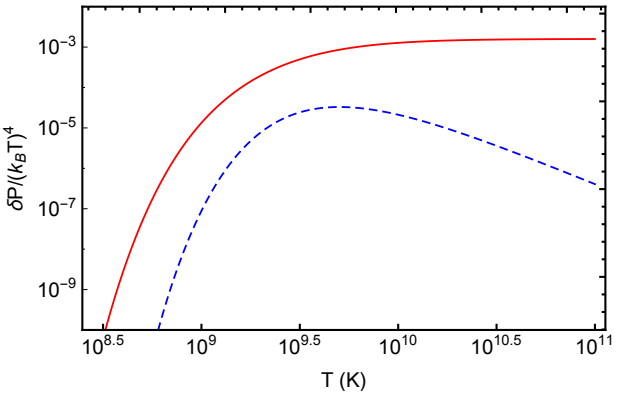

FIG. 7 *Red continuous line* : $\overline{\delta P}_\mathrm{d}$. *Blue dashed line* : $\overline{\delta P}_\mathrm{s}$. Definitions are given in Eq. (49).

The modification of the plasma energy density is then obtained from the thermodynamic identity[8]

$$\rho = -P + T\frac{\mathrm{d}P}{\mathrm{d}T}\,, \tag{50}$$

so that we get immediately

$$\overline{\delta\rho} \equiv \frac{\delta\rho}{T^4} = 3\overline{\delta P} + \frac{\partial\overline{\delta P}}{\partial\ln T}\,. \tag{51}$$

[8] Choosing T and V to describe the state of a system, then P and ρ are functions of T only since they are intensive quantities. It follows from $T\mathrm{d}S = \mathrm{d}(\rho V) + P\mathrm{d}V$ that $\mathrm{d}S = (P+\rho)/T\mathrm{d}V + V/T(\mathrm{d}\rho/\mathrm{d}T)\mathrm{d}T$. From the integrability conditions we then get $\partial_T[(\rho+P)/T] = \partial_V(V/T\mathrm{d}\rho/\mathrm{d}T)$ and the identity (50) follows.

Lopez and Turner (1999) defined corrected relativistic degrees of freedom by

$$\delta g_\rho \equiv 2\frac{\overline{\delta\rho}}{\bar\rho_\gamma} = \frac{30}{\pi^2}\overline{\delta\rho}\,, \quad \delta g_P \equiv 2\frac{\overline{\delta P}}{\bar P_\gamma} = \frac{90}{\pi^2}\overline{\delta P}\,. \tag{52}$$

At high temperatures, that is for $T \gg m_e$, we obtain using $I_+^{(0,1)}(x=0) = \pi^2/12$ (see table IX in appendix A.1) the limits

$$\overline{\delta\rho} \simeq -\frac{5}{96}(4\pi\alpha)\,, \qquad \overline{\delta P} \simeq \frac{1}{3}\overline{\delta\rho}\,, \tag{53}$$

which expressed in terms of corrected relativistic degrees of freedom read

$$\delta g_\rho \simeq \delta g_P \simeq -\frac{25\alpha}{4\pi} \simeq 0.01452\,. \tag{54}$$

These corrections are plotted in Fig. 8 together with the high temperature limit.

The QED plasma corrections enter in four places.

- First they imply that the entropy of the plasma as given in Eq. (30b) must be modified and we must use

$$\mathcal{S}^{\rm QED} = \mathcal{S} + \frac{\bar\rho_\gamma}{\bar s_\gamma}\frac{\delta g_\rho}{2} + \frac{\bar P_\gamma}{\bar s_\gamma}\frac{\delta g_P}{2} = \mathcal{S} + \frac{\delta g_P + 3\delta g_\rho}{8} \tag{55}$$

  where the last equality follows from Eqs. (25). $\mathcal{S}^{\rm QED}$ must be used instead of $\mathcal{S}$ in Eq. (31) in order to obtain $a(T)$.

- Second, this entropy modification also affects the evolution of z and we find

$$(z_0^{\rm QED})^3 = S^{\rm QED}(T \gg m_e) = \frac{11}{4}\left(1 - \frac{4}{11}\frac{25\alpha}{8\pi}\right)\,, \tag{56}$$

  that is $z_0^{\rm QED} \simeq 1.39979$. This affects the neutrino temperature scaling which then becomes

$$T_\nu^{\rm QED} = \frac{a_0 T_0}{a\, z_0^{\rm QED}}\,. \tag{57}$$

  This neutrino temperature must be used in Eq. (42) when computing the energy density of neutrinos for the Friedmann equation (40).

- Third, the plasma QED correction must also be incorporated in the energy density of the plasma when solving the Friedmann equation (40), meaning that we must modify Eqs. (41) and use instead

$$\mathcal{E}^{\rm QED} = \mathcal{E} + \frac{\delta g_\rho}{2}\,, \tag{58}$$

  when computing $\rho_{\rm pl}$ for the Friedmann equation (40).

- Finally, the electron mass shifts modifies the statistics of electrons and positrons in the weak-interactions.

An important comment is in order here on the last effect. Since the mass shift (44) is exactly Eq. (5.12) of (Brown and Sawyer, 2001) (that is $2E\Delta E = \delta m_e^2$), the effect of the electron mass shift is one of the several effects involved in finite-temperature radiative corrections for the weak rates. Hence, following Brown and Sawyer (2001), we consider that the modification of the statistics through the mass shift is part of the finite-temperature corrections and we do not consider that it is part of the QED plasma corrections. This point of view is similar to Esposito *et al.* (2000a); Serpico *et al.* (2004) but different from Lopez and Turner (1999). Hence comparisons on the magnitude of the correction must take into account the point of view on the effect of mass shifts, since either they are reported as QED effects or finite-temperature radiative corrections.

It turns out that the QED plasma corrections (that is without the effect of the mass shift on the weak-interaction rates), coming from the modifications (55),(57) and (58), are very small since they modify the Helium production by approximately $\Delta Y_{\rm P}^{(4)} = -0.1$ (see § V.C).

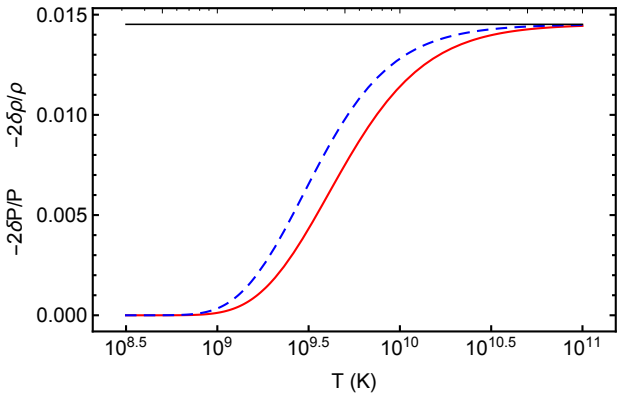

FIG. 8 Effective degrees of freedom in the plasma from QED corrections. *Red continuous line* : $-\delta g_P = -2\delta P/P$. *Blue dashed line* : $-\delta g_\rho = -2\delta\rho/\rho$. *Black thin line* : High temperature asymptotic value $25\alpha/(4\pi)$.

F. Incomplete neutrino decoupling

The effect of incomplete neutrino decoupling has been studied in details in Birrell *et al.* (2014); Dodelson and Turner (1992); Dolgov *et al.* (1997, 1999); Esposito *et al.* (2000b); Fields *et al.* (1993); Gnedin and Gnedin (1998); Grohs *et al.* (2016); Hannestad (2002); Hannestad and Madsen (1995); Mangano *et al.* (2002, 2005, 2006); de Salas and Pastor (2016). Electron-positron annihilations lead to a small reheating of the neutrino bath which must be studied in the context of coupled Boltzmann equations since it also leads to spectral distortions in the neutrino spectrum. Furthermore the complete study,

that we do not reproduce here, requires to consider neutrino flavor oscillations.

Let us first study the effect of incomplete neutrino decoupling (ID) on the plasma. If there is heat exchange, that is energy exchange between the plasma and the neutrinos, then the evolution of the plasma entropy is dictated by Eq. (20) with the chemical potential neglected, that is

$$\dot{S}_{\rm pl} = \frac{\dot{Q}_{\rm pl}}{T}\,. \tag{59}$$

This is always true for the plasma because it is always at local thermodynamic equilibrium, but not necessarily true for the neutrinos for which we should rely on Eq. (17) if we were to compute the evolution of their entropy. The numerical studies of the effect of incomplete neutrino decoupling gives a fit to the heating rate of the plasma in Pisanti *et al.* (2008). More precisely, we define the dimensionless function $\mathcal{N}(T)$ related to the heating rate as

$$\frac{\dot{q}_{\rm pl}}{HT} = -T^3\mathcal{N}(T)\,, \tag{60}$$

where we remind $\dot{Q} = a^3\dot{q}$. The function $T^4\mathcal{N}$ can be viewed as the volume heating rate in units of the Hubble rate H. The fit given in Pisanti *et al.* (2008, Eqs. A24-A25) is a 13-order polynomial in $x = m_e/T$ valid for $x < 4$, and we plot it in Fig. 9.

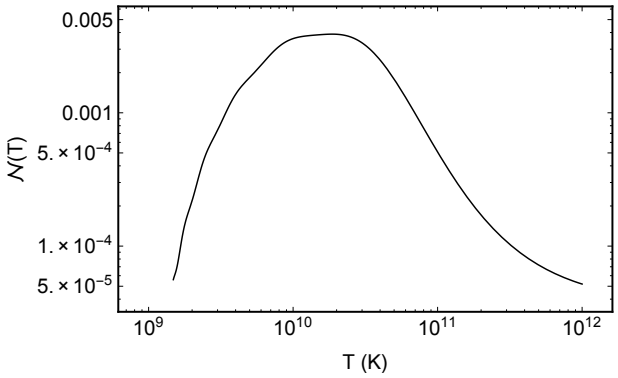

FIG. 9 $\mathcal{N}(T)$ as defined in Eq. (60).

From Eqs. (59) and (60), the evolution of the plasma reduced entropy is dictated by

$$\frac{1}{(aT)^3}\frac{{\rm d}[\bar{s}_{\rm pl}(aT)^3]}{{\rm d}\ln a} = -\mathcal{N}\,. \tag{61}$$

From the definition (30b) we obtain

$$\frac{{\rm d}\ln(aT)}{{\rm d}\ln T} = \frac{\mathcal{N} - \frac{{\rm d}\mathcal{S}}{{\rm d}\ln T}}{\mathcal{N}+3\mathcal{S}} \tag{62}$$

where $\mathcal{S}$ must be replaced by $\mathcal{S}^{\rm QED}$ when including plasma QED effects. We recover when $\mathcal{N} = 0$, that is for complete neutrino decoupling, that $z = aT \propto \mathcal{S}^{-1/3}$. This equation can be integrated numerically to obtain $a(T)$ in the case of incomplete neutrino decoupling, and a numerical inversion allows to obtain subsequently $T(a)$. z is modified because of the non-conservation of plasma entropy, and we get $z_0^{\rm ID} \simeq 1.39911$ if QED plasma effects are not included and $z_0^{\rm ID,QED} \simeq 1.39788$ if they are also included, in agreement (except for the last digit) with table 1 of de Salas and Pastor (2016). Our results are summarized in table I.

Let us now focus on the effect of incomplete neutrino decoupling on neutrinos. Since the energy taken from the plasma is gained by the neutrinos, we have necessarily $q_{\rm pl} = -q_\nu$. Hence we can solve for the evolution of the neutrino energy density from Eq. (12) which is

$$\frac{1}{a^4}\frac{{\rm d}(a^4\rho_\nu)}{{\rm d}\ln a} = -\frac{\dot{q}_{\rm pl}}{H} = T^4\mathcal{N}\,. \tag{63}$$

Since $T^4\mathcal{N}$ is a function of T it can be considered as a function of a using the $T(a)$ previously obtained. Solving numerically this differential equation gives $\rho_\nu(a)$. Together with the previously solved $T(a)$ [which allows to get $\rho_{\rm pl}(a)$ from Eq. (41)] and the QED correction (58), we obtain $\rho(a)$ and thus the relation $a(t)$ and its inverse $t(a)$ from numerically solving the Friedmann equation (40).

This approach to compute the variation of the neutrino energy density from Eq. (63) is correct even if incomplete neutrino decoupling and neutrino reheating by electron-positron annihilations create spectral distortions in the neutrino spectra. That is, the gravitational effect of incomplete neutrino decoupling is taken into account correctly with our approach. However it cannot fully take into account the effect on the weak rates which we discuss further in § III.I and V.C.5.

G. Effective description of neutrinos

Neutrinos are not in local thermodynamical equilibrium and their temperature is not well defined. Indeed, the full characterization of the neutrinos requires to solve the coupled Boltzmann equations dictating the evolution of neutrino distribution functions, and we must in principle build a temperature definition from the energy spectrum (see e.g. Pitrou and Stebbins (2014)). In the BBN context it is convenient to define a brightness temperature, being the temperature of the Fermi-Dirac distribution with no chemical potential that would have the same energy density. Hence we define T_ν as in Eq. (42) by

$$\rho_\nu = N_\nu\bar{\rho}_\nu T_\nu^4 \quad \Rightarrow \quad \rho_\nu a^4 = N_\nu\bar{\rho}_\nu z_\nu^4\,, \tag{64}$$

where ρ_ν results from the integration of Eq. (63). z_ν[9] is deduced from the value of $\rho_\nu a^4$ obtained numerically,

[9] Note that we still define z_ν as in the LTE case [Eq. (28)].

and we find $z_{\nu,0} = 1.00144$. It corresponds to a neutrino energy density increase of a factor $z_{\nu,0}^4 = 1.00576$ compared to the complete decoupling scenario.

The ratio between neutrino and photon temperature is simply

$$\frac{T_\nu}{T} = \frac{z_\nu}{z}\,. \tag{65}$$

Using this ratio, Eq. (64) can be rewritten to define an effective number of neutrinos as

$$\rho_\nu = N_{\rm eff}\bar{\rho}_\nu \left(\frac{T}{z^{\rm stand}}\right)^4 \qquad N_{\rm eff} \equiv N_\nu \left(\frac{z_\nu z^{\rm stand}}{z}\right)^4 . \tag{66}$$

This is the number of neutrinos that would be required to have the same energy density if the ratio T_ν/T was taken from the complete decoupling result without QED correction, that is $1/z^{\rm stand}$. $N_{\rm eff}$ today is completely determined by the values of z_0 and $z_{\nu,0}$. Its evolution is plotted in Fig. 10.

We find $N_{\rm eff}^{\rm ID} = 3.0337$ today if QED plasma effects are ignored [z obtained from Eq. (62) and z_ν from Eqs. (63) and (65)] but non-instantaneous decoupling is taken into account. We find $N_{\rm eff}^{\rm QED} = 3.0106$ for the reverse situation ($z_\nu = 1$ but $z = z^{\rm QED}$). If both effects are taken into account [z obtained from Eq. (62) with $\mathcal{S}^{\rm QED}$ instead of $\mathcal{S}$, and z_ν from Eqs. (63) and (65)], we find $N_{\rm eff}^{\rm ID,QED} = 3.0444$, in very close agreement with the last results of de Salas and Pastor (2016).

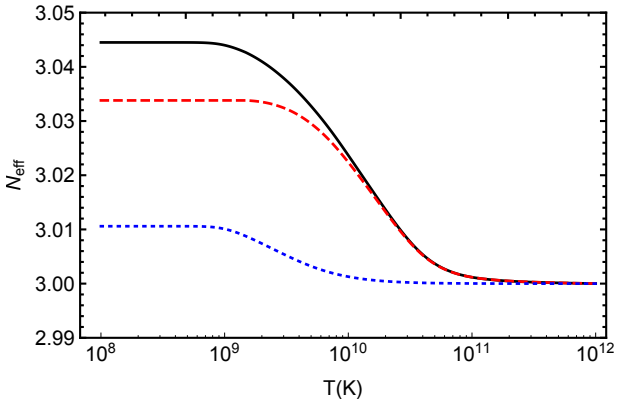

FIG. 10 $N_{\rm eff}(T)$. *Black continuous line* : both QED plasma effects and incomplete neutrino decoupling. *Red long dashes*: Incomplete decoupling but no QED corrections. *Blue small dashes*: QED correction with complete decoupling

After BBN, e.g. for the evolution of initial perturbations through baryon acoustic oscillations, only the energy density of neutrinos is important through its gravitational effect. Distortions in the neutrino spectra can have in principle an effect on CMB and structure formation when considering its joint effect with neutrino masses at late times. However this effect is expected to be extremely small and it is enough to assume that after

TABLE I z_0, $z_{\nu,0}$ and $N_{\rm eff}$ depending on the effects.

QED	Decoupling	$z_0 = aT$	$z_{\nu,0} = aT_\nu$	$N_{\rm eff}$
No	Yes	1.40102	1.00000	3.0000
Yes	Yes	1.39979	1.00000	3.0106
No	No	1.39911	1.00144	3.0338
Yes	No	1.39788	1.00144	3.0445

BBN neutrinos follow a Fermi-Dirac distribution. Hence $N_{\rm eff}$ is used in CMB codes such as CAMB (Lewis and Challinor, 1999; Lewis *et al.*, 2000) and CLASS (Blas *et al.*, 2011; Lesgourgues, 2011) to take into account the effect of incomplete decoupling during BBN. From the definition (66) the total energy density of radiation after BBN is

$$\rho_{\rm R} = \rho_\nu + \rho_\gamma = \rho_\gamma \left(1 + \frac{7}{8} N_{\rm eff} \left(\frac{4}{11}\right)^{4/3}\right) \tag{67}$$

meaning that we can forget about the QED plasma corrections and the incomplete neutrino decoupling during BBN if we use $N_{\rm eff}$ instead of $N_\nu = 3$.

The values of z_0, $z_{\nu,0}$ and $N_{\rm eff}$ for the various cases are reported in table I. Let us comment on the value $N_{\rm eff} \simeq 3.02$ found in Grohs *et al.* (2016) for the effect of QED alone. It is important to realize that we must be careful not to replace the mass shifts (44) and (46) directly in the distribution function inside the general expression (A2c) for pressure to obtain the pressure shift (47), since this would overestimate it by a factor 2. This subtlety is detailed in Heckler (1994) and is correctly taken into account in Mangano *et al.* (2002). Since this is what has been done in Grohs *et al.* (2016), it explains why the effect of QED on the plasma as measured by $N_{\rm eff}$ found in this reference is around 3.02 instead of 3.01.

III. WEAK INTERACTIONS

Once the dynamics of the background has been solved, it is possible to study the evolution of the abundance of neutrons. This determines the final amount of chemical species since atomic nuclei form from the fusion of neutrons and protons. Throughout we assume that all particles are in local thermodynamical equilibrium. If this is certainly true for the plasma of photons strongly coupled with electrons and positrons, this is not exactly true for neutrinos. Indeed, as we have seen in § II.F, neutrinos are not fully decoupled when BBN takes place and there is a residual heating of neutrinos which cannot be fully described as an increased neutrino temperature, since it also leads to a distorted neutrino spectrum.

A. General formulation

The weak interaction reactions correspond to a set of reactions which are all related by crossing symmetry. These are the six reactions

$$n + \nu \leftrightarrow p + e^- \tag{68a}$$
$$n \leftrightarrow p + e^- + \bar{\nu} \tag{68b}$$
$$n + e^+ \leftrightarrow p + \bar{\nu} \tag{68c}$$

where n (p) stands for neutrons (protons). The two reactions $n + e^+ + \nu \leftrightarrow p$ are not possible energetically since $m_n > m_p$, as can be seen considering the reaction in the proton rest mass frame. However it can exist if there is a photon in the final state of the forward reaction, see appendix § B.7.

It follows that the number density of neutrons and protons is not just diluted by expansion, but varies according to the reaction rates. The general form for the neutron-proton density evolution is

$$\dot{n}_n + 3Hn_n = -n_n\Gamma_{n\to p} + n_p\Gamma_{p\to n} \tag{69a}$$
$$\dot{n}_p + 3Hn_p = -n_p\Gamma_{p\to n} + n_n\Gamma_{n\to p} \tag{69b}$$

where the reaction rates Γ are associated to the corresponding collision terms in the Boltzmann equation. Here we have gathered the rates according to

$$\Gamma_{n\to p} = \Gamma_{n+\nu\to p+e} + \Gamma_{n\to p+e+\bar{\nu}} + \Gamma_{n+e\to p+\bar{\nu}} \tag{70a}$$
$$\Gamma_{p\to n} = \Gamma_{p+e\to n+\nu} + \Gamma_{p+e+\bar{\nu}\to n} + \Gamma_{p+\bar{\nu}\to n+e} \tag{70b}$$

The general expression for these reaction rates is detailed in App. B. For all rates with the nucleon a in the initial state and nucleon b in the final state, they take the form

$$n_a\Gamma_{a\to b} = \int \frac{\mathrm{d}^3\mathbf{p}_a\mathrm{d}^3\mathbf{p}_e\mathrm{d}^3\mathbf{p}_\nu}{2^4(2\pi)^8}\delta\left(E_a - E_b + \alpha_e E_e + \alpha_\nu E_\nu\right)\frac{|M|^2_{a\to b}}{E_nE_pE_eE_\nu}f_a(E_a)f_\nu(\alpha_\nu E_\nu)f_e(\alpha_e E_e) \tag{71}$$

where $\alpha_\nu = 1$ if the neutrino is in the initial state and $\alpha_\nu = -1$ if it is in the final state, and a similar definition for α_e according to the $\mathrm{e}^\pm$ position. These coefficients appear obviously in the Dirac delta function ensuring energy conservation in reactions, and they are also used to express the final nucleon momentum as $p_b = p_a + \alpha_\nu p_\nu + \alpha_e p_e$. They also appear in the distribution functions of the electrons and neutrinos, because either the particle is in the initial state and the corresponding distribution function appears in the expression, or it is in the final state and it becomes a Pauli-blocking factor thanks to the relation

$$f(-E) = 1 - f(E)\,, \tag{72}$$

valid for a Fermi-Dirac distribution with vanishing chemical potential. For a given reaction, $|M|^2_{a\to b}$ is the corresponding matrix-element of the weak interaction summed over all initial and final states. For weak interactions in the Fermi theory, it is of the form (Fidler and Pitrou, 2017)

$$\frac{|M|^2}{2^7G_F^2} = c_{LL}\mathcal{M}_{LL} + c_{RR}\mathcal{M}_{RR} + c_{LR}\mathcal{M}_{LR}\,, \tag{73}$$

with the coupling factors $c_{..}$ given in Eqs. (B11). The expressions for $\mathcal{M}_{LL}, \mathcal{M}_{RR}, \mathcal{M}_{LR}$ are reported in Eqs. (B12). The LL term (resp. RR) corresponds to purely left-chiral (resp. right-chiral) couplings, and the LR term is an interference term.

B. Infinite nucleon mass approximation

Let us define the energy gap

$$\Delta \equiv m_n - m_p \simeq 1.29333\ \mathrm{MeV}\,. \tag{74}$$

Throughout we use $g(E)$ for the Fermi-Dirac distribution at temperature of electrons T and $g_\nu(E)$ for the Fermi-Dirac distribution at the neutrino temperature T_ν.

$$g(E) \equiv \frac{1}{\left(\mathrm{e}^{\frac{E}{T}} + 1\right)} \qquad g_\nu(E) \equiv \frac{1}{\left(\mathrm{e}^{\frac{E}{T_\nu}} + 1\right)}\,. \tag{75}$$

In § II, details are given on how these temperatures can be computed in function of the scale factor a and the time t.

In the infinite nucleon mass limit (but keeping Δ constant), also called the Born approximation, the reaction rates take simple forms (see App. B). First, the factors entering the matrix element (73) are in that limit simply

$$\frac{\mathcal{M}_{LL}}{E_nE_pE_\nu E_e} = \frac{\mathcal{M}_{RR}}{E_nE_pE_\nu E_e} = \frac{\mathcal{M}_{LR}}{E_nE_pE_\nu E_e} = 1\,. \tag{76}$$

The last equality is correct only if it is understood that an angular average either on electrons momentum or neutrino momentum is performed[10] (see the detailed explanation at the end of § B.2). Hence from Eq. (71), we

[10] The LR coupling is at the origin of the asymmetry (B22b) in the decay product of neutron beta decay (Ivanov *et al.*, 2013) from which the value of g_A is inferred.

find the Born rates (Bernstein *et al.*, 1989; Brown and Sawyer, 2001; Lopez and Turner, 1999; Weinberg, 1972)

$$\overline{\Gamma}_{n\to p} = \overline{\Gamma}_{n\to p+e} + \overline{\Gamma}_{n+e\to p} \quad (77)$$

$$= K\int_0^\infty p^2 \mathrm{d}p[\chi_+(E) + \chi_+(-E)]\,, \quad (78)$$

with $E = \sqrt{p^2+m_e^2}$ and

$$\chi_\pm(E) \equiv (E_\nu^\mp)^2 g_\nu(E_\nu^\mp) g(-E)\,, \quad (79)$$

$$E_\nu^\mp \equiv E \mp \Delta\,, \quad (80)$$

$$K \equiv \frac{4G_W^2(1+3g_A^2)}{(2\pi)^3}\,. \quad (81)$$

The first contribution in Eq. (77) corresponds to the $n \to p$ processes (68a) and (68b) added, that is for all processes where the electron is in the final state. It can be checked indeed that the electron distribution is evaluated as $g(-E) = 1 - g(E)$. Furthermore, if the neutrino is in the initial state (when $E > \Delta$) its energy is $E_\nu = E - \Delta$ and its distribution function appears as $g_\nu(E_\nu)$, but if it is in the final state (when $E < \Delta$) its energy is $E_\nu = \Delta - E$ and the neutrino distribution function is evaluated as $g_\nu(E-\Delta) = 1 - g_\nu(\Delta - E)$.

The second term of Eq. (77) corresponds to the reaction (68c), that is to the process where the positron is in the initial state. The energy of the positron is E and its distribution function appears as an initial state $[g(E)]$, whereas the neutrinos in the final state have energy $E_\nu = \Delta + E$ and their distribution function appear thus as Pauli-blocking factor $g_\nu(-E-\Delta) = 1-g_\nu(E+\Delta)$.

The reaction rate for protons, that is $\Gamma_{p\to n}$, is obtained by the simple replacement $\Delta \to -\Delta$, which amounts to $\chi_+ \to \chi_-$. We give it for completeness

$$\overline{\Gamma}_{p\to n} = \overline{\Gamma}_{p\to n+e} + \overline{\Gamma}_{p+e\to n} \quad (82)$$

$$= K\int_0^\infty p^2 \mathrm{d}p[\chi_-(E) + \chi_-(-E)]\,. \quad (83)$$

Similarly the second term corresponds to the reverse processes (68a) and (68b) added since the electron distribution function is always in an initial state $[g(E)]$, and the neutrino is in the initial or final state depending on the sign of $E_\nu = -E + \Delta$. The first term corresponds to the reverse process (68c) with the positron always in the final state $[g(-E) = 1 - g(E)]$ and the neutrino always in the initial state $[g_\nu(E+\Delta)]$.

Finally, note that using

$$g(-E) = 1 - g(E) = \mathrm{e}^{E/T} g(E)\,, \quad (84)$$

we get in the case of thermal equilibrium between neutrinos and the plasma (that is when $T_\nu = T$)

$$\chi_+(E) = \mathrm{e}^{\Delta/T}\chi_-(-E)\,. \quad (85)$$

This implies that if neutrinos have the same temperature as the plasma, the reaction rates satisfy the Born approximation detailed balance relation

$$\overline{\Gamma}_{p\to n} = \mathrm{e}^{-\Delta/T}\overline{\Gamma}_{n\to p}\,. \quad (86)$$

It is important that detailed balance be satisfied in our estimation of the weak rates since it is at the origin of the enforcement of the thermodynamical equilibrium between neutrons and protons. When adding corrections to the Born approximation weak rates in the form $\Gamma \equiv \delta\Gamma + \overline{\Gamma}$, then the relative corrections of the forward and reverse rates must be equal, that is

$$\frac{\delta\Gamma_{p\to n}}{\overline{\Gamma}_{p\to n}} = \frac{\delta\Gamma_{n\to p}}{\overline{\Gamma}_{n\to p}}\,, \quad (87)$$

in order that the corrected rates also satisfy the detailed balance property (86). When estimating the corrections to the Born rates, we systematically discuss how this detailed balance is kept valid with the corrections and we highlight our differences on that crucial property with previous literature.

C. Calibration from free neutron decay rate

The interaction rates are proportional to the factor K defined in Eq. (81). It is proportional to

$$G_W^2 \equiv G_F^2\cos^2(\theta_\mathrm{C}) \quad (88)$$

where G_F is the Fermi constant and θ_C is a CKM angle, and also to $1+3g_A^2$ where g_A is the axial current constant for the nucleons (see App. D for numerical values). Given the uncertainty in these parameters, it is more precise to obtain K from the free neutron decay[11]. Indeed, at low temperatures, $\Gamma_{n\to p}$ should be equal to the free neutron decay rate $1/\tau_n$. The low temperature corresponds to (77) restricted to $E_\nu < 0$, that is

$$\frac{1}{\tau_n} = \Gamma_{n\to p}(T=0) = K\int_0^{\sqrt{\Delta^2-m_e^2}} p^2 E_\nu^2 \mathrm{d}p\,, \quad (89)$$

with $E_\nu = \sqrt{p^2+m_e^2} - \Delta$. We define

$$\lambda_0 \equiv m_e^{-5}K^{-1}\Gamma_{n\to p}(T=0) \quad (90)$$

so K is obtained from the free neutron decay rate as

$$K = 1/(\tau_n\lambda_0 m_e^5) \quad (91)$$

instead of Eq. (81). At the Born approximation level, that is using $\overline{\Gamma}_{n\to p}$ in Eq. (90), λ_0 takes the value (Bern-

[11] The relative precision on $\cos(\theta_\mathrm{C})$ and g_A are respectively 2.0×10^{-4} and 1.8×10^{-3}. If τ_n was to be obtained theoretically from these constants, then its uncertainty $\delta\tau_n/\tau_n \simeq 2\delta\cos(\theta_\mathrm{C})/\cos(\theta_\mathrm{C}) + 1.66\delta g_A/g_A$ would be of order 3×10^{-3} which is larger than the experimental uncertainty which is of order 1.0×10^{-3}. However improvements in the measurements of g_A by a factor 3 would make this direct estimation of τ_n competitive.

stein *et al.*, 1989)

$$\begin{aligned}\bar{\lambda}_0 &\equiv m_e^{-5}\int_0^{\sqrt{\Delta^2-m_e^2}} p^2E_\nu^2\mathrm{d}p \\ &= \sqrt{\bar{\Delta}^2-1}\left(\frac{-8-9\bar{\Delta}^2+2\bar{\Delta}^4}{60}\right)+\frac{\bar{\Delta}}{4}\operatorname{arccosh}\bar{\Delta} \\ &\simeq 1.63609, \end{aligned} \tag{92}$$

where $\bar{\Delta}\equiv\Delta/m_e$.

D. Neutron abundance and freeze-out

It is enough to consider the weak rates in the Born approximation to estimate the freeze-out temperature. The Born rates are plotted in Fig. 11 together with the Hubble rate. A first estimation of the freeze-out temperature

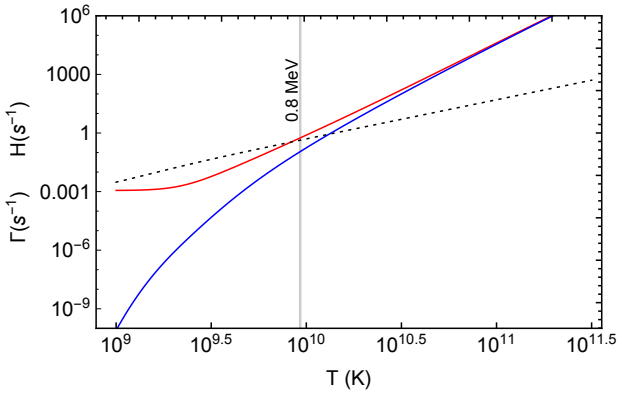

FIG. 11 Γ. *Continuous line* : Upper red curve is $n\to p$ rate and lower blue curve is $p\to n$ rate . *Dashed line* : Hubble rate.

consists in noting that expansion overcomes both rates for $T_F\simeq 8\times10^9$K which we can take as the freeze-out temperature.

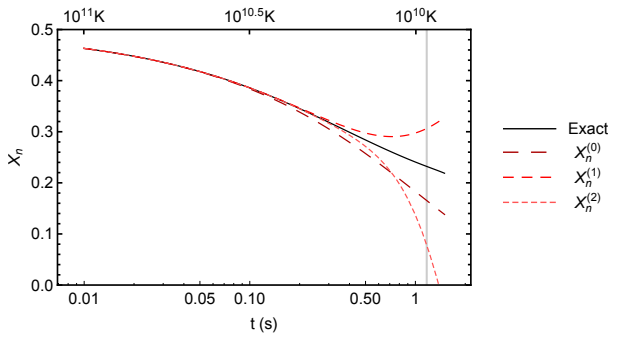

FIG. 12 *Black continuous line* : numerical solution. *red dashed lines* : solutions (95) for $p=0,1,2$. The vertical bar corresponds to $T_F=0.8\,\mathrm{MeV}$

We can justify this estimation by finding an approximate solution for the neutron abundance. Its evolution, in absence of nuclear reactions, is dictated by

$$\dot{X}_n = X_p\Gamma_{p\to n}-X_n\Gamma_{n\to p}\,. \tag{93}$$

Using $X_p=1-X_n$, we get

$$X_n=\frac{\Gamma_{p\to n}}{\Lambda}-\frac{1}{\Lambda}\dot{X}_n\,,\qquad \Lambda\equiv\Gamma_{p\to n}+\Gamma_{n\to p}\,. \tag{94}$$

We obtain tight-coupling solutions to order m by recursive replacement of X_n and we get

$$X_n^{(m)}=\sum_{k=0}^{m}\left(\frac{-1}{\Lambda}\frac{\mathrm{d}}{\mathrm{d}t}\right)^k\frac{\Gamma_{p\to n}}{\Lambda}\,. \tag{95}$$

$m=0$ corresponds to the pure thermodynamical equilibrium and higher order corrections are due to the fact that the neutron abundance has less and less time to approach this equilibrium value. This expansion is equivalent to Bernstein *et al.* (1989, Eq. 2.8). We can estimate the freeze-out temperature, that is the temperature at which weak interactions fail to maintain the thermodynamical equilibrium value, by computing the temperature for which the first correction is of order of the equilibrium value, that is when $|X_n^{(1)}-X_n^{(0)}|=X_n^{(0)}$. Assuming that the neutrino temperature does not differ significantly from the plasma temperature before freeze-out, we can use Eq. (86) to estimate this condition which reads

$$H\frac{Q}{T}\frac{\mathrm{e}^{Q/T}}{1+\mathrm{e}^{Q/T}}=\Lambda\,. \tag{96}$$

We find $T_F\simeq 8.9\times10^9\mathrm{K}\simeq0.77\,\mathrm{MeV}$ and replacing in the thermodynamical equilibrium abundance we get

$$X_n^F\equiv X_n^{(0)}(T_F)\simeq 0.156\,. \tag{97}$$

Finally, another estimation consists in determining visually when the neutron abundance is only affected by beta decay. In Fig. 3, this leads to $T_F\simeq3.3\times10^9\,\mathrm{K}\simeq0.28\,\mathrm{MeV}$ and $X_n^F\simeq0.17$.

After the freeze-out, the neutron abundance is only affected by the neutron beta decay. The nucleosynthesis starts approximately when $T<T_{\rm Nuc}=0.078\,\mathrm{MeV}$, or 0.9 GK (see § V.B) corresponding to roughly $t_{\rm Nuc}=200\,\mathrm{s}$. The neutron abundance when the nucleosynthesis starts is thus approximately given by

$$X_n(T_{\rm Nuc})=X_n^F\exp\left(-\frac{t_{\rm nuc}-t_F}{\tau_n}\right)\approx0.13\,. \tag{98}$$

E. Radiative corrections at $T=0$

1. Standard computation

Radiative corrections at $T=0$ correspond to two types of corrections (Abers *et al.*, 1968; Dicus *et al.*, 1982; Kernan, 1993; Sirlin, 1967). First the radiative corrections per se, that is for which a virtual photon is emitted and

absorbed inside the interaction and which interfere with the lowest order or Born diagram. Hereafter we call these *pure radiative corrections* and the relevant diagrams in the infinite nucleon mass limit are depicted in Fig. 13 (see also Ivanov *et al.* (2013, App. C)). As shown in the seminal article by Sirlin (1967), the other diagrams involving virtual photons[12] can be reabsorbed in the redefinitions of G_F and g_A.

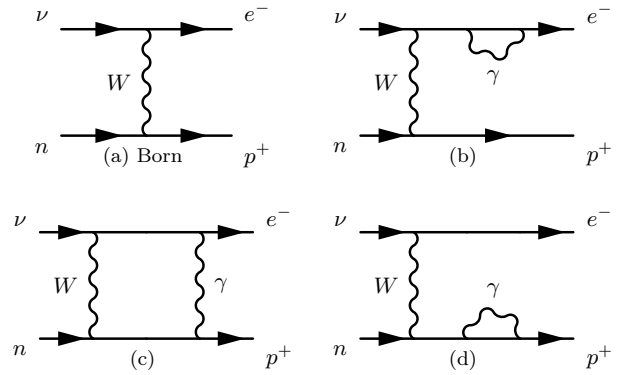

FIG. 13 Born diagram and virtual photon radiative corrections.

Second it also contains the corrections due to the emission of real photon (Abers *et al.*, 1968, Fig 2e,2f). These processes are generically called bremsstrahlung (BS), and in the infinite nucleon mass approximation only the emission from the electron line (Fig. 14a) contributes.

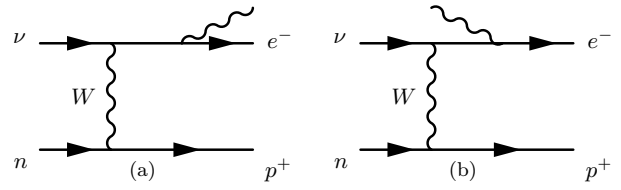

FIG. 14 Bremsstrahlung (left) and absorption (right).

It is necessary to handle these two types of corrections simultaneously, because each of these contributions contains an infrared divergence in the photon momentum. But as is well known, when both are considered, these divergences exactly cancel provided they are correctly regularized. The usual procedure consists in letting the photon have a mass for the computation of each type of correction, and then noticing that the log-divergences which appear are exactly opposite, leading to a finite result in the limit $m_\gamma \to 0$ (Abers *et al.*, 1968); (Ivanov *et al.*, 2013, App. B). These radiative corrections are very well understood for the neutron beta decay (Abers *et al.*, 1968; Czarnecki *et al.*, 2004; Marciano and Sirlin, 2006; Sirlin, 1967). The main result is that radiative corrections can be taken into account by a multiplicative factor whose expression involves Sirlin's universal function (Sirlin, 1967, Eq. 20b). This was subsequently refined mainly to improve the expression of the high energy cut-off which was related to the mass of the vector boson once weak interactions were properly understood, and we use Czarnecki *et al.* (2004) as the most accurate account on this issue.

A careful analysis however indicates that only pure radiative corrections take a universal form which can be used for all the reactions (68). They are given by Abers *et al.* (1968, Eq. 6.2) and depend only on the electron velocity $\beta = p/E$ [13]. The total corrections for the neutron beta decay include also the bremsstrahlung (Abers *et al.*, 1968, Eq. 6.6) and these are computed specifically for the neutron beta decay, with a maximum photon energy being $\Delta - E$.

Hence, the radiative corrections for the reactions (68) should in principle be recomputed to take into account the correct bremsstrahlung corrections for each reaction. However it proves much more convenient to temporarily forget about this issue and assume that the radiative corrections computed for the neutron beta decay can be used without modification for all weak reactions. We postpone the correct treatment of bremsstrahlung to the next section.

Note that even for the neutron beta decay this approximation amounts to ignoring the Pauli-blocking effects of the neutrinos which is modified by the energy subtracted from the photon. In this approximation, the maximum energy of emitted photons is chosen to be the maximum energy of the neutrino when in the final state. For the neutron beta decay this is $\Delta - E$, but for reaction (68c) this is $\Delta + E$.

Under this assumption, our method to compute the radiative correction at $T = 0$ follows exactly the approach by Dicus *et al.* (1982) and subsequent literature based on it, for which the same assumption was implicitly made. The radiative corrections can be separated between a Coulomb correction, which accounts for the motion of the electron in the Coulomb field of the proton, and the other corrections. It is customary to factorize the Coulomb corrections as they can be taken into account multiplicatively by the Fermi function[14]. The diagram 13c corresponds to the interaction between the

[12] These extra diagrams correspond first to a virtual photon exchange between the electron and the gauge boson, and between the electron and the neutron (Sirlin, 1967, Fig. 1), and second to a virtual photon exchange between the proton and the gauge boson and between the proton and the neutron (Sirlin, 1967, Fig. 3).

[13] Even though they have been derived for neutron beta decay, they remain formally identical for other reactions because they are related by crossing symmetry under which β is left invariant.

[14] This amounts to including some radiative corrections which are higher order in $\alpha_{\rm FS}$.

proton and the electron, and since this is accounted for by the Fermi function, its Coulomb part is subtracted so as to avoid double counting.

The non-relativistic Fermi function is

$$F(E) \equiv \frac{y}{1-\mathrm{e}^{-y}}\,, \qquad y \equiv \frac{2\pi\alpha_{\rm FS}}{\beta} \quad \beta = \frac{p}{E}\,. \tag{99}$$

The relativistic Fermi function is given by (Ivanov *et al.*, 2013, Eq. 5)

$$F(E) \equiv \frac{4\left(1+\frac{\gamma}{2}\right)(2r_p m_e\beta)^{2\gamma}}{\Gamma^2(3+2\gamma)}\frac{\mathrm{e}^{\pi\alpha_{\rm FS}/\beta}}{(1-\beta^2)^{\gamma}} \times\left|\Gamma\left(1+\gamma+\mathrm{i}\frac{\alpha_{\rm FS}}{\beta}\right)\right|^2 \tag{100}$$

where $\gamma \equiv \sqrt{1-\alpha_{\rm FS}^2}-1$ and r_p is the proton radius. In practice the non-relativistic function is enough as long as we do not focus on a precision on $Y_{\rm P}^{(4)}$ better than unity. The modification on light elements yields is evaluated in § V.C and we find $\Delta Y_{\rm P}^{(4)} \simeq 0.3$ when using the relativistic Fermi function (see also Smith and Fuller (2010) which reports $\Delta Y_{\rm P}^{(4)} \simeq 0.4$). In this work we use the relativistic Fermi function whenever it is not specified differently. The relative difference between the two Fermi functions is plotted in Fig. 15 and it remains smaller than 0.06%.

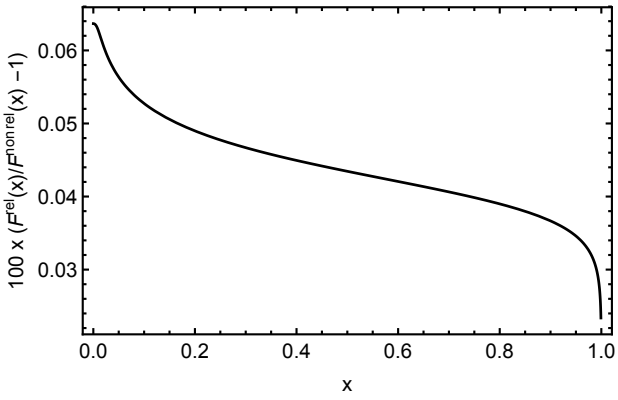

FIG. 15 Relative difference between the relativistic and the non-relativistic Fermi function.

Considering the contributions of Coulomb and other radiative corrections, the Born rates are modified as

$$\Gamma_{n\to p}^{\rm RC0} = K\int_0^\infty p^2{\rm d}p[\mathcal{F}_+(E)R(E,|\Delta-E|)\chi_+(E) +\mathcal{F}_+(-E)R(E,\Delta+E)\chi_+(-E)]\,. \tag{101}$$

The Coulomb corrections occur only if both the electron and the proton are either in the initial or the final state. We have thus defined the compact notation

$$\mathcal{F}_\pm(x) = \begin{cases} F(|x|) & \text{if} \quad \pm x > 0 \\ 1 & \text{if} \quad \pm x \le 0\,, \end{cases} \tag{102}$$

which ensures that this is the case.

The factor $R(.,.)$ takes into account pure radiative corrections and bremsstrahlung (but only in the form of neutron beta decay in vacuum as evoked above) and is of the form

$$R(E,k_{\rm max}) \equiv 1+\frac{\alpha_{\rm FS}}{2\pi}\mathcal{C}\left(E,k_{\rm max}\right)\,. \tag{103}$$

The function $\mathcal{C}$ is given in Eq. (B30). However we find it better to use the most recent form (B35) for the radiative correction $R(E,k_{\rm kmax})$ which amounts to resumming higher order corrections, since it is more accurate (Czarnecki *et al.*, 2004; Esposito *et al.*, 1999). We show in § V.C that it modifies the ^{4}He production by $\Delta Y_{\rm P}^{(4)} \simeq 0.2$.

The rate for protons is obtained by the replacement $\Delta \to -\Delta$ in (101), that is from $\chi_+ \to \chi_-$, together with the replacement $\mathcal{F}_+ \to \mathcal{F}_-$ to ensure that the Fermi function appears when the proton and the electron are on the same side. Hence it is given by

$$\Gamma_{p\to n}^{\rm RC0} = K\int_0^\infty p^2{\rm d}p[\mathcal{F}_-(E)R(E,E+\Delta)\chi_-(E) +\mathcal{F}_-(-E)R(E,|E-\Delta|)\chi_-(-E)]\,. \tag{104}$$

Given our choice to take into account the bremsstrahlung corrections of neutron beta decay for all processes and our choice for the maximum energy of emitted photons $k_{\rm max}$, then by construction the detailed balance property (86) is preserved using again the property (85), that is we get by construction

$$\Gamma_{p\to n}^{\rm RC0} = \mathrm{e}^{-\Delta/T}\Gamma_{n\to p}^{\rm RC0}\,. \tag{105}$$

The relative variations of the weak rates from radiative corrections are plotted in Fig. 16.

The radiative corrections also affect the free decay rate of neutrons and thus the value of λ_0 which is increased to

$$\lambda_0^{\rm RC0} \equiv m_e^{-5}\int_0^{\sqrt{\Delta^2-m_e^2}} F(E)R(E,E_\nu)p^2E_\nu^2{\rm d}p \simeq 1.75767\,, \tag{106}$$

with $E_\nu = \Delta - E$.

2. Bremsstrahlung corrections

It was argued in Brown and Sawyer (2001) that the detailed balance relation (86) should hold even including radiative corrections at order $\alpha_{\rm FS}$, as long as we work in the infinite nucleon mass approximation. Hence the derivation of radiative corrections due to interactions with the surrounding bath of particles, which are usually called finite-temperature corrections, must satisfy this detailed balance relation. These corrections correspond to real photon processes which are the absorption diagram 14b

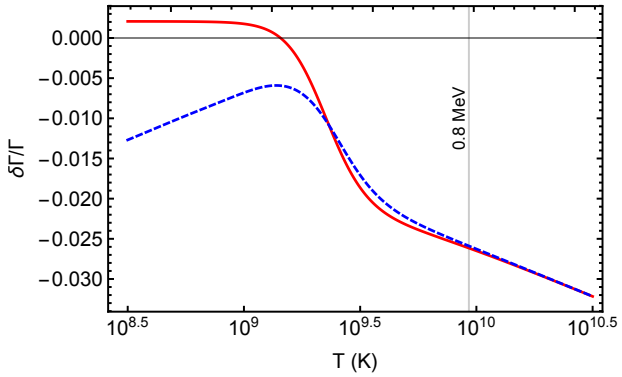

FIG. 16 $\delta\Gamma/\Gamma$ due to Coulomb and null-temperature radiative corrections. *Red continuous line* : $n \to p$. *Blue dashed line* : $p \to n$. The relative variations are equal at high temperature, when $T_\nu \simeq T$, and the detailed balance is still satisfied when including these corrections. This plot reproduces Lopez and Turner (1999, Fig. 8).

together with the stimulated emission part of 14a, and to mass shift effects illustrated by the diagrams 17.

The full computation of the finite temperature radiative corrections was carefully carried out in Brown and Sawyer (2001), following the guideline of detailed balance and with a detailed discussion on misconceptions in earlier efforts (Cambier *et al.*, 1982; Chapman, 1997; Dicus *et al.*, 1982; Esposito *et al.*, 2000a; Sawyer, 1996) concerning the so called wave-function renormalization. However the authors of Brown and Sawyer (2001) reported that when combining their results with the null-temperature radiative corrections discussed in the previous section, the rates failed to satisfy the detailed balance relation. We argue that this is because bremsstrahlung was inconsistently taken into account. As long as we take into account only null-temperature radiative corrections, it is reasonable to consider that the bremsstrahlung effects are those of the neutron beta decay for all reactions, so as to maintain the detailed balance relation (86). This is what has been done in the previous section.

Strictly speaking it is a mistake because part of the null-temperature corrections are left out. However it is the most reasonable procedure if one ignores the full details of the finite-temperature radiative corrections. Here since we take into account the interactions with the bath of photons and electrons in the finite temperature radiative corrections, we must also correct for this ad-hoc and incorrect treatment of bremsstrahlung in the previous section. The details are reported in appendix B.7 and the result is that we need to add the corrections

$$\delta\Gamma^{\rm BS}_{n\to p} = \frac{\alpha_{\rm FS}K}{2\pi}\int_{m_e}^{\infty} {\rm d}E\,\big[g(-E)\mathcal{F}_+(E)\gamma^{\rm BS}_{n\to p+e} + g(E)\mathcal{F}_+(-E)\gamma^{\rm BS}_{n+e\to p}\big] \quad (107a)$$

$$\delta\Gamma^{\rm BS}_{p\to n} = \frac{\alpha_{\rm FS}K}{2\pi}\int_{m_e}^{\infty} {\rm d}E\,\big[g(-E)\mathcal{F}_-(E)\gamma^{\rm BS}_{p\to n+e} + g(E)\mathcal{F}_-(-E)\gamma^{\rm BS}_{p+e\to n}\big]\,, \quad (107b)$$

with the definitions (B48-B49). Note that we have added the Fermi factor contribution for consistency with the rest of the radiative corrections. Their temperature dependence is plotted in Fig. 18. Even though these BS corrections correspond to null temperature radiative corrections, unless specified we include them as part of the finite temperature radiative corrections discussed in the next section, since they must be added only to maintain consistently the detailed balance relation when finite temperature radiative corrections are included. We report in § V.C that these BS corrections are responsible for a non-negligible modification of ^{4}He production which is $\Delta Y_{\rm P}^{(4)} \simeq -3.1$.

F. Finite temperature radiative corrections

The finite-temperature corrections can be separated in three parts. Using a notation similar to Brown and Sawyer (2001), these three contributions are noted

$$\Gamma^{T}_{n\to p} \equiv \Gamma^{\gamma,T}_{n\to p} + \Gamma^{\Delta E,T}_{n\to p} + \Gamma^{ep+ee,T}_{n\to p}\,, \quad (108)$$

and similar notation for the $p \to n$ processes.

The first part is the stimulated emission and absorption of real photons (Brown and Sawyer, 2001, Eq. 5.9), see Fig. 14. When combined with a contribution coming from the diagram 17a it gives

$$\Gamma^{\gamma,T}_{n\to p} = \frac{\alpha_{\rm FS}K}{2\pi}\int_0^\infty \frac{{\rm d}k}{k}\int_{m_e}^{\infty}{\rm d}E\,\times \quad (109a)$$
$$\big\{A(E,k)\,\big[g(-E)\widetilde{\chi}^A_+(E,k) + g(E)\widetilde{\chi}^A_+(-E,k)\big] - kB(E,k)\,\big[g(-E)\widetilde{\chi}^B_+(E,k) + g(E)\widetilde{\chi}^B_+(-E,k)\big]\big\}$$

$$\Gamma^{\gamma,T}_{p\to n} = \Gamma^{\gamma,T}_{n\to p}\big|_{\widetilde{\chi}^{A/B}_+\to\widetilde{\chi}^{A/B}_-} \quad (109b)$$

with

$$\widetilde{\chi}^A_\pm(E,k) \equiv \widetilde{\chi}_\pm(E-k) + \widetilde{\chi}_\pm(E+k) - 2\widetilde{\chi}_\pm(E) \quad (110)$$

$$\widetilde{\chi}^B_\pm(E,k) \equiv \pm\,[\widetilde{\chi}_\pm(E-k) - \widetilde{\chi}_\pm(E+k)]\,. \quad (111)$$

It does not satisfy the detailed balance relation. However when the bremsstrahlung corrections (107) are added the sum does satisfy it. This crucial point is detailed in App. B.7.c.

The second part of finite temperature radiative corrections is made of the electron energy shift (Brown and

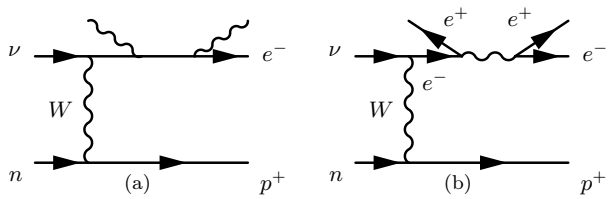

FIG. 17 Feynman diagram interpretation of finite temperature radiative corrections, that is of the effect of the interactions with the surrounding plasma.

Sawyer, 2001, Eq. 5.13), and it originates partly from the diagrams 17. It reads

$$\Gamma^{\Delta E,T}_{n\to p} = -\frac{2\alpha_{\rm FS}K}{\pi}\int \mathrm{d}p\,[\chi_+(E)+\chi_+(-E)] \qquad (112a)$$
$$\times\left[\frac{\pi^2T^2}{6}+\int_{m_e}^{\infty}\mathrm{d}E'p'g(E')\left(1-\frac{m_e^2}{E'^2-E^2}\right)\right]$$
$$\Gamma^{\Delta E,T}_{p\to n} = \Gamma^{\Delta E,T}_{n\to p}\big|_{\chi_+\to\chi_-}\,, \qquad (112b)$$

where $E'\equiv\sqrt{p'^2+m_e^2}$.

The third and last part is made of proton-electron interactions, which is a finite temperature correction to the diagram 13c, and electron self-energy and wave-function renormalization (Brown and Sawyer, 2001, Eq. 5.10), which come partly from the diagram 17b. It reads

$$\Gamma^{ep+ee,T}_{n\to p} = \frac{\alpha_{\rm FS}K}{2\pi}\int_{m_e}^{\infty}\mathrm{d}E\,[\chi_+(E)+\chi_+(-E)]$$
$$\times\int_{m_e}^{\infty}\mathrm{d}E'g(E')\frac{E}{E'^2-E^2}$$
$$\times\left\{8pp'-(E'^2+E^2)\ln\left(\frac{p+p'}{p-p'}\right)^2\right. \qquad (113a)$$
$$\left.-\frac{E'}{E}(E'^2+E^2)\ln\left[\frac{(EE'+pp')^2-m_e^4}{(EE'-pp')^2-m_e^4}\right]\right\}$$
$$\Gamma^{ep+ee,T}_{p\to n} = \Gamma^{ep+ee,T}_{n\to p}\big|_{\chi_+\to\chi_-}\,. \qquad (113b)$$

The second and third contributions [Eqs. (112) and (113)] satisfy manifestly the detailed balance relation thanks to the property (85). Furthermore, they can be recast in a form which does not involve principal parts of integrals and are thus better suited for numerical integration (Brown and Sawyer, 2001, Eq 5.15)]. We report it in App. B.8.

The modification of the rates from these finite temperature corrections is plotted in Fig. 18. We also show the BS corrections and the sum of the two. By construction for the sum, it can be checked that whenever the neutrinos have the same temperature, that is for $T > 10^{10}\,\mathrm{K}$, the relative variation of the rates are equal and the detailed balance property (86) is preserved.

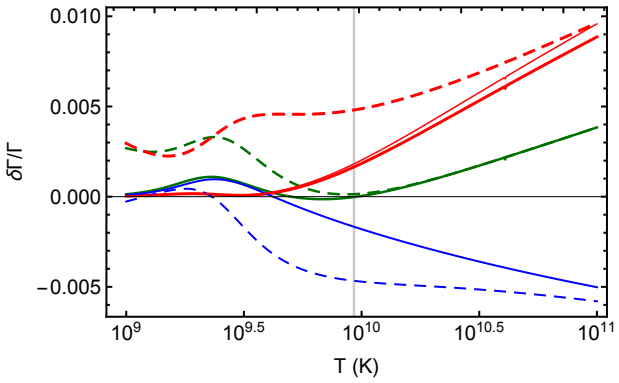

FIG. 18 $\delta\Gamma/\Gamma$ from finite-temperature radiative corrections. *Continuous line* : $n\to p$. *Dashed line* : $p\to n$. The red lines are the corrections of Brown and Sawyer (2001) in very good agreement with their Fig. 2. In the thin continuous red line, the $n+\bar\nu+e^+\to p+\gamma$ has been added to the $n\to p$ corrections, as advocated in Brown and Sawyer (2001) and we check that it results in a very small modification, as also found in their Fig. 3, and most notably it is insufficient to satisfy detailed balance. The blue lines are the Bremsstrahlung corrections (107). Finally the green lines are the total corrections, that is the corrections of (Brown and Sawyer, 2001) with all bremsstrahlung corrections added. We check that above $T > 10^{10}$K, that is when $T_\nu = T$, the relative variations of the total corrections are equal, implying that the detailed balance is satisfied.

G. Finite nucleon mass corrections

It is not fully correct to consider that nucleons have an infinite mass. Indeed, the typical energy transfer in weak-interactions to electrons and neutrinos is of the order of the mass gap $\Delta \simeq 1.29\,\mathrm{MeV}$, which is 1.4×10^{-3} smaller than the nucleon mass. It corresponds to a temperature of 1.5×10^{10}K which is not much larger than the freeze-out temperature. In the infinite nucleon mass approximation, we have thus neglected factors of the type E_ν/m_N, E_e/m_N or Δ/m_N (where m_N is the average nucleon mass $m_N\equiv(m_p+m_n)/2$) which represent order 10^{-3} corrections with respect to the leading one around 10^{10}K and even larger corrections at higher temperature. Our method consists in expanding the full reaction rate in power of a small parameter $\epsilon\equiv T/m_N$. Terms of the type E_ν/m_N or E_e/m_N are obviously of order ϵ and terms of the type Δ/m_N are also treated as being of order ϵ. Our implementation of the finite mass corrections consists in including all the terms up to order ϵ, but neglecting terms of order ϵ^2. This means that we neglect terms whose importance is of order 10^{-6} which is justified given our goal in precision.

If we ignore radiative corrections at null temperature,

these corrections take the form

$$\delta\Gamma^{\rm FM}_{n\to p} = K\int_0^\infty p^2{\rm d}p \times [\chi^{\rm FM}_+(E,g_A)+\chi^{\rm FM}_+(-E,g_A)] \quad (114a)$$

$$\delta\Gamma^{\rm FM}_{p\to n} = K\int_0^\infty p^2{\rm d}p \times [\chi^{\rm FM}_-(E,-g_A)+\chi^{\rm FM}_-(-E,-g_A)]\,, \quad (114b)$$

and the functions $\chi^{\rm FM}_\pm$ are reported in App. B.3. However since finite mass effects and radiative corrections can be rather important, they cannot be added linearly and one should also include radiative corrections inside finite nucleon mass corrections[15]. Hence the corrections to the rates are

$$\delta\Gamma^{\rm RC+FM}_{n\to p} = K\int_0^\infty p^2{\rm d}p \times [\mathcal{F}_+(E)R(E,|E-\Delta|)\chi^{\rm FM}_+(E,g_A) + \mathcal{F}_+(-E)R(E,E+\Delta)\chi^{\rm FM}_+(-E,g_A)] \quad (115a)$$

$$\delta\Gamma^{\rm RC+FM}_{p\to n} = K\int_0^\infty p^2{\rm d}p \times [\mathcal{F}_-(E)R(E,E+\Delta)\chi^{\rm FM}_-(E,-g_A) + \mathcal{F}_-(-E)R(E,|E-\Delta|)\chi^{\rm FM}_-(-E,-g_A)]\,. \quad (115b)$$

The expression for $\chi^{\rm FM}_\pm(E,g_A)$ is given in App. B.3. The relative modifications to the rates are depicted in Fig. 19. It is not obvious that the finite nucleon mass corrections preserve the detailed balance relation. In fact when including these corrections the detailed balance ratio between neutrons and protons is given by Eq. (A15). Since this must also be the ratio $\Gamma_{p\to n}/\Gamma_{n\to p}$ we define α following Lopez *et al.* (1997) as

$$\frac{\overline{\Gamma}_{p\to n}+\delta\Gamma^{\rm FM}_{p\to n}}{\overline{\Gamma}_{n\to p}+\delta\Gamma^{\rm FM}_{n\to p}} \equiv {\rm e}^{-\frac{\Delta}{T}}\left[1+(1+\alpha)\frac{3\Delta}{2m_N}\right]. \quad (116)$$

α characterizes the deviation from the detailed balance equality and must vanish if detailed balance with finite mass corrections is satisfied. It is plotted in Fig. 20. We observe that for $T<m_e$ deviations from detailed balance occur because the neutrino temperature is not equal to the plasma temperature. Hence we have also plotted α with $T_\nu = T$ artificially enforced. At low temperature, that is below $T=m_e$, detailed balance is very well satisfied because the parameter $\epsilon = T/m_N$ is small. At higher temperatures we see deviations, and this comes from the fact that we considered only corrections which are first order in ϵ.

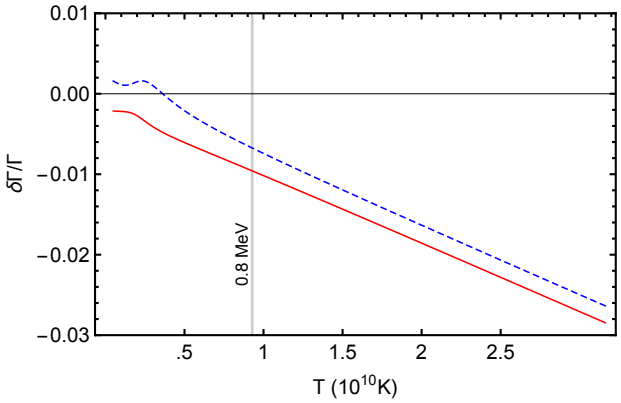

FIG. 19 $|\delta\Gamma/\bar{\Gamma}|$ from finite nucleon mass effects. *Red continuous line* : $n\to p$. *Blue dashed line* : $p\to n$. This plot is to be compared with Lopez and Turner (1999, Fig. 9).

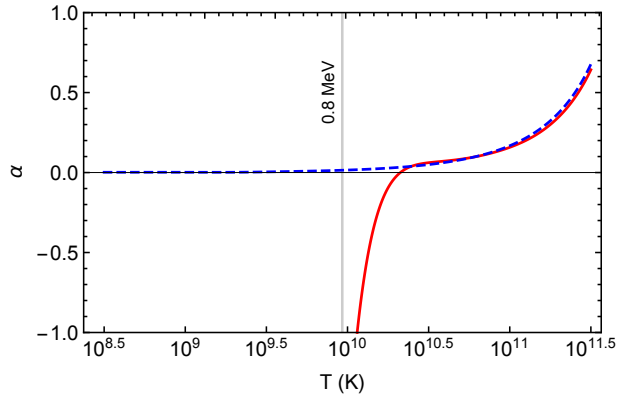

FIG. 20 α defined in Eq. (116). *Red continuous line* : With T_ν differing from T when electron-positron annihilations occur. *Blue dashed line* : With $T_\nu = T$ artificially enforced. This plot is to be compared with Lopez *et al.* (1997, Fig. 4).

Finally, the total neutron rate at null temperature is

$$\Gamma_{n\to p}(T=0) = \Gamma^{\rm RC0}_{n\to p}(T=0)+\delta\Gamma^{\rm FM}_{n\to p}(T=0)\,, \quad (117)$$

that is there is a correction to λ_0 due to finite nucleon mass effects. If Eq. (114) is used, this is

$$\delta\lambda^{\rm FM}_0 = m_e^{-5}\int_0^{\sqrt{\Delta^2-m_e^2}} p^2{\rm d}p\ \chi^{\rm FM}_+(E,g_A)\big|_{T=0} \quad (118)$$

combined with Eq. (B26), and we obtain $\delta\lambda^{\rm FM}_0 \simeq -3.3828\times10^{-3}$, that is $\delta\lambda^{\rm FM}_0/\bar{\lambda}_0 \simeq -0.002068$. This is in agreement with the result $\delta\lambda^{\rm FM}_0/\bar{\lambda}_0 \simeq -0.00206$ found in Lopez *et al.* (1997) with an exact method to compute the finite nucleon mass effects. We recomputed this ratio with the method of Lopez *et al.* (1997, Eq. 20) and found it is more precisely given by -0.0020637. The tiny difference with our value $\delta\lambda^{\rm FM}_0/\bar{\lambda}_0$ is only due to the fact

[15] In principle one should rederive all radiative corrections including consistently all finite nucleon mass effects. This is absent from the literature, and is certainly a daunting task. Our procedure consists in postulating that the multiplicative factor introduced by radiative corrections also multiplies the finite nucleon mass correction as in Cooper *et al.* (2010); Czarnecki *et al.* (2004)

that we kept only first order finite nucleon mass corrections, that is we kept terms of order ϵ, and ignored terms of higher order ϵ^2. Furthermore, if we also include radiative corrections, that is if we use $\delta\Gamma^{\rm RC+FM}_{n\to p}$ instead of $\delta\Gamma^{\rm FM}_{n\to p}$ in Eq. (117), hence corresponding to an extra factor $F(E)R(E,\Delta-E)$ in the integrand of Eq. (118), we get $\delta\lambda_0^{\rm FM}\simeq -3.6201\times10^{-3}$. These values are summarized in table II.

H. Weak magnetism

We show in B.4 that the effect of weak magnetism is exactly similar to the finite mass correction which arises from the coupling between the axial current and the vector current. This has been noticed earlier by Seckel (1993). That is, it brings corrections which are exactly of the same type as those proportional to g_A in Eq. (73). The weak magnetism corrections amount to a simple redefinition of the constant factors (B11) as

$$c_{LL} \equiv \frac{(1+g_A)^2}{4} + f_{\rm wm} g_A \tag{119a}$$

$$c_{RR} \equiv \frac{(1-g_A)^2}{4} - f_{\rm wm} g_A \tag{119b}$$

$$c_{LR} \equiv \frac{g_A^2-1}{4} \tag{119c}$$

when computing the finite nucleon mass corrections. The associated couplings (B24) must be replaced accordingly.

The weak magnetism, if considered independently of radiative corrections, induces no modification of λ_0, at least up to the order ϵ of our finite nucleon mass expansion, as explained in appendix § B.4. However when this is combined with the radiative corrections, this brings a residual increase to $\delta\lambda_0^{\rm FM}\simeq -3.6333\times10^{-3}$. Summing this value of the finite nucleon mass corrections (which includes weak-magnetism and which is coupled to radiative corrections), to the radiative corrections themselves (106) leads to

$$\lambda_0^{\rm RC+FM} = \lambda_0^{\rm RC} + \delta\lambda_0^{\rm FM} \simeq 1.75474\,. \tag{120}$$

This is to be compared with Cooper *et al.* (2010) where it is reported $\lambda_0 \simeq 1.03887\times1.6887\simeq 1.75434$, a modest 0.023% smaller than the value (120). This close agreement can also be seen by noting that $(\hbar 2\pi^3)/(m_e^5c^{10}G_F^2\lambda_0^{\rm RC+FM}) \simeq 4907.4\,$s, which is very close to the value 4908 s given by Czarnecki *et al.* (2004, Eq. 17) or the refined value 4908.7s of Marciano and Sirlin (2006, Eq. 18).

I. Effect of incomplete neutrino decoupling

Neutrino heating also induces modification of the weak rates. In our thermal approximation of the incomplete neutrino decoupling (see § II.F), this is taken into account by putting the effective neutrino temperature defined in Eq. (64) in all expressions for the weak rates.

TABLE II Value of $\delta\lambda_0^{\rm FM}$ depending on the effects considered.

RC	FM	WM	FM+WM
No	-3.3828×10^{-3}	0	-3.3828×10^{-3}
Yes	-3.6201×10^{-3}	-0.0132×10^{-3}	-3.6333×10^{-3}

This amounts to assuming that all neutrinos receive the same share of the heating and ignoring the spectral distortions. We postpone a more detailed discussion on the effect of incomplete neutrino decoupling on the weak rates and thus the ^{4}He production in § V.C.5. Briefly, the most notable effect of incomplete neutrino decoupling is to affect the time-temperature relation, and this is also the case from QED corrections in the plasma but the effect is much smaller. Indeed, since for a given plasma temperature, neutrino heating induces an increase of the total energy density, the Hubble rate is increased and so is the rate of variation $\mathrm{d}T/\mathrm{d}t$. In practice this means that the Universe is younger when nucleosynthesis starts around $T_{\rm Nuc}=0.078$MeV and the neutron beta decay results in a lower loss of neutrons, and thus a higher production of ^{4}He at the end of the BBN. This is the *clock effect* explained in Dodelson and Turner (1992); Fields *et al.* (1993).

J. Total correction to the weak rates

The total weak reaction rates are given by summing the various effects [Eqs. (101), (108), (107) and (115)], that is

$$\Gamma_{n\to p} = \Gamma^{\rm RC0}_{n\to p} + \Gamma^{T}_{n\to p} + \delta\Gamma^{\rm BS}_{n\to p} + \delta\Gamma^{\rm FM}_{n\to p}\,, \tag{121}$$

and a similar sum for $p\to n$ processes. The constant K involved in all contributions is then calibrated on neutron beta decay from λ_0 given by Eq. (120) replaced in Eq. (91). We recall that when including weak-magnetism in finite nucleon mass effects, that is in Eqs. (115), one must use the constants (119) in (B24), so as to evaluate the $\chi^{\rm FM}_{\pm}$ given by Eqs. (B23).

The size of all corrections relative to the Born approximation is plotted in Fig. 21. Around $T\simeq 3.3\times10^9$K for which the neutron are only subject to beta decay, we find $\delta\Gamma_{n\to p}/\bar\Gamma_{n\to p}\simeq -0.023$. From the rule (7) this should lead to $\Delta Y_{\rm P}^{(4)}\simeq 42$, quite in nice agreement with the total correction $\Delta Y_{\rm P}^{(4)}\simeq 44.7$ that we report in § V.C.

IV. NUCLEOSYNTHESIS

Once the weak interaction rates are determined and computed with great precision, it is possible to solve for the nucleosynthesis by adding the effect of nuclear reactions which form nuclei. Hence we need to build the

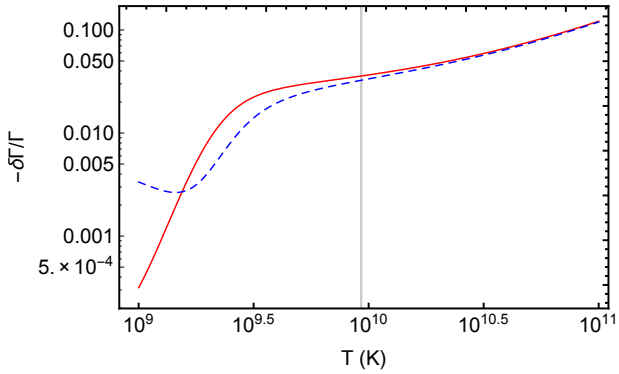

FIG. 21 Total relative rate corrections, including all the effects discussed, $-\delta\Gamma/\overline{\Gamma}$. $n \to p$ in red continuous line and $p \to n$ in blue dashed line. The vertical line corresponds to $T_F = 0.8$MeV.

differential system which rules the evolution of all (neutrons, protons and main isotopes) abundances. We describe how this is performed in this section and turn to report and discuss the numerical results obtained for final abundances in § V.

We remind that, for a general reaction of the type

$$A + b \to C + d \tag{122}$$

the conventional notation in experimental nuclear physics is $A(b,d)C$ to keep in mind that A is the target nucleus at rest, b is the projectile from the beam, d is the outgoing, detected, particle and C is left generally undetected, possibly not escaping the target. Hence, usually, but not always, A and C are the heaviest nuclei. The same notation is used in theoretical nuclear physics, regardless of the experimental details.

A. Thermonuclear reaction rates

We summarize here a few results, to be used in this review, and refer to (Angulo *et al.*, 1999; Clayton, 1983; Iliadis, 2007; Longland *et al.*, 2010) for a detailed treatment. It is assumed that the medium is in local thermodynamical equilibrium so that the distribution of ion velocities/energies follows a Maxwell–Boltzmann distribution (see § A.3),

$$\phi_{\rm MB}(v)v\mathrm{d}v = \sqrt{\frac{8}{\pi m}}\frac{1}{(k_BT)^{3/2}}e^{-\frac{E}{k_BT}}E\mathrm{d}E. \tag{123}$$

It is understood that for the distribution of relative velocities between two reacting nuclei, m is their reduced mass. In such conditions, one defines the thermonuclear reaction rate by

$$N_A\langle\sigma v\rangle = N_A\int_0^\infty \sigma(v)\phi_{\rm MB}(v)v dv \tag{124}$$

in $\mathrm{cm^3 s^{-1} mole^{-1}}$ units where N_A is Avogadro's number ($\mathrm{mole^{-1}}$). For reactions involving charged particles, since the kinetic energies are below the Coulomb barrier, the energy dependence of the cross section is dominated by the tuneling effect through the barrier. The Coulomb plus centrifugal barrier penetration probability is given by

$$P_\ell(E) = \frac{kR}{F_\ell^2(\eta,kR)+G_\ell^2(\eta,kR)} \tag{125}$$

where F_ℓ and G_ℓ are the Coulomb functions (Fröberg, 1955), $k = \sqrt{2mE}/\hbar$ is the wave number, ℓ the orbital angular momentum and

$$\eta \equiv \frac{Z_1Z_2e^2}{\hbar v} \tag{126}$$

the Sommerfeld parameter. To account for this strong energy dependency of the cross section, it is convenient to introduce the astrophysical S–factor:

$$\sigma(E) \equiv \frac{S(E)}{E}\exp(-2\pi\eta) \tag{127}$$

which, in the absence of resonances removes most of the energy dependence. A resonance, associated to a nuclear level in the compound nucleus formed by the fusion of the projectile and target nuclei, induces a strong but localized variation of the S–factor. Hence, the presence of a resonance can increase by several orders of magnitude a reaction rate.

B. General form

The evolution of abundances, defined in Eq. (1), is deduced from the evolution of number densities found from Eq. (10). Since both nuclear and weak reactions preserve the number of baryons, we obtain

$$\frac{\mathrm{d}n_\mathrm{b}}{\mathrm{d}t} + 3Hn_\mathrm{b} = 0, \tag{128}$$

that is baryon volume density is only affected by dilution and $n_\mathrm{b} \propto 1/a^3$.

For a given isotope i, the evolution of the volume density depends on the reaction rates in which it is involved. It is of the form

$$\frac{\mathrm{d}n_i}{\mathrm{d}t} + 3Hn_i = \mathcal{J}_i\,, \tag{129}$$

where $\mathcal{J}_i$ is the net rate of evolution of number density due to all nuclear reactions. A decay of species i ($i \to \dots$) and a decay reaction in which species i is the end product ($j \to i + \dots$) contribute as

$$\mathcal{J}_i \supset -n_i\Gamma_{i\,\to\dots} + n_j\Gamma_{j\to i+\dots} \tag{130}$$

where the Γ are the decay rates (usually given in $\mathrm{s^{-1}}$). A two-body reaction of the type $i + j \leftrightarrow k + l$ contributes instead as

$$\mathcal{J}_i \supset n_kn_l\gamma_{kl\to ij} - n_in_j\gamma_{ij\to kl}\,. \tag{131}$$

with

$$\gamma_{ij\to kl} \equiv \langle \sigma v \rangle_{ij\to kl} \,. \tag{132}$$

Since both the individual n_i and the total n_b are affected similarly by expansion, it proves much simpler to study directly the evolution of abundances defined as [16]

$$Y_i \equiv \frac{n_i}{n_\mathrm{b}} \,, \tag{133}$$

since one finds

$$\dot{Y}_i = C[Y_i] \,, \qquad C[Y_i] \equiv \frac{\mathcal{J}_i}{n_\mathrm{b}} \,. \tag{134}$$

Obviously the decay reactions considered in Eq. (130) contribute as

$$C[Y_i] \supset -Y_i \Gamma_{i\,\to\ldots} + Y_j \Gamma_{j\to i+\ldots} \,. \tag{135}$$

However two-body reactions contribute as

$$C[Y_i] \supset Y_k Y_l \Gamma_{kl\to ij} - Y_i Y_j \Gamma_{ij\to kl} \,, \tag{136}$$

where we related the rates for abundances to those of number densities through

$$\Gamma_{ij\to kl} \equiv n_\mathrm{b} \gamma_{ij\to kl} \,. \tag{137}$$

Eq. (131) is straightforwardly generalized to reactions with more bodies. In full generality, and without restricting to decay reactions or two-body reactions, the evolution of abundances takes the form (Fowler *et al.*, 1967; Wagoner, 1969)

$$\dot{Y}_{i_1} = \sum_{i_2\ldots i_p, j_1\ldots j_q} N_{i_1} \left(\Gamma_{j_1\ldots j_q \to i_1\ldots i_p} \frac{Y_{j_1}^{N_{j_1}} \ldots Y_{j_q}^{N_{j_q}}}{N_{j_1}! \ldots N_{j_q}!} - \Gamma_{i_1\ldots i_p \to j_1\ldots j_q} \frac{Y_{i_1}^{N_{i_1}} \ldots Y_{i_p}^{N_{i_p}}}{N_{i_1}! \ldots N_{i_p}!} \right) \,, \tag{138}$$

where N_i is the stoichiometric coefficient of species i in the reaction and with the relation between abundance rates and number density rates given by

$$\Gamma_{i_1\ldots i_p \to j_1\ldots j_q} = n_\mathrm{b}^{(N_{i_1}+\cdots+N_{i_p})-1} \gamma_{i_1\ldots i_p \to j_1\ldots j_q} \,. \tag{139}$$

Note that for a decay reaction $\Gamma_{i\to\ldots} = \gamma_{i\to\ldots}$.

In practice the reaction rates for many-body reactions are given as tables for the quantities $N_A^{(N_{i_1}+\cdots+N_{i_p})-1} \gamma_{i_1\ldots i_p \to j_1\ldots j_q}$, as detailed in App. C on the steps required to deduce them from the nuclear physics tables. Furthermore the rates are only given for forward reactions. Indeed, since when there is nuclear statistical equilibrium (NSE) reverse reactions should balance with forward reactions, we can always relate the reverse reactions to the forward reactions from the detailed balance relation

$$\frac{\gamma_{i_1\ldots i_p \to j_1\ldots j_q}}{\gamma_{j_1\ldots j_q \to i_1\ldots i_p}} = \frac{N_{i_1}! \ldots N_{i_p}!}{N_{j_1}! \ldots N_{j_q}!} \left[\frac{n_{j_1}^{N_{j_1}} \ldots n_{j_q}^{N_{j_q}}}{n_{i_1}^{N_{i_1}} \ldots n_{i_p}^{N_{i_p}}} \right]^\mathrm{NSE} \tag{140}$$

where the NSE densities are given in Eq. (A22). Since nuclear reactions in many-body reactions do not change the nature of nucleons[17], that is they conserve the number of protons and neutrons, then using the relation (139) the reverse reactions are related to the forward reactions by

$$\begin{aligned} \frac{\gamma_{j_1\ldots j_q \to i_1\ldots i_p}}{\gamma_{i_1\ldots i_p \to j_1\ldots j_q}} &= \frac{\Pi_{i=i_1\ldots i_p} \frac{1}{N_i!} \left[g_i \left(\frac{m_i T}{2\pi} \right)^{3/2} \right]^{N_i}}{\Pi_{j=j_1\ldots j_q} \frac{1}{N_j!} \left[g_j \left(\frac{m_j T}{2\pi} \right)^{3/2} \right]^{N_j}} \\ &\times \exp\left(\frac{\sum_{j=1}^q m_j - \sum_{i=1}^p m_i}{T} \right) . \end{aligned} \tag{141}$$

We check easily that we recover the particular cases of Fowler *et al.* (1967, Eqs. 15, 18, 25). Hence the relation between forward and reverse reactions is of the form

$$\frac{\gamma_{j_1\ldots j_q \to i_1\ldots i_p}}{\gamma_{i_1\ldots i_p \to j_1\ldots j_q}} = \alpha \left(\frac{T}{10^9\mathrm{K}} \right)^\beta \exp\left(\frac{\gamma \times 10^9\mathrm{K}}{T} \right) \,, \tag{142}$$

which depends only on 3 constants. In practice, for a given reaction, the forward reaction rate is tabulated for various values of T or is approximated by an analytic fit, and the constants (α, β, γ) needed to obtain the reverse reaction rate are also computed once for all from Eq. (141) using the tabulated masses and spins of isotopes [we use the table `nubase2016.asc` described in Audi *et al.* (2017)].

C. Nuclear network and reaction rates uncertainties

The nuclear reaction network used here has been fully described in Coc *et al.* (2012): it includes 59 nuclides

[17] This is not the case for decay reactions but for these we neglect the reverse reactions.

from neutron to ^{23}Na (see table III), linked by 391 reactions involving neutrons, protons, deuterium, tritium (^{3}H), ^{3}He and α–particles induced reactions, and 33 β-decay processes. The complete list of reactions can be found in Table 4 of Coc *et al.* (2012), together with the references for the values of the reaction rates. Each of these reactions is systematically supplemented ($ij \rightarrow kl$) by its reverse ($kl \rightarrow ij$) whose rate is obtained as described above, except for decay reactions whose rates are from Audi *et al.* (2017).

This network is adapted to the prediction of the primordial abundances of the light elements, but also to the calculation of the abundances of the ^{6}Li, ^{9}Be, ^{10}B, ^{11}B and CNO isotopes. As listed in Table 4 of Coc *et al.* (2012), reaction rates and their associated uncertainties were taken primarily from Angulo *et al.* (1999); Descouvemont *et al.* (2004); Iliadis *et al.* (2010); Xu *et al.* (2013) evaluations when available. For many reactions, in the absence of sufficient experimental data, the rates come from theory (TALYS code) (Goriely *et al.*, 2008). An extensive sensitivity study, performed by Coc *et al.* (2012), identified ten reactions that needed further analyses, and it was followed by their re–evaluations (shown in boldface in Table 4 of Coc *et al.* (2012)). Finally, out of these hundreds of reactions, the most important ones are displayed in Fig. 22. They were identified in sensitivity studies, i.e. (Coc and Vangioni, 2010; Cyburt, 2004; Nollett and Burles, 2000) for the light elements (^{4}He, D, ^{3}He and ^{7}Li) and Coc *et al.* (2012); Coc *et al.* (2014) for others and correspond to the main nuclear flow.

TABLE III Nuclides considered in the nuclear network.

Z \ N	0	1	2	3	4	5	6	7	8	9	10	11	12	13
0		n												
1	H	^{2}H	^{3}H											
2		^{3}He	^{4}He	^{5}He	^{6}He									
3				^{6}Li	^{7}Li	^{8}Li	^{9}Li							
4				^{7}Be	^{8}Be	^{9}Be	^{10}Be	^{11}Be	^{12}Be					
5				^{8}B	^{9}B	^{10}B	^{11}B	^{12}B	^{13}B	^{14}B	^{15}B			
6				^{9}C	^{10}C	^{11}C	^{12}C	^{13}C	^{14}C	^{15}C	^{16}C			
7						^{12}N	^{13}N	^{14}N	^{15}N	^{16}N	^{17}N			
8						^{13}O	^{14}O	^{15}O	^{16}O	^{17}O	^{18}O	^{19}O	^{20}O	
9									^{17}F	^{18}F	^{19}F	^{20}F		
10									^{18}Ne	^{19}Ne	^{20}Ne	^{21}Ne	^{22}Ne	^{23}Ne
11										^{20}Na	^{21}Na	^{22}Na	^{23}Na	

Experimental uncertainties on Y_P are due to the ^{1}H(n,γ)^{2}H, D(d,n)^{3}He and D(d,p)^{3}H reaction rates and to the neutron lifetime. For these three reactions, one finds (e.g. Coc *et al.*, 2015; Cyburt, 2004)

$$\Delta Y_P \approx (1.5 \times 10^{-3}) \frac{\Delta\langle\sigma v\rangle}{\langle\sigma v\rangle}, \qquad (143)$$

and $\Delta Y_P \approx 0.18 \Delta\tau_n/\tau_n$ from Eq. (7). Since the experimental uncertainties are of the order of 10^{-2} for the rates and 10^{-3} for the lifetime, they may all contribute to the error budget.

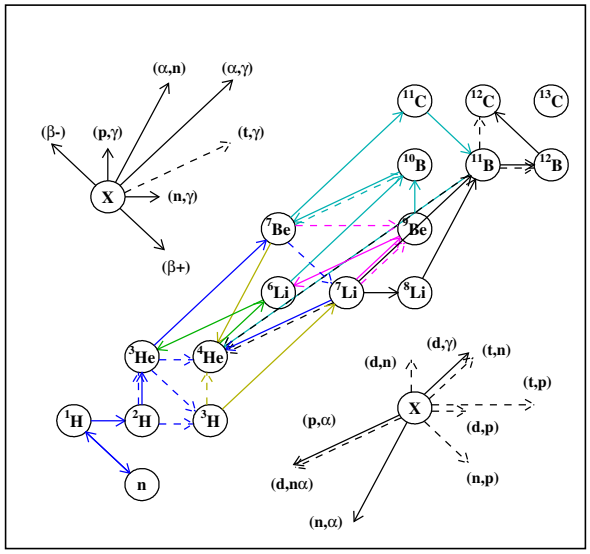

FIG. 22 Nuclear network of the most important reactions in BBN (out of the 424) up to^{7}Li (blue), including ^{6}Li (green), ^{10,11}B (light blue), ^{9}Be (pink) and up to CNO (black). The yellow arrows indicate the reactions that are now considered as unimportant.

There are basically two methods for the experimental determination of the neutron lifetime: detecting dying neutrons i.e. their decay rate ("beam experiments") or surviving neutrons after being left in a magnetic "bottle" for a certain time. Both methods produce slightly different results (see e.g. Fig. 8 in Young *et al.*, 2014). This is most probably due to different systematic uncertainties but it might also be real and be explained by an undetected decay into a dark sector (see e.g. Fornal and Grinstein, 2018). Note that in that case it would be the "bottle" results, corresponding to the surviving neutrons counting, that would be important for BBN. Hence, the value of the neutron lifetime has been revised several times by the Particle Data Group (PDG) from 885.7±0.8 s (Amsler *et al.*, 2008), used, e.g. in Coc and Vangioni (2010), to 879.4±0.6 s resulting from an average of "bottle" experiments (Czarnecki *et al.*, 2018), slightly below the current PDG average (Patrignani and Particle Data Group, 2016 and 2017 update) which is 880.2 ± 1.0 s. We use the average over post-2000 experiments, 879.5 ± 0.8 s (Serebrov *et al.*, 2017), which is extremely close to the average on bottle experiments, but with more conservative errors.

The cross section of the ^{1}H(n,γ)^{2}H reaction is obtained from calculations in the framework of Effective Field Theory whose results are estimated to be reliable to within 1% error (Ando *et al.*, 2006). Indeed, the few experimental information available for this cross section at BBN energies are in very good agreement with theory (see Fig. 1 in Coc (2013)).

The D(p,γ)^{3}He, D(d,n)^{3}He and D(d,p)^{3}H reactions are the main source of nuclear uncertainty for deuterium nucleosynthesis while the two last one may affect the error budget of $Y_{\rm P}$. The relative variations of D/H are related to the variation of these rates (see e.g. Coc and Vangioni, 2010) by

$$\frac{\Delta({\rm D/H})}{\rm D/H} = -0.32\frac{\Delta\langle\sigma v\rangle_{\rm d(p,\gamma)^3He}}{\langle\sigma v\rangle_{\rm d(p,\gamma)^3He}}$$
$$\frac{\Delta({\rm D/H})}{\rm D/H} = -0.54\frac{\Delta\langle\sigma v\rangle_{\rm d(d,n)^3He}}{\langle\sigma v\rangle_{\rm d(d,n)^3He}} - 0.46\frac{\Delta\langle\sigma v\rangle_{\rm d(d,p)^3H}}{\langle\sigma v\rangle_{\rm d(d,p)^3H}}$$

so that to achieve the $\sim$1% precision required by observations, one needs a similar precision on reaction rates. None of them are affected by resonances, so that the only questions are to model the slowly varying energy dependence of the S–factors and precisely determine their absolute scale. There are basically two options: either empirically fit both the energy dependence and scale so as to follow closely the data, or use theoretical energy dependences from nuclear physics models and only determine the absolute normalization. We adopted the rates from the new evaluations of Iliadis *et al.* (2016) and Gómez Iñesta *et al.* (2017) that use both the second option, together with Bayesian methods. The theoretical, *ab initio* energy dependences were taken from Marcucci *et al.* (2005) for D(p,γ)^{3}He and from Arai *et al.* (2011) for D(d,n)^{3}He and D(d,p)^{3}H. The main difficulty to determine the absolute scale of the S–factors is that one needs to combine results from different experiments.

Coc *et al.* (2015), using traditional statistics found a normalization factor of 0.9900$\pm$0.0368 for the D(p,γ)^{3}He theoretical S–factor of Marcucci *et al.* (2005), while the Bayesian analysis gives $1.000^{+0.038}_{-0.036}$ (Iliadis *et al.*, 2016). This shows that, starting from the same experimental data and theoretical model, different statistical analyses can lead to a, significant, 1% difference. Figure 23 displays the D(p,γ)^{3}He experimental S–factor normalised to the theoretical model of Marcucci *et al.* (2005). The solid horizontal line corresponds to the scaling of the theoretical S–factor adopted by Coc *et al.* (2015). It is obvious that experimental data are scarce at BBN energies and slightly below the scaled S–factor (an overall 9% systematic uncertainty is not shown however), while the empirical fit by Adelberger *et al.* (2011) or (Descouvemont *et al.*, 2004) follows closely, by construction, the experimental data. Note also that Marcucci *et al.* (2016) have included higher order terms in their *ab initio* model resulting in a $\approx$10% increase with respect with their previous result (Marcucci *et al.*, 2005), this time well above the experimental data (see Fig. 23). Using this new theoretical S–factor, one would obtain an additional reduction of Δ(D/H) = -0.072$\times10^{-5}$ that nevertheless would vanish if we rescale it (by 0.915) to fit experimental data. This rate is thus a major source of uncertainty for D/H prediction that should be resolved when the new experimental data (Gustavino, 2017) from LUNA at the Gran Sasso underground facility will be released, supplementing the low energy ones (Casella *et al.*, 2002).

In a similar way, the D(d,n)^{3}He and D(d,p)^{3}H rates have been evaluated by (Coc *et al.*, 2015) and later by (Gómez Iñesta *et al.*, 2017), using the *ab initio* S–factor from Arai *et al.* (2011) scaled according to experimental data. They found negligible differences in scaling factors: 0.959$\pm$0.010 and 0.955$\pm$0.010 for the traditional analysis to be compared with 0.961$\pm$0.010 and 0.956$\pm$0.010 for the Bayesian one. However, the theoretical work of Arai *et al.* (2011) was focused on low energies and does not correctly reproduce the D(d,n)^{3}He and D(d,p)^{3}H experimental data above $\approx$600 keV. It is highly desirable that these calculations be extended up to $\approx$2 MeV, to cover the range of experimental data that encompass BBN energies.

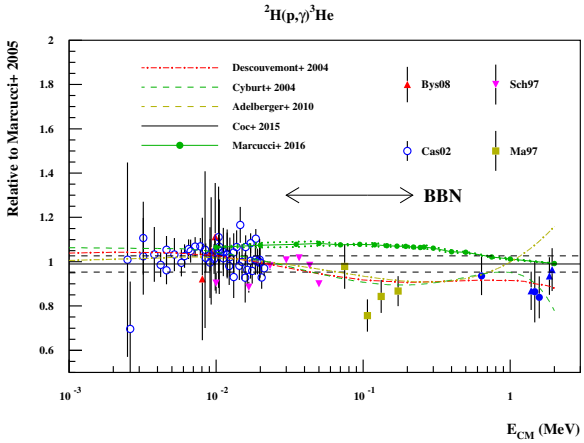

FIG. 23 Ratio of experimental (Bystritsky *et al.*, 2008; Casella *et al.*, 2002; Ma *et al.*, 1997; Schmid *et al.*, 1997), fitted (Adelberger *et al.*, 2011; Coc *et al.*, 2015; Cyburt, 2004; Descouvemont *et al.*, 2004) and new theoretical (Marcucci *et al.*, 2016) S–factors to the theoretical one (Marcucci *et al.*, 2005); the horizontal lines correspond to the theoretical S–factor scaled according to Coc *et al.* (2015). (Systematic uncertainties, i.e. global normalization errors, in the range 4.5–9% are shown in keys).

At the CMB deduced density, ^{7}Li is produced through the formation of ^{7}Be via the ^{3}He$(\alpha,\gamma)^7$Be reaction as ^{7}Be will decay much later to ^{7}Li. The destruction of ^{7}Be occurs through the ^{7}Be(n,p)^{7}Li(p,α)^{4}He channel which is limited by the scarcity of late time neutron abundance. The most influential reaction rates on ^{7}Li nucleosynthesis are (e.g. Table 1 in Coc and Vangioni, 2010) ^{1}H(n,γ)^{2}H (indirectly by affecting the neutron abundance) and ^{3}He$(\alpha,\gamma)^7$Be, but large deviations from their nominal cross sections are strongly constrained by experiments. Even though, there has not been new experimental data, since it is the major source of uncertainty on the ^{7}Li production, the ^{3}He$(\alpha,\gamma)^7$Be reaction rate has also been recently re-evaluated using Bayesian methods (Gómez Iñesta *et al.*, 2017) to scale the theoretical S–

factor of Neff (2011). It was known that the ^{7}Be(n,α)^{4}He reaction could not help solve the lithium problem, but its rate was highly uncertain and affected the ^{7}Li production at the few percent level. Until recently, the only published rate came from an evaluation by Wagoner (1969) based on very scarce data. We used either this rate or the one obtained by TALYS (Goriely *et al.*, 2008) in previous publications (Coc *et al.*, 2012; Coc *et al.*, 2014). A new re-evaluation (Hou *et al.*, 2015) and experiments (Barbagallo *et al.*, 2016; Kawabata *et al.*, 2017) confirmed that the ^{7}Be(n,α)^{4}He rate is approximately, one order of magnitude below the Wagoner one, rendering negligible the effect this reaction. Hence, we now use the rate provided by the n_TOF collaboration (Barbagallo *et al.*, 2016) that now has no impact on ^{7}Be.

Lithium–6 nucleosynthesis is quite simple given that it is only produced by the D(α,γ)^{6}Li reaction and destroyed by ^{6}Li(p,α)^{4}He. While the rate of the latter has been precisely known for a long time, the rate of the former suffered from large uncertainties (Angulo *et al.*, 1999). This has now been solved, thanks to experiments (Anders *et al.*, 2014; Hammache *et al.*, 2010), and theory (Mukhamedzhanov *et al.*, 2016).

Elements with atomic number above 7 are not expected to be significantly produced in BBN, unless some of the reaction rates involved in their production differ strongly from their current estimates (Coc *et al.*, 2014; Iocco *et al.*, 2007). Indeed, some of them rely on theoretical models not well adapted to low mass nuclei. Figure 22 displays the main reactions producing or destructing the beryllium, boron and C, N and O stable isotopes.

Table IV displays the few reaction rates that have been updated in Coc *et al.* (2015, 2014), and now in this work, with respect to the Table 4 of Coc *et al.* (2012).

TABLE IV Updated reaction rates with respect to Coc *et al.* (2012)

Reaction	Previous	Present
D(p,γ)^{3}He	Descouvemont *et al.* (2004)[a,b] Coc *et al.* (2015)[c]	Iliadis *et al.* (2016)
D(d,p)^{3}H and D(d,n)^{3}He	Descouvemont *et al.* (2004)[a,b] Coc *et al.* (2015)[c]	Gómez Iñesta *et al.* (2017)
^{3}He(α,γ)^{7}Be	Cyburt and Davids (2008)[a,b] deBoer *et al.* (2014)[c]	Iliadis *et al.* (2016)
^{8}Li(p,n)2α	Becchetti *et al.* (1992)[a]	Mendes *et al.* (2012)[c]
^{7}Be(n,α)^{4}He	Goriely *et al.* (2008)[a] Wagoner (1969)[b] Hou *et al.* (2015)[c]	Barbagallo *et al.* (2016)
^{14}C(α,γ)^{18}O and ^{14}C(p,γ)^{15}N	Error in tabulated rates[a,b,c]	Goriely *et al.* (2008)

Used in: [a]Coc *et al.* (2012), [b]Coc *et al.* (2014), or [c]Coc *et al.* (2015)

V. NUMERICAL RESULTS

A. Overview of PRIMAT

To our knowledge, apart from the Kawano code (Kawano, 1992) which is based on the historical code of Wagoner (Wagoner, 1969, 1973; Wagoner *et al.*, 1967), there exist only two public BBN codes, which are PArthENoPE (Consiglio *et al.*, 2017; Pisanti *et al.*, 2008) and AlterBBN (Arbey, 2012). The method followed in PRIMAT differs slightly from these two recent implementations, in that we integrate directly differential equations in time, instead of integrating differential equations in the plasma temperature which are obtained by the replacement of dT/dt derived from the Friedmann equation. The code is abundantly commented and refers to equations of the previous sections of this article. Let us summarize the main steps of the code.

- First we solve for the thermodynamics of the plasma following the details provided in § II. This allows to obtain $a(T)$ either using entropy conservation (31) if the effect of incomplete neutrino decoupling is neglected, or using the variation of entropy from the heat transfer between the plasma and the neutrinos (62). When QED plasma effects are included we use the corresponding (55). The relation $T(a)$ is obtained by a numerical inversion. The temperature of neutrinos is either deduced from (29), or (57) when QED plasma effects are included, if we assume they are fully decoupled. If we take into account the incomplete neutrino decoupling, then their effective temperature is obtained from Eqs. (63) and (64). The evolution of baryon energy density follows the simple scaling (34), and similarly for cold dark matter. Then the cosmological expansion is solved using the total energy density (43) [with QED effects included for the plasma energy density (Eq. 58) if the choice is made], inside the Friedmann equation (40), so to obtain $a(t)$ by numerical resolution of the differential equation. The relation $t(a)$ is obtained by numerical inversion. Eventually we obtain $T(t)$ as $T(a(t))$ that we can use later in the reaction rates since they depend on temperature.

- Once the thermodynamics and the cosmological expansion are known, we compute the weak rates for a grid of plasma temperatures so as to interpolate them. The total rates are obtained by considering all relevant corrections discussed in § III, which are added as in Eq. (121). The constant K involved in all rates is obtained from Eq. (91) with λ_0 given by the value (120). Since the weak rates computation can be very long, especially when including finite temperature radiative corrections which involve two-dimensional integrals, we store them on hard disk for later use. An option allows to recompute them when desired and various options allow

to switch on or off the various corrections.

- Finally we build the system of equations for the nuclear network, that is the system of Eqs. (138) including the weak rates. The nuclear reaction rates are read from tabulated values in function of temperature, or from analytical fits and the reverse rates are obtained from (141). The evolution of the nuclides abundances is numerically solved in three periods.

  1. For $10^{11}\mathrm{K} \geq T \geq 10^{10}\mathrm{K}$ we solve only for the abundance of neutrons and protons and totally ignore the nuclear reactions. Photodissociation reactions are too strong for this period and only the abundance of neutrons and protons is relevant at this stage. Nuclear reactions are anyway not tabulated above 10^{10}K.
  2. Then for $10^{10}\,\mathrm{K} \geq T \geq 1.25 \times 10^{9}\,\mathrm{K}$ we solve for a small nuclear network, made of light elements only (protons, neutron, ^{2}H, ^{3}H, ^{3}He, ^{4}He, ^{6}Li, ^{7}Li and ^{7}Be) and starting from the NSE abundance, apart for neutrons and protons which are taken from the previously solved period. For this period the system is very stiff and we use a first order BDF scheme (backward differentiation formula), which is equivalent to a backward Euler method.
  3. Finally for $1.25 \times 10^{9}\mathrm{K} \geq T \geq 6 \times 10^{7}\mathrm{K}$ we solve numerically for all nuclides, using the full network of reactions. The system is less stiff and it is possible to fasten the numerical integration by using a second order BDF scheme.

B. Temperature of nucleosynthesis

One can estimate the temperature of nucleosynthesis as the temperature for which the NSE value of deuterium is equal to the abundance of neutrons found from the simple freeze-out plus beta decay model (98). At this temperature deuterium would have gobbled up all free neutrons and this definition corresponds essentially to the end of nucleosynthesis. Hence $T_{\rm Nuc}$ is defined by

$$Y_n(T_{\rm Nuc}) \equiv Y_d^{\rm NSE}(T_{\rm Nuc})\,. \tag{144}$$

These two abundances are plotted in Fig. 24 and we find numerically $T_{\rm Nuc} \simeq 7.7 \times 10^8\mathrm{K} \simeq 0.066\,\mathrm{MeV}$ and a corresponding $t_{\rm Nuc} \simeq 300\,\mathrm{s}$. On Fig. 3, we see that nearly all neutrons are hidden in ^{4}He which is energetically more favored than deuterium. Overall the deuterium is only a catalytic agent, necessary to convert free neutrons in ^{4}He, and we find only traces of it at the end of BBN. The nucleosynthesis of all rare light elements is over when the temperature is around 6×10^7K, corresponding to $t_{\rm end} \simeq 5 \times 10^4\,\mathrm{s}$. In our code, the decay reactions of elements whose half-life is much longer than $t_{\rm end}$ are not included. However when reporting the final abundances of elements, it is customary to consider that these elements have been fully converted into stable elements. For instance the half-life of ^{7}Be is 53.22 days, as it decays into ^{7}Li. Hence when reporting the latter abundances, we add the former ones. Similarly, tritium (^{3}H) decays in ^{3}He in 12.32 years and the former is added to the latter in the final abundances reported. The evolution of the isotopes as a function of time is depicted in Fig. 25[18].

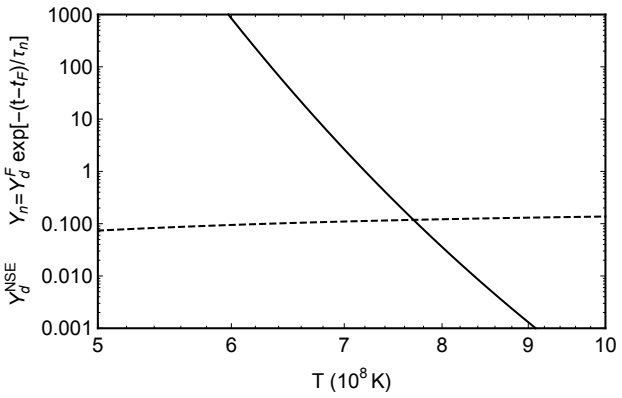

FIG. 24 Evolution of NSE deuterium abundance (continuous line) and Y_n^F found from a simple freeze-out and beta decay model (dashed line).

C. Effect of corrections on abundances

The effects of the various corrections in the weak rates have been estimated numerically and are reported in table V. We have assessed the importance of individual corrections as well as the interplay of some corrections when they do not add simply linearly. Let us now comment in details the effect of these corrections.

1. Radiative corrections

Using the non-relativistic Fermi function and Sirlin's function (B30) without resummation of higher order corrections, we find $\Delta Y_{\rm P}^{(4)} = 31.0$, exactly as in Lopez and Turner (1999, Table V, line 2). With the resummed radiative corrections (B35) and using the relativistic Fermi function brings an extra $\Delta Y_{\rm P}^{(4)} = 0.5$, worth being considered for precise predictions.

[18] The time evolution of ^{14}C in Fig. 25, left panel, strongly differs from the one in Fig. 13 of Coc *et al.* (2012). This was due to an error in the ^{14}C(α,γ)^{18}O and ^{14}C(p,γ)^{15}N reaction rates that are now fixed. It has, however no consequences on the total CNO production.

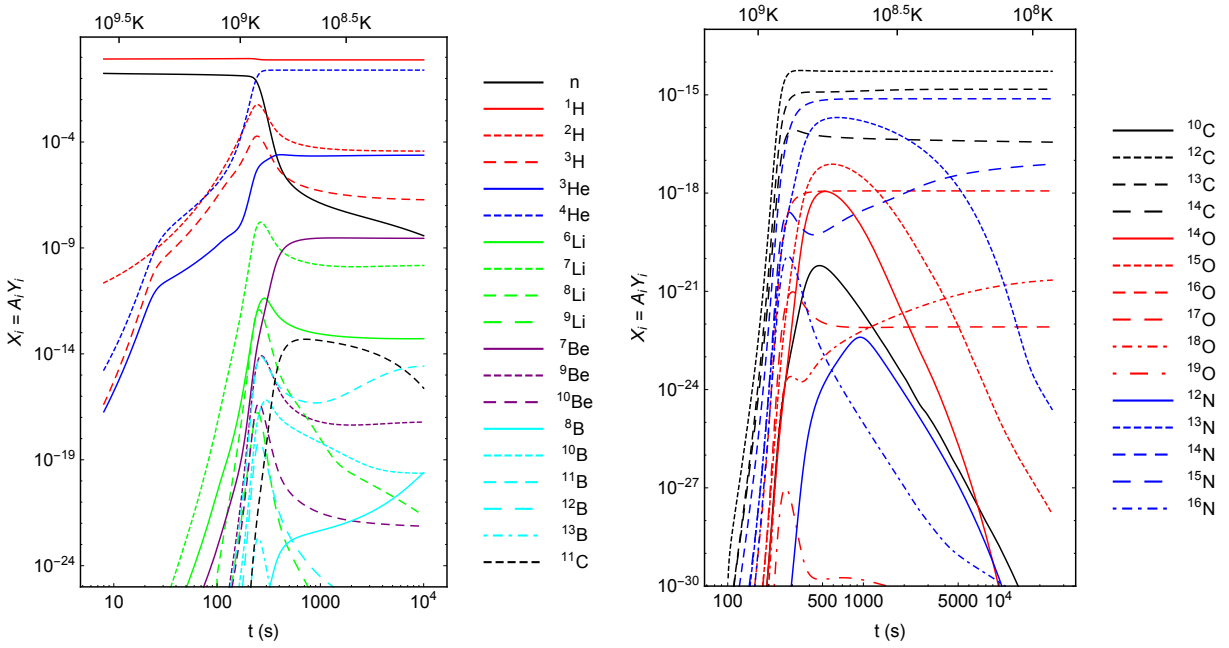

FIG. 25 *Left* : Evolution of light elements abundances. *Right* : Evolution of heavier elements abundances[18].

2. Finite nucleon mass corrections

We find that the cumulated effect of finite nucleon mass corrections and weak-magnetism brings $\Delta Y_{\rm P}^{(4)} = 12.8$ corresponding to $+0.53\%$ This is slightly more than found by Lopez and Turner (1999, Table V, line 3) which is $\Delta Y_{\rm P}^{(4)} = 12$ corresponding to $+0.50\%$, also evoked in Lopez *et al.* (1997). Given the smallness of the difference we consider that our results are in agreement with these references. Note that weak-magnetism accounts for around 12% of the finite nucleon mass corrections.

It is worth commenting that when finite nucleon mass effects are considered together with incomplete neutrino decoupling, the total effect is less than the sum of the effects taken individually and there is a reduction $\Delta Y_{\rm P}^{(4)} \simeq -0.6$. We found that this is because finite nucleon mass corrections are very sensitive to the neutrino temperature (see Fig. 20). Hence we advocate that a correct treatment of neutrino decoupling needs not only to be performed with the full machinery of the Boltzmann equation, with the inclusion of neutrino oscillations, but it should also be performed jointly with the inclusion of finite nucleon mass corrections. So far this joint treatment is lacking in the literature.

3. Finite temperature radiative corrections

In table V, we report that the finite radiative corrections bring $\Delta Y_{\rm P}^{(4)} \simeq 3.1$, reduced to $\Delta Y_{\rm P}^{(4)} \simeq 0$ when bremsstrahlung corrections are added to obtain a consistent detailed balance of weak rates. Indeed in Fig. (18) we check that around freeze-out, finite radiative corrections and bremsstrahlung corrections are almost opposite. In both cases this is very different from the modification computed in Esposito *et al.* (2000a) where $\Delta Y_{\rm P}^{(4)} \simeq -4$ is reported.

It is important to realize that the electron mass shift (44) is part of the finite-temperature corrections when it comes to considering the corrections to the weak rates. Hence we adopt the point of view of Brown and Sawyer (2001) which is different from Lopez and Turner (1999). In order to allow a comparison with that reference, we evaluated independently the effect of the electron mass shift following their method, that is replacing the electron mass shift directly in the distribution functions, and we found a modification $\Delta Y_{\rm P}^{(4)} \simeq +1.4$. Hence from the estimation of Lopez and Turner (1999) for finite-temperature radiative corrections $\Delta Y_{\rm P}^{(4)} \simeq 3$ one should instead use $\Delta Y_{\rm P}^{(4)} \simeq 4.4$ to compare with our results. This is slightly larger than our value $\Delta Y_{\rm P}^{(4)} \simeq 3.1$ without BS corrections but certainly larger than our value $\Delta Y_{\rm P}^{(4)} \simeq 0$ with BS corrections.

In general, an enhancement of the rates induces a decrease of $Y_{\rm P}$ thanks to Eq. (7). In Lopez and Turner (1999) the rates are increased by the finite temperature radiative corrections, and one would expect a decrease $Y_{\rm P}$. However since the corrected rates no longer satisfy the detailed balance relation (86) as they should, Eq. (7)

TABLE V Final abundances depending on the corrections included. ID is incomplete decoupling of neutrinos. FM is finite nucleon mass effect without weak-magnetism, WM is weak-magnetism, and FM+WM are both effects. RC are radiative corrections. ThRC are finite temperature radiative corrections without bremsstrahlung corrections, and BS are bremsstrahlung corrections. QED-MS is the QED electron mass shift effect considered alone when replaced directly in distribution functions (see discussion in §V.C.3), and QED-Pl are the QED effects on the plasma thermodynamics (§II.E).

Corrections	$Y_{\rm P}$	$\delta Y_{\rm P} \times 10^4$	$\delta Y_{\rm P}/Y_{\rm P}(\%)$	D/H $\times 10^5$	Δ (D/H) (%)	^{3}He/H $\times 10^5$	^{7}Li/H $\times 10^{10}$
Born	0.24262	0	0	2.423	0	1.069	5.635
Born+ID	0.24274	1.2	0.05	2.432	0.37	1.070	5.613
Born+FM	0.24374	11.2	0.46	2.430	0.25	1.070	5.651
Born+FM+WM	0.24390	12.8	0.53	2.430	0.29	1.070	5.654
RCa [Eq. (B30), Non. Rel. Fermi]	0.24572	31.0	1.27	2.440	0.70	1.071	5.681
RCb [Eq. (B35), Non. Rel. Fermi]	0.24575	31.3	1.29	2.440	0.70	1.071	5.682
RC [Eq. (B35), Rel. Fermi]	0.24577	31.5	1.30	2.440	0.70	1.071	5.682
RC+QED-MS	0.24591	32.9	1.36	2.441	0.74	1.071	5.684
RC+QED-Pl	0.24577	31.5	1.30	2.443	0.82	1.072	5.674
RC+ID	0.24588	32.6	1.34	2.449	1.07	1.073	5.660
RC+ID+QED-Pl	0.24588	32.6	1.34	2.452	1.19	1.073	5.652
RC+FM+WM	0.24705	44.3	1.82	2.447	0.99	1.072	5.701
RC+FM+WM+QED-MS	0.24718	45.6	1.87	2.448	1.03	1.073	5.701
RC+FM+WM+QED-Pl	0.24704	44.2	1.81	2.450	1.11	1.073	5.693
RC+FM+WM+ID	0.24720	44.8	1.84	2.456	1.36	1.074	5.678
RC+FM+WM+ThRC (No BS)	0.24736	47.4	1.95	2.449	1.07	1.073	5.706
RC+FM+WM+ThRC+BS	0.24705	44.3	1.82	2.447	0.99	1.072	5.701
RC+FM+WM+ThRC+BS+ID+QED-Pl	0.24709	44.7	1.84	2.459	1.49	1.074	5.670

cannot be used and the effect is not opposite. In our case this can be seen when using the radiative corrections, without the BS corrections added. The weak rates are increased (see Fig. 18) and still it leads to $\Delta Y_{\rm P}^{(4)} \simeq 3.1$. This highlights the extreme importance of constructing corrections which respect the detailed balance, in order to obtain meaningful results. Any corrections added which does not satisfy the correct detailed balance relation Eq. (7) is somehow equivalent to a modification of the value of the mass gap Δ, modifying artificially the thermal equilibrium value. Stated more directly, it is obvious that an overestimated enhancement of $\Gamma_{p\to n}$ as in Lopez and Turner (1999) leads to an artificial increase of Y_n and thus of $Y_{\rm P}$. When a correction does not satisfy the detailed balance relation, the primary effect is no more a delayed or advanced freeze-out, that is a lower or larger freeze-out temperature, but an artificially different freeze-out abundance for the same freeze-out temperature since one rate is overestimated and the thermal equilibrium is artificially displaced.

4. QED effects on plasma thermodynamics

The effect of QED corrections on $Y_{\rm P}$ is negligible. In Lopez and Turner (1999), it is estimated to be around $\Delta Y_{\rm P}^{(4)} \simeq 1$ only because it is also cumulated with the electron mass shift effects which are part of finite temperature corrections of the weak rates in our terminology. We find $\Delta Y_{\rm P}^{(4)} \simeq 1.4$ when computing it with the same method.

5. Incomplete neutrino decoupling

The pure clock effect evoked at the end of § III.I is not the only effect, because one must also consider the effect of incomplete neutrino decoupling on the weak rates. In our approximate description, we have implicitly assumed in § II.G that all neutrino flavors share the same ratio of heating, that is we assume that $\delta\rho_{\nu_e}/\rho_{\nu_e} = \delta\rho_{\nu_\mu}/\rho_{\nu_\mu} = \delta\rho_{\nu_\tau}/\rho_{\nu_\tau}$ so that it is meaningful to define a common effective temperature. It is certainly not correct since there is more energy gained by electronic neutrino than other types of neutrino. Indeed electronic neutrinos couple to electrons and positron with charged and neutral currents whereas the other flavors of neutrinos couple only through neutral currents. However, first this is less the case when considering neutrino flavor mixing (Mangano *et al.*, 2005), and second in the early stage of neutrino heating by electron-positron annihilations, the heating is more efficiently redistributed among the three species. Hence it is not a too bad approximation to assume that the heating is distributed in the same ratio among flavors when considering the effect on weak rates. This means that we assume that all neutrino flavors share always $1/N_\nu$ of the total energy density. Even though we know that they have distorted spectra, we still defined an effective neutrino temperature from their energy density. That is we still use Eq. (42) to define the neutrino tem-

perature T_ν, and by construction it is the temperature for thermalized neutrino distributions that would have the same energy density.

Apart from the clock effect mentioned earlier, there are two competing effects in the weak rates which nearly fully cancel (Dodelson and Turner, 1992; Fields *et al.*, 1993; Mangano *et al.*, 2005). First the higher energy density in neutrinos results in an increase of the weak rates, inducing a freeze-out which happens later, with less neutrons and thus producing less ^{4}He. However the energy gained by neutrinos is lost from the plasma, and the reduction in electrons-positrons energy density results in lower weak rates, inducing an earlier freeze-out which results in more neutrons and then more ^{4}He production. It has been shown in Fields *et al.* (1993) that both effects level off when the freeze out is complete, that is around $T = 3.3 \times 10^9$K. Indeed we find that in our simple thermal approximation, the relative variation in the neutron fraction at that temperature is a modest relative increase of 2×10^{-5}. Without the clock effect this would result in a negligible $\Delta Y_{\rm P}^{(4)} \simeq 0.05$. It is only the clock effect (see § V.C), that is the fact that neutrons have slightly less time to beta decay, which results in $\Delta Y_{\rm P}^{(4)} \simeq 1.2$. When taking more carefully into account the fact that neutrinos do not get the same share of the heating, and that furthermore there are spectral distortions which affect the neutrino distribution functions entering the weak-rates, it is found a slightly larger increase in $Y_{\rm P}^{(4)}$ (Mangano *et al.*, 2005).

However note that our variations for $Y_{\rm P}$, D/H, ^{3}He/H and ^{7}Li/H are in very close agreement with those found in Grohs *et al.* (2016) (Table IV, second line), where these spectral distortions effects (but not the flavor oscillations) have been fully taken into account. It is puzzling that with our thermal approximation based on a heating rate found from Pisanti *et al.* (2008), that is from the result of Mangano *et al.* (2005), we do not recover the results of table 3 in Mangano *et al.* (2005) but we recover with very good agreement the results of Grohs *et al.* (2016). We found that the argument presented in Grohs *et al.* (2016) for the variations of D/H, ^{3}He/H and ^{7}Li/H are very convincing and we recover them in our numerics. Indeed the clock effect results in less time to destroy deuterium through D(d,n)^{3}He, D(p,γ)^{3}He and D(d,p)^{3}H, ending up in more deuterium being left out at the end of BBN. Since two of these deuterium destroying reactions are producing ^{3}He [namely D(d,n)^{3}He and D(p,γ)^{3}He], this results in more ^{3}He. As for ^{7}Li it is reduced only because the production of ^{7}Be has less time to proceed, but we found that the ^{7}Li (without ^{7}Be added) is increased since it has also less time to be destroyed down from its peak value during BBN. Hence the signs of variations for D/H, ^{3}He/H and ^{7}Li/H have a clear physical origin, when incomplete neutrino decoupling is taken into account, and these signs are opposite to those reported in table 3 of Mangano *et al.* (2005).

TABLE VI First coefficients of Eq. (145). These provide abundances with precision better than 0.01% for $Y_{\rm P}$ and 0.03% for other abundances, in the range of 10% variations in $\Omega_{\rm b}h^2$, 2% variation in τ_ν and $2 \leq N_\nu \leq 4$. However these are still subject to reaction rates uncertainties which are estimated below in table VII.

	$Y_{\rm P}$	D/H	^{3}He/H	^{7}Li/H
C_{100}	0.039 039	−1.645 50	−0.566 99	2.076 05
C_{010}	0.163 552	0.409 01	0.135 87	−0.276 75
C_{110}	−0.000 044	−0.612 29	−0.121 57	−0.292 77
C_{200}	−0.029 351	2.041 37	0.533 03	0.586 39
C_{020}	−0.036 124	−0.005 99	−0.012 65	0.038 88
C_{300}	0.017 891	−2.408 17	−0.518 55	−0.882 43
C_{210}	−0.001 037	0.801 50	0.120 83	0.510 82
C_{120}	−0.000 354	−0.004 77	0.009 28	−0.103 35
C_{030}	0.009 938	0.002 24	0.002 70	0.008 84
C_{001}	0.731 614	0.422 20	0.140 52	0.438 29
C_{101}	−0.009 741	−0.660 30	−0.123 90	1.226 19
C_{011}	0.018 321	0.193 66	0.040 40	−0.330 69
C_{111}	−0.003 423	−0.331 58	−0.038 79	−0.709 23
C_{201}	0.004 189	0.906 17	0.121 21	0.924 63
C_{021}	−0.011 981	0.004 98	−0.003 28	0.135 30

D. Dependence on main parameters

The variations of the yields for small variations of the main parameters can be given with expansions of the type

$$\frac{\Delta Y_{\rm P}}{\overline{Y_{\rm P}}} = \sum_{pqr} C_{pqr} \left(\frac{\Delta \Omega_{\rm b} h^2}{\overline{\Omega_{\rm b} h^2}}\right)^p \left(\frac{\Delta N_\nu}{\overline{N_\nu}}\right)^q \left(\frac{\Delta \tau_n}{\overline{\tau_n}}\right)^r \quad (145)$$

with similar expansions for the other abundances (D/H,^{3}He/H,^{7}Li/H). The reference abundances are given by the last line of table V and the reference parameters are $\overline{\Omega_{\rm b} h^2} = 0.02225$, $\overline{\tau_n} = 879.5\,$s and $\overline{N_\nu} = 3$. The meaning of varying the number of neutrinos is further discussed in § VI.D. The first coefficients of these expansions are given in table VI.

Leaving aside the non-standard BBN physics which corresponds to a variation of the number of neutrinos, we can restrict this expansion to the linear behaviour to estimate rapidly the variations of the abundances in function of changes in the baryon abundance or the neutron lifetime. Hence if these parameters are slightly modified in the future, our results can be transposed easily. We

find

$$\frac{\Delta Y_{\rm P}}{\overline{Y_{\rm P}}} = 0.0390\frac{\Delta\Omega_{\rm b}h^2}{\overline{\Omega_{\rm b}h^2}} + 0.732\frac{\Delta\tau_n}{\overline{\tau_n}} \quad (146a)$$

$$\frac{\Delta {\rm D/H}}{\overline{\rm D/H}} = -1.65\frac{\Delta\Omega_{\rm b}h^2}{\overline{\Omega_{\rm b}h^2}} + 0.422\frac{\Delta\tau_n}{\overline{\tau_n}} \quad (146b)$$

$$\frac{\Delta {}^3{\rm He/H}}{\overline{{}^3{\rm He/H}}} = -0.567\frac{\Delta\Omega_{\rm b}h^2}{\overline{\Omega_{\rm b}h^2}} + 0.141\frac{\Delta\tau_n}{\overline{\tau_n}} \quad (146c)$$

$$\frac{\Delta {}^7{\rm Li/H}}{\overline{{}^7{\rm Li/H}}} = 2.08\frac{\Delta\Omega_{\rm b}h^2}{\overline{\Omega_{\rm b}h^2}} + 0.438\frac{\Delta\tau_n}{\overline{\tau_n}}\,. \quad (146d)$$

As expected, $Y_{\rm P}$ is very sensitive to the weak rates and thus to τ_n but not to the baryon abundance. Hence even though uncertainty is larger in baryon abundance, the theoretical uncertainty of $Y_{\rm P}$ is dominated by the uncertainty in the determination of the neutron lifetime. From the measured value of τ_n reported in appendix D, this corresponds to a 0.068 % uncertainty in $Y_{\rm P}$ or $\sigma(Y_{\rm P}) \simeq 0.00017$ which is lower than the value $\sigma(Y_{\rm P}) \simeq 0.0003$ used in Ade *et al.* (2016, p47), implying that we find errors approximately 40% smaller in $Y_{\rm P}$. The predicted and observed abundances as functions of η are plotted in Fig. 26.

E. Distribution of abundance predictions

We use the method described in Coc *et al.* (2014) to estimate the uncertainty in light elements productions during BBN due to uncertainty in nuclear rates and weak-rates (that is the uncertainty on τ_n that we assume to follow a normal distribution). It has been found (Longland *et al.*, 2010), that probability density functions of reaction rates can be well approximated by lognormal distributions

$$f(x) = \frac{1}{\sigma\sqrt{2\pi}}\frac{1}{x}e^{-(\ln x-\mu)^2/(2\sigma^2)} \quad (147)$$

(with $x \equiv N_A\langle\sigma v\rangle$ for short is the rate). This is equivalent to the assumption that $\ln(x)$ is Gaussian distributed with expectation value μ and variance σ^2 (both functions of temperature). The lognormal distribution allows to cope with large uncertainty factors ($\equiv e^\sigma$) together with ensuring that the rates remain positive. If these parameters are tabulated as a function of the temperature, they can be used to perform subsequent Monte-Carlo nucleosynthesis calculations. The quantile of the distributions of the abundances obtained by such a method are reported in table VII for which we used 20 000 Monte-Carlo points.

The variations of $Y_{\rm P}$ are nearly entirely due to the uncertainty on τ_n because it is almost completely controlled by weak rates which set the abundance of free neutrons before nucleosynthesis starts. This Monte-Carlo method allows to construct the probability $P(Y_i|\omega_{\rm b})$ for each species, where $\omega_{\rm b} \equiv \Omega_{\rm b}h^2$. This probability reflects the uncertainty in all parameters affecting the reaction rates, independently of cosmology and it is used to plot the $\pm\sigma$ width of curved in Fig. 26 by computing the quantiles $\{0.15865, 0.84135\}$.

TABLE VII Monte-Carlo estimation of light elements uncertainties due to nuclear rates, and τ_n (aka weak rates) uncertainties.

Quantile	2.275%	15.865%	50%	84.135%	97.725%	mean	$\frac{\sigma}{\rm mean}$
$Y_{\rm P}$	0.24676	0.24693	0.24709	0.24726	0.24742	0.24709	0.068%
D/H $\times 10^5$	2.386	2.423	2.460	2.496	2.532	2.459	1.49%
^{3}He/H $\times 10^5$	1.023	1.048	1.074	1.100	1.127	1.074	2.43%
^{7}Li/H $\times 10^5$	5.123	5.392	5.627	5.858	6.105	5.623	4.39%
^{6}Li/H $\times 10^{14}$	0.61	0.85	1.20	1.68	2.35	1.27	35%
CNO/H $\times 10^{15}$	0.14	0.52	1.02	3.07	65.6	15.3	13.4

For elements for which the uncertainty is small, it proves useful to approximate these probabilities by a normal distribution as

$$P(Y_i|\omega_{\rm b}) \simeq \mathcal{N}\left[\bar{Y}_i\left(\omega_{\rm b}\right), \sigma_i^{\rm th}\left(\omega_{\rm b}\right)\right]\left(Y_i\right) \quad (148)$$

where the normal distribution is noted

$$\mathcal{N}[\mu,\sigma](x) \equiv \frac{1}{\sqrt{2\pi}\sigma}\exp\left[-\frac{(x-\mu)^2}{2\sigma^2}\right]. \quad (149)$$

If we use the CMB to obtain a prior distribution on $\omega_{\rm b}$ that we assume to follow a normal distribution (the mean and standard deviation are reported in appendix D), then we can build the joint probability

$$P(Y_i, \omega_{\rm b}|{\rm CMB}) = P(Y_i|\omega_{\rm b})P(\omega_{\rm b}|{\rm CMB})\,, \quad (150)$$

and marginalizing over $\omega_{\rm b}$ we get probabilities in predicted abundances

$$P(Y_i|{\rm CMB}) = \int P(Y_i, \omega_{\rm b}|{\rm CMB}){\rm d}\omega_{\rm b}\,. \quad (151)$$

In practice we use also a Monte-Carlo method to obtain directly $P(Y_i|{\rm CMB})$. We only need to vary $\omega_{\rm b}$, according to its normal distribution, in addition to varying the reaction rates. With this method we can predict the underlying abundances that are reported in table VIII. The predicted abundance for deuterium is noticeably lower than the one in Ade *et al.* (2016, Eq. 74) which uses `PArthENoPE` (Pisanti *et al.*, 2008), and this has consequences when inferring the chemical potential of neutrinos (see § VI.C).

F. Comparison with observations

Except for ^{4}He, and the weak rates, the predicted abundances, displayed in Table VIII, do not differ significantly from those of Coc *et al.* (2015). As can be seen in Table IV, very few reaction rates have been updated, and if so, either the rate changes are tiny or the reactions have, in any case, a negligible effect. On the contrary, there are significative differences with the results

TABLE VIII Primordial abundances compared to observations.

	Observations	(a) $\tau_n = 880.3(1.1)$ s	**This work (h)** $\tau_n = 879.5(8)$ s	(f) $\tau_n = 880.3(1.1)$ s	Planck 2015 (g) $\tau_n = 880.3(1.1)$ s
$Y_{\rm P}$	0.2449±0.0040(b)	0.2484±0.0002	**0.24709±0.00017**	0.24709±0.00025	0.24667±0.00062
D/H ($\times 10^{-5}$)	2.527±0.030 (c)	2.45±0.05	**2.459±0.036**	2.58±0.13	2.614±0.13
^{3}He/H ($\times 10^{-5}$)	<1.1±0.2 (d)	1.07±0.03	**1.074±0.026**	1.0039±0.0090	
^{7}Li/H ($\times 10^{-10}$)	$1.58^{+0.35}_{-0.28}$ (e)	5.61±0.26	**5.623±0.247**	4.68±0.67	

(a) Coc *et al.* (2015), (b) Aver *et al.* (2015), (c) Cooke *et al.* (2018), (d)Bania *et al.* (2002), (e) Sbordone *et al.* (2010), (f) Cyburt *et al.* (2016), (g)Ade *et al.* (2016, TT+TE+EE+LowP, 95%CL), (h) we get $Y_{\rm P} = 0.24726$ when using $\tau_n = 880.3$ s

of Cyburt *et al.* (2016) which are mostly, and probably entirely, due to the different choice of reaction rates. Apparently, Cyburt *et al.* (2016) use for some of the most important reactions, D(p,γ)^{3}He, D(d,n)^{3}He, D(d,p)^{3}H, and ^{3}He$(\alpha,\gamma)^7$Be, the rates from NACRE II (Xu *et al.*, 2013), now superseded for these reactions by Coc *et al.* (2015); Gómez Iñesta *et al.* (2017); Iliadis *et al.* (2016). This is clearly the origin of the differences concerning D and ^{7}Li. There is an even greater difference with the D/H value reported by *Planck* (Ade *et al.*, 2016; Di Valentino *et al.*, 2014) using the `PArthENoPE` code (Pisanti *et al.*, 2008). This is again, probably due to a different choice of reaction rates for deuterium destruction.

Since the results for deuterium and lithium are not significantly different from our earlier works (Coc *et al.*, 2015, 2014) the comparison with observations is very similar. As explained in § I.A.3 we do not consider ^{3}He as a constraint.

1. Helium

Thanks to the re–evaluation of the corrections to the weak rates, we claim a precision of a few 10^{-4} on $Y_{\rm P}$ i.e. smaller than one unit on $Y_{\rm P}^{(4)}$ before taking into account the experimental uncertainty on the neutron lifetime and a few reaction rates (§ IV.C). We finally obtained $Y_{\rm P} = 0.24705\pm0.00019$, fully consistent with the value $Y_{\rm P} = 0.2449 \pm 0.0040$ deduced from Izotov *et al.* (2014) observations by Aver *et al.* (2015) (see Fig. 26), without the need for extra relativistic degrees of freedom as in (Izotov *et al.*, 2014).

Since this work is focused on ^{4}He and is an improved continuation of previous works it is worthwhile tracking the evolution of our calculation of $Y_{\rm P}$. In our earliest works (e.g. Coc *et al.* (2004)), since the observational uncertainties on $Y_{\rm P}$ were large, we neglected some of the corrections discussed here because we were unable to calculate them (e.g. including six–fold integrals). The corrections that we took into account corresponds to line RCa line in Table V and our (Fortran) calculated corrections did amount to $\delta Y_{\rm P}^{(4)} = 31.6$ (Coc *et al.*, 2014). When the observational uncertainties were reduced, it become important to include the neglected corrections, by artificially increasing $Y_{\rm P}^{(4)}$ by 18 at the the very end of the calculation. It corresponded to the finite-nucleon mass correction ($\delta Y_{\rm P}^{(4)} = 12$ (Lopez and Turner, 1999)), finite-temperature radiative correction ($\delta Y_{\rm P}^{(4)} = 3$) (Lopez and Turner, 1999)), QED plasma ($\delta Y_{\rm P}^{(4)} = 1$ (Lopez and Turner, 1999)) and neutrino decoupling ($\delta Y_{\rm P}^{(4)} = 2$ (Mangano *et al.*, 2005)), for a total of $\delta Y_{\rm P}^{(4)} = 18$, that we could not easily directly re-calculate. Hence, before this final correction, the $Y_{\rm P}$ value from Coc *et al.* (2015) was 0.2466 (i.e. 0.2484 minus 0.0018) to be compared to 0.24572 (RCa in Table V). This difference of $\delta Y_{\rm P}^{(4)} = 9$, which is in fact only $\delta Y_{\rm P}^{(4)} = 7$ if we account for the different τ_n used, was reduced to $\delta Y_{\rm P}^{(4)} \simeq 0.5$ by improving the Fortran code (time steps, temperature grid,...) at the expense of execution time[19].

2. Deuterium

Our present result differs by less than 3%, and agrees within error bars with the latest value inferred from Cooke *et al.* (2018) observations. Since the theoretical value lies on the lower bound of the observational one, this leaves only little room for models of lithium (i.e. ^{7}Be) destruction that byproduct extra deuterium (see below). Tiny differences with previous results (Coc *et al.*, 2015) come in part from the corrections to the weak rates (see Table V), to the re-evaluation of the three nuclear reaction rates (Gómez Iñesta *et al.*, 2017; Iliadis *et al.*, 2016) that govern deuterium destruction and improvements in the numerical method. With the high precision reached by D/H observations, these reaction rates [D(p,γ)^{3}He, D(d,n)^{3}He and D(d,p)^{3}H] need to be known at the percent level! This demands accurate measurement at BBN energies where data are scarce and theoretical improvement to better constrain the energy dependence of the S–factors.

[19] Details to appear elsewhere.

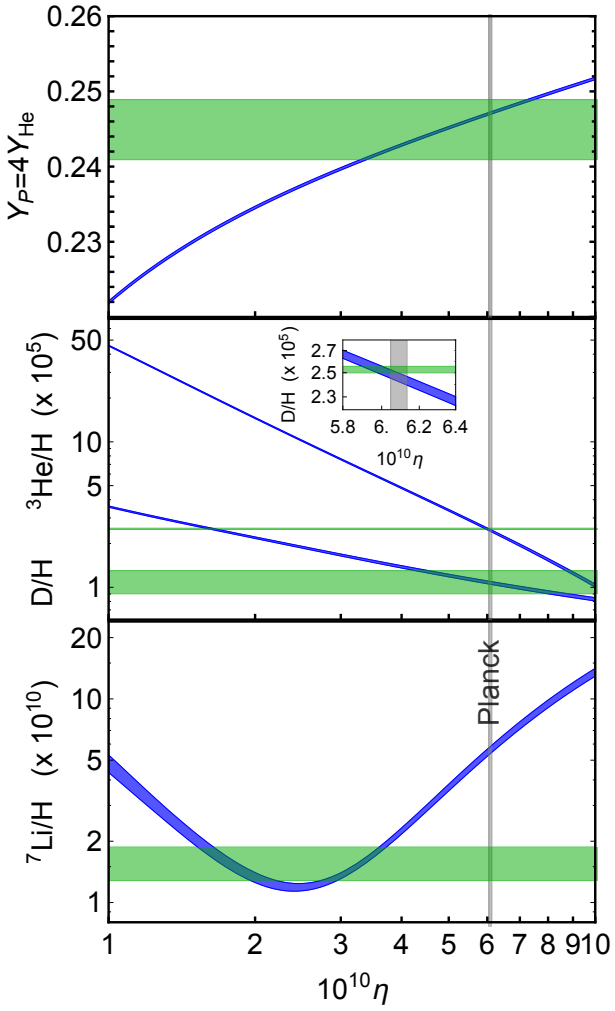

FIG. 26 *Top* : Dependence of $Y_{\rm P} = 4Y_{^4{\rm He}}$ in η and observational constraints. *Middle* : Dependence of deuterium (to curve) and ^{3}He (bottom curve) in η with observational constraints. The ^{3}H has been added since it decays radioactively in ^{3}He. *Bottom* : Dependence of ^{7}Li in η with observational constraints. The ^{7}Be has been added since it decays radioactively in ^{7}Li. In all these plots, the width of the curves represents the $\pm\sigma$ uncertainty from nuclear rates and neutron lifetime.

3. Lithium

There remains a factor of 3.6 between the predicted and observed Li/H values. This discrepancy has not yet found a fully satisfactory solution. On the contrary, the problem had worsened because of an updated reaction rate (Cyburt and Davids, 2008; Cyburt *et al.*, 2008) and because many solutions have been ruled out by the improved precision on D/H observations (Cooke *et al.*, 2018). We present below the kinds of solutions that have been considered so far.

- *There is no nuclear solution to the lithium problem.* Extensive sensitivity studies (Coc *et al.*, 2012, 2004) have not identified reactions, beyond those already known, that could have a strong impact on lithium nucleosynthesis. The most promising was ^{7}Be(d,p)2α (Coc *et al.*, 2004; Cyburt and Pospelov, 2012): an increase of its rate by a factor of $\approx$100 would have solved the problem. However, measurements of its average cross section (Angulo *et al.*, 2005) or properties of candidate resonances (Kirsebom and Davids, 2011; O'Malley *et al.*, 2011; Scholl *et al.*, 2011) ruled out this possibility. More generally, other destruction channels have recently been proposed (Chakraborty *et al.*, 2011) : ^{7}Be+n, p, d, t, ^{3}He and ^{4}He. In particular, the existence of a relatively narrow state around 15 MeV in the compound nucleus ^{10}C formed by ^{7}Be+^{3}He or the existence of a state close to 8 MeV in the compound nucleus ^{11}C formed by ^{7}Be+^{4}He could help reduce the ^{7}Be production. However, a recent search (Hammache *et al.*, 2013) for missing levels in the relevant excitation energy regions of ^{10}C and ^{11}C, via the reactions ^{10}B(^{3}He,t)^{10}C and ^{11}B(^{3}He,t)^{11}C, respectively, did not find any new level, whose corresponding resonances, in any case, would have too low strengths (Broggini *et al.*, 2012) because of the Coulomb barrier. It seems now that all extra ^{7}Be destructing reactions have been considered and found inefficient.

- *The effect of electron screening or modification of decay lifetime is negligible.* For reactions of interest to BBN, screening affects the laboratory cross sections at too low energies [e.g. $\lesssim$ 20 keV for D(d,p)^{3}H (Greife *et al.*, 1995) or ^{3}He(d,p)^{4}He (Aliotta *et al.*, 2001)] to affect measurement at BBN energies [$\approx$100 keV], on the one hand. On the other hand, the effect of screening during BBN is completely negligible (Famiano *et al.*, 2016; Wang *et al.*, 2011). It is well known that the lifetime of ^{7}Be that decays by electron capture depends on the probability of presence of an electron (from an atomic s orbital or from a plasma) inside the nucleus; for instance it is increased to $\sim$ 100 days at the center of the Sun (Adelberger *et al.*, 2011). To have an impact on lithium prediction, the ^{7}Be lifetime must be reduced to a value of $\sim 10^3$ s. However, because of the Boltzmann suppression factor, at T <0.5 GK, when ^{7}Be is present, the electron density becomes smaller than in the Sun so that one can expect an even longer lifetime. This can be confirmed if one extrapolates the results of Simonucci *et al.* (2013, Fig. 1), to $T \lesssim 500 \times 10^6$K and $\rho \lesssim 10^{-5}$ g/cm^3.

- Many exotic solutions to the lithium problem have been investigated (e.g. Yamazaki *et al.* (2014)), but most rely on extra neutron sources to boost ^{7}Be destruction through the ^{7}Be(n,p)^{7}Li(p,α)^{4}He

channel. However, these extra neutrons, inevitably, also boost the D and ^{3}H production through the ^{1}H(n,γ)^{2}H and ^{3}He(n,p)^{3}H channels, respectively (Coc *et al.*, 2015; Kusakabe *et al.*, 2014). This is shown in Figs. 1 in Olive *et al.* (2012), 4 in Kusakabe *et al.* (2014), and 14 in Coc *et al.* (2015) that display results of various types of models that succeed in solving the lithium problem, but at the expense of deuterium overproduction to levels now excluded by observations (Cooke *et al.*, 2014, 2016, 2018). Very few solutions, even beyond the Standard Model, that do not suffer from this drawback are left, e.g. Goudelis *et al.* (2016).

- *Stellar physics solutions require a uniform reduction of surface lithium over a wide range of effective temperature and metallicity.* Some amount of surface lithium destruction is unavoidable, because of atomic diffusion that transport lithium down to deeper and hotter layers where it is destroyed by a factor of 1.5 to 2 (Michaud *et al.*, 1984). The difficulty comes from the small thickness of the lithium plateau over a wide range of metallicity and temperature and the absence of stars between the plateau and the BBN prediction (Fig. 2). This could possibly be circumvented if an additional mixing process is included in the outer layers of these stars (Richard *et al.*, 2005). This is supported by the comparison between lithium observations in the metal–poor globular cluster NGC 6397 with stellar depletion models (Korn *et al.*, 2006). Another recent proposition relies on full lithium destruction but followed by a self–regulated reenrichment of lithium by late time accretion from the interstellar gas (Fu *et al.*, 2015). In addition, the Spite plateau does not exist anymore at the metallicity below [Fe/H]=-3, and is replaced by an increased spread of abundances, below the plateau value (Sbordone *et al.*, 2010). This "meltdown" of the Spite plateau is not understood yet. All this suggests that lithium observations cannot be used anymore to constrain BBN models.

- *There is no* ^{6}Li *problem anymore.* A few years ago, observations (Asplund *et al.*, 2006) of ^{6}Li in a few metal poor stars had suggested the presence of a plateau, at typically ^{6}Li/H $\approx 10^{-11}$, orders of magnitude higher than the BBN predictions of ^{6}Li/H $\approx 1.3\times10^{-14}$ (Hammache *et al.*, 2010). However, later, the observational ^{6}Li plateau has been questioned due to line asymmetries which were neglected in previous abundance analyses. Hence, there is no remaining evidence for a plateau at very low metallicity (Lind *et al.*, 2013) that can be used to derive a primordial ^{6}Li abundance.

4. Other elements

Leaving aside the ^{9}Be, ^{10}B and ^{11}B isotopes for which no primordial abundance can be inferred from observations (Coc *et al.*, 2014), it is worth mentioning the CNO abundance. Here, we call CNO all isotopes with masses larger than 12 (^{11}C mostly decays to ^{11}B). Even though, there are no primordial CNO abundance either, it is of peculiar interest since it may affect the evolution of the first stars (Population III) within the first structures of the Universe. Hydrogen burning in the first generation of stars proceeds through the slow pp–chains until enough carbon is produced (through the triple-alpha reaction) to activate the CNO cycle. The minimum value of the initial CNO mass fraction that would affect Population III stellar evolution is estimated to be 10^{-11} (Cassisi and Castellani, 1993) or even as low as 10^{-13} (in number of atoms relative to hydrogen, CNO/H) for the less massive stars (Ekström *et al.*, 2008). Table VII shows that the median abundance (0.5 quantile) is in agreement with previous works (Coc *et al.*, 2012; Iocco *et al.*, 2007), if taking into account that the distribution is not Gaussian (Coc *et al.*, 2014; Coc and Vangioni, 2014). As a result, the 0.97725 quantile corresponds to CNO/H$\approx 0.7\times10^{-13}$, close to the limit to have an impact on some first stars. As this is explained in Coc *et al.* (2014), this value, much larger than the median comes from the simultaneous variations, during the Monte Carlo, of a few reaction rates around ^{10}Be. Since very few or no experimental data are available for these reactions, the actual rates may differ by a few orders of magnitudes, from the TALYS (Goriely *et al.*, 2008) theoretical predictions. Experimental efforts are needed to confirm or infirm this possibility.

VI. COSMOLOGY WITH BBN

A. Cosmological perturbations

Cosmological fluctuations are of order 10^{-5}, and whatever their effect, we have neglected them given our precision goal. However it is easy to estimate the effect of adiabatic perturbations seeded by inflation. Indeed, since the Hubble radius is extremely small during BBN, most modes can be considered as super-Hubble modes, that is longer than the Hubble radius. In that case their effect can be described by a simple coordinate transformation applied on a homogeneous cosmology (Creminelli *et al.*, 2011; Mirbabayi and Zaldarriaga, 2015; Weinberg, 2003).

Let us consider a perturbed metric (expressed in conformal time defined by $\mathrm{d}t = a\mathrm{d}\eta$)

$$\mathrm{d}s^2 = a^2(\eta)\left(-(1+2\Phi)\mathrm{d}\eta^2 + (1-2\Psi)\delta_{ij}\mathrm{d}x^i\mathrm{d}x^j\right) . \tag{152}$$

It can be put in the homogeneous form using a coordinate transformation. Or conversely the dynamics of a spacetime perturbed by long modes can be deduced from the homogeneous dynamics thanks to a coordinate transformation. Not all such transformations lead to a physical

long mode dynamics, and one must ensure some conditions. In the case where the Universe dynamics is dominated by radiation, as is the case for BBN, the relevant coordinate transformation is (Creminelli *et al.*, 2011)

$$\tilde{\eta} = \eta\left(1 - \frac{\zeta}{3}\right), \qquad \tilde{x}^i = x^i(1+\zeta) \tag{153}$$

where ζ is the comoving curvature perturbation.

It follows using Eq. (10) that the number density in the perturbed universe $\tilde{n}_i$ is related to the one of a homogeneous cosmology n_i thanks to

$$\tilde{n}_i = n_i - \frac{\eta\zeta}{3}\partial_\eta n_i = (1+\zeta)n_i - \frac{\eta\zeta}{3} a\mathcal{J}_i\,, \tag{154}$$

where we used that for radiation domination $a \propto \eta$ and $\partial_\eta a/a = 1/\eta$. At the end of BBN, when all reactions are inefficient, all net creation rates $\mathcal{J}_i$ vanish and we find that all number densities are simply rescaled by $1+\zeta$. Note that this could have been anticipated because for super-Hubble modes, ζ is equal to density perturbations on isocurvature surfaces (Vernizzi, 2005). Since abundances are ratios of number densities, they remain unchanged by the long mode perturbation. Hence, provided we can neglect the effect of modes which are smaller than the Hubble radius during BBN, standard adiabatic cosmological perturbations have no effect on BBN predictions. Intuitively, an adiabatic perturbation enhances baryon and photons number densities in the same proportions, leaving η constant. Since this analysis is based on long modes only, one cannot infer the consequences of fluctuations on scales smaller than the Hubble radius during BBN from the homogeneous cosmology results. For these small scales, only a complete treatment of all perturbed equations dictating the evolution of species can lead to a meaningful result.

Finally, it is worth noting that long modes of entropy perturbation, that is perturbations which do not modify the total energy density (and for which $\zeta = 0$) but which modify the ratios $\rho_\mathrm{b}/\rho_\gamma$ have an effect on abundances. Since during BBN the total energy density is dominated by radiation, and long mode entropy perturbation can be rephrased as a perturbation in ρ_b alone, that is a perturbation of η. As a consequence, its effect is directly evaluated by the sensitivity of BBN final abundances on η.

B. Measurement of baryon abundance from BBN

The observed abundances are related to the underlying one by an assumed normal distribution, that is for each isotope observed, the likelihood is

$$P(Y_i^\mathrm{obs}|Y_i) = \mathcal{N}\left[Y_i, \sigma_i^\mathrm{obs}\right](Y_i^\mathrm{obs})\,. \tag{155}$$

The observed values and their standard deviations are reported in § I.A. Then we can consider

$$P(Y_i^\mathrm{obs}|\omega_\mathrm{b}) \equiv \int \mathrm{d}Y_i P(Y_i^\mathrm{obs}|Y_i)P(Y_i|\omega_\mathrm{b})\,,$$

and we deduce using Eqs. (148) and (155) that it follows approximately a normal distribution

$$P(Y_i^\mathrm{obs}|\omega_\mathrm{b}) \simeq \mathcal{N}\left[\bar{Y}_i(\omega_\mathrm{b}), \Sigma_i(\omega_\mathrm{b})\right](Y_i^\mathrm{obs}) \tag{156}$$

with $\Sigma_i^2(\omega_\mathrm{b}) \equiv (\sigma_i^\mathrm{obs})^2 + \left[\sigma_i^\mathrm{th}(\omega_\mathrm{b})\right]^2$. In practice we do not use the approximation (148) and use instead the full result of our Monte-Carlo method to estimate the distribution of abundances due to reaction rates uncertainties. However, the results obtained are extremely similar given that (148) is a very good approximation.

If we then use an uniform prior on ω_b, that is if we do not use our knowledge from CMB observations, the posterior distribution for ω_b is immediately given from $P(\omega_\mathrm{b}|Y_i^\mathrm{obs}) \propto P(Y_i^\mathrm{obs}|\omega_\mathrm{b})$. Otherwise we use the CMB prior to build the posterior distribution for ω_b as

$$\begin{aligned} P(\omega_\mathrm{b}|Y_i^\mathrm{obs}, \mathrm{CMB}) &\propto P(Y_i^\mathrm{obs}, \omega_\mathrm{b}|\mathrm{CMB}) \\ &= P(Y_i^\mathrm{obs}|\omega_\mathrm{b})P(\omega_\mathrm{b}|\mathrm{CMB}). \end{aligned} \tag{157}$$

When including all observed abundances, we use that the total probability is the product of individual ones. In practice, only ^{4}He and ^{2}H are determined with enough precise experimental precision to be taken into account.

The CMB prior distribution and the posterior distribution from the observations of BBN are plotted in Fig. 27. The posterior bounds from BBN and CMB are $\Omega_\mathrm{b}h^2 = 0.02215 \pm 0.00014$, whereas from BBN alone on gets $\Omega_\mathrm{b}h^2 = 0.02190 \pm 0.00025$. Note that if we had used a code which predicts $\mathrm{D/H} \simeq 2.61 \times 10^{-5}$ instead of $\mathrm{D/H} \simeq 2.46 \times 10^{-5}$ for the Planck parameters, we would have obtained the constraint $\Omega_\mathrm{b}h^2 = 0.02271 \pm 0.00025$ from BBN alone, having exactly the same central value than found in Consiglio *et al.* (2017), using `PArthENoPE`.

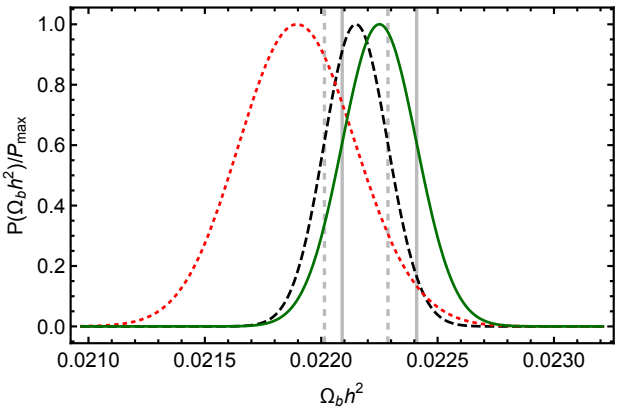

FIG. 27 $P(\Omega_\mathrm{b}h^2)$ normalized to a unit maximum. *Green continuous line :* CMB prior distribution. *Black dashed line* BBN posterior distribution (BBN+CMB). *Red dotted line :* baryon abundance distribution determined only from BBN. The vertical gray lines are the $\pm\sigma$ CMB (continuous) and CMB+BBN (dashed) bounds.

C. Neutrino chemical potential from BBN

If there is a neutrino asymmetry, that is a non-vanishing neutrino chemical potential, then for each flavor we have necessarily

$$\mu_\nu + \mu_{\bar\nu} = 0 \tag{158}$$

because of processes like $\nu + \bar\nu \leftrightarrow e^- + e^+ \leftrightarrow 2\gamma$ and photons have a vanishing chemical potential. Furthermore cosmological expansion affects only the particle momenta and $\xi_\nu \equiv \mu_\nu/T_\nu$ is frozen at its initial value, whose consequences on BBN can be investigated (Iocco *et al.*, 2009; Serpico and Raffelt, 2005; Simha and Steigman, 2008).

The neutrino asymmetry (defined for each neutrino flavor) is defined by the excess of neutrinos over antineutrinos as

$$\begin{aligned}\eta_\nu \equiv \frac{n_\nu - n_{\bar\nu}}{n_\gamma} &= \frac{I_+^{(1,1)}(0,\xi_\nu) - I_+^{(1,1)}(0,-\xi_\nu)}{2I_-^{(1,1)}} \\ &\simeq \frac{1}{12\zeta(3)}\left(\frac{T_\nu}{T}\right)^3 \left(\pi^2\xi_\nu + \xi_\nu^3\right). \end{aligned}\tag{159}$$

The neutrino oscillations imply that the various flavors must reach an equilibrium for which the chemical potentials are equal (Dolgov *et al.*, 2002; Wong, 2002). Assuming accordingly that the asymmetry is the same for all flavors, the first modification of the neutrino asymmetry is an excess of energy densities stored in neutrinos which can be absorbed by a redefinition of the number of neutrino generations N_ν as

$$\begin{aligned}\tilde N_\nu &= N_\nu\left(1 + \frac{I_+^{(2,1)}(0,\xi_\nu) + I_+^{(2,1)}(0,-\xi_\nu)}{2I_+^{(2,1)}}\right) \\ &\simeq N_\nu\left(1 + \frac{30\xi_\nu^2}{7\pi^2} + \frac{15\xi_\nu^4}{7\pi^4}\right). \end{aligned}\tag{160}$$

This effect is very small for small values of ξ_ν since it is at least quadratic in ξ_ν.

There is a second modification for the weak-interaction rates in which one must use instead of Eq. (75)

$$g_\nu(E) \equiv \begin{cases} g_\nu^+(E) \equiv \frac{1}{\mathrm{e}^{(E/T_\nu - \xi_\nu)}+1} & n \to p \text{ rates} \\ g_\nu^-(E) \equiv \frac{1}{\mathrm{e}^{(E/T_\nu + \xi_\nu)}+1} & p \to n \text{ rates}. \end{cases} \tag{161}$$

For instance in the definition (79) of $\chi_\pm$, one must use $g_\nu^\pm$ instead of g_ν. To show this we used that the Pauli-blocking factor of the antineutrino (resp. neutrino) is still related to the distribution of the neutrino (resp. antineutrino) according to (72) thanks to the property (158). This modification is the most important one and modifies the thermodynamical equilibrium ratio between neutrons and protons (A15) because from Eq. (A14) we get $\mu_n - \mu_p = -\mu_\nu$. We get that at thermodynamical equilibrium

$$\frac{n_n}{n_p} = \left.\frac{n_n}{n_p}\right|_{\xi_\nu=0} \times \mathrm{e}^{-\xi_\nu}, \tag{162}$$

and one expects a modification of the freeze-out abundance (for small ξ_ν) of order

$$\frac{\Delta Y_n^F}{Y_n^F} \simeq \frac{\Delta Y_\mathrm{P}}{Y_\mathrm{P}} \simeq -(1 - Y_n^F)\xi_\nu. \tag{163}$$

Finally there is a third modification when one considers the effect of incomplete neutrino decoupling (Grohs *et al.*, 2017) but this is negligible since the effect without the asymmetry is already very small. For small ξ_ν we find the abundance modifications

$$\frac{\Delta Y_\mathrm{P}}{Y_\mathrm{P}} \simeq -0.96\,\xi_\nu \tag{164a}$$

$$\frac{\Delta \mathrm{D/H}}{\mathrm{D/H}} \simeq -0.53\,\xi_\nu \tag{164b}$$

$$\frac{\Delta^3\mathrm{He/H}}{^3\mathrm{He/H}} \simeq -0.18\,\xi_\nu \tag{164c}$$

$$\frac{\Delta^7\mathrm{Li/H}}{^7\mathrm{Li/H}} \simeq -0.62\,\xi_\nu. \tag{164d}$$

The modification of Y_P is in very good agreement with the estimation (163) since $(1 - Y_n^F) \simeq 0.92$. Since BBN has no free parameter when assuming non-degenerate neutrinos ($\xi_\nu = 0$), the observational constraints on Y_P and D/H can be used to obtain bounds on the degeneracy parameter ξ_ν if we consider instead that it is unknown.

We repeat the analysis of § VI.B, using the pair of cosmological parameters $(\omega_\mathrm{b}, \xi_\nu)$ instead of ω_b alone. However, we still assume that the CMB prior determines only ω_b. Again, for each species the uncertainty from nuclear rates $\sigma_i^\mathrm{th}(\omega_\mathrm{b}, \xi_\nu)$ is obtained from a Monte-Carlo method. The posterior distribution for $(\omega_\mathrm{b}, \xi_\nu)$ from BBN combined with CMB is plotted in Fig. 28. Once marginalized over baryon abundance we get

$$\xi_\nu = 0.001 \pm 0.016, \tag{165}$$

which is a much tighter constraint than the constraints from CMB alone (Oldengott and Schwarz, 2017, $\xi_\nu = -0.002^{+0.053}_{-0.060}$) or than earlier BBN constraints such as Simha and Steigman (2008, $\xi_\nu = 0.037 \pm 0.026$), thanks to the recent improvement on both deuterium and ^{4}He abundance measurements.

Even though the bounds (165) are tighter, they are also surprisingly still highly compatible with a vanishing neutrino chemical potential. Since we find $|\xi_\nu| < 0.016\,(68\%\,\mathrm{CL})$, it corresponds to $(\tilde N_\nu - N_\nu)/N_\nu < 0.011\%$ and $\eta_\nu < 4.0 \times 10^{-3}$.

Note that if we had used `Parthenope` (Pisanti *et al.*, 2008), as is the case in Ade *et al.* (2016), which predicts $\mathrm{D/H} \simeq 2.61 \times 10^{-5}$ rather than $\mathrm{D/H} \simeq 2.46 \times 10^{-5}$ for Planck parameters, we would have found rather $\xi_\nu = 0.021 \pm 0.016$ less compatible with a vanishing neutrino chemical potential. Indeed, in our case the observed value for Y_P (resp. D/H) is lower (resp. higher) than the averaged value inferred from the CMB measured baryon abundance, and given the linearized dependences (164)

which have the same sign, this results in a compensation and a central value very close to zero. However if the prediction for deuterium from a BBN code is also above its observed value, then both $Y_{\rm P}$ and D/H tend to favor a positive ξ_ν.

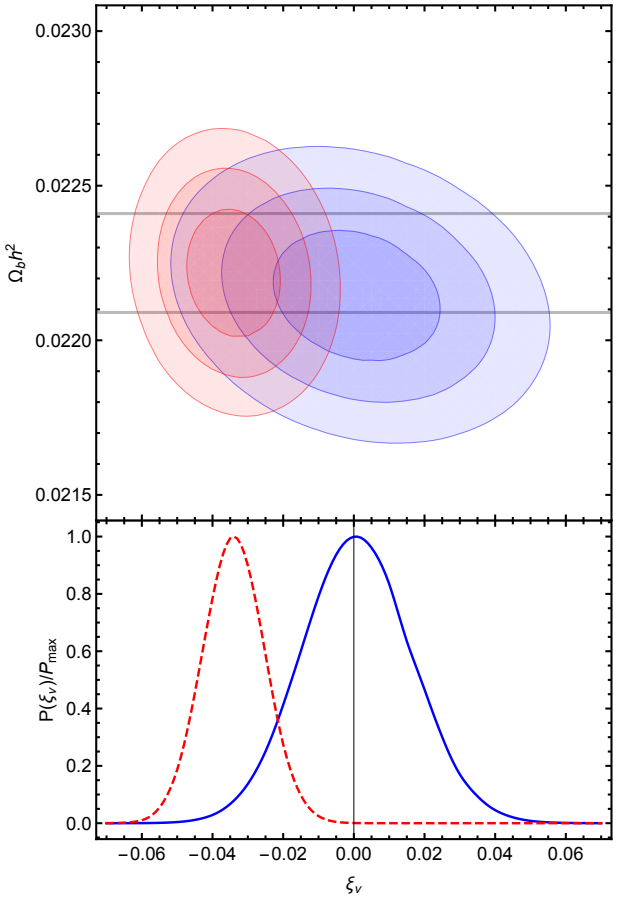

FIG. 28 *Top :* $P(\Omega_{\rm b}h^2, \xi_\nu)$ with 68.27%, 95.45% and 99.73% contours. *Blue :* using the ^{4}He bounds (4). *Red :* using the bounds $Y_{\rm P} = 0.2551 \pm 0.0022$ of Izotov *et al.* (2014). The gray horizontal bars are the $\pm\sigma$ CMB constraints on baryon abundance. *Bottom :* marginalized distribution for ξ_ν. Continuous line uses (4) whereas the dashed line uses the bounds $Y_{\rm P} = 0.2551 \pm 0.0022$ of Izotov *et al.* (2014).

D. Number of neutrinos

We repeat the analysis of § VI.B but for the pairs of cosmological parameters $(\Omega_{\rm b}h^2, N_\nu)$ instead of the baryon abundance alone. We use the CMB prior $P(\Omega_{\rm b}h^2, N_\nu|{\rm CMB})$ obtained from the Monte-Carlo Markov chains `base_nnu_plikHM_TTTEEE_lowTEB` of Ade *et al.* (2016) (TT+TE+EE+lowP analysis). The constraints from CMB are given directly in terms of $N_{\rm eff}$ (see § II.G) since they are obtained as the model-independent gravitational contribution of relativistic degrees of freedom. However, during BBN the effective number of neutrinos evolves as can be seen in Fig. 10, and this evolution is model-dependent. We assume that if there are extra relativistic degrees of freedom, they do not share any of the energy which is brought to neutrinos by incomplete decoupling. Hence for these extra neutrinos, or what is described phenomenologically as extra neutrinos, $z_\nu = 1$ throughout BBN. Given these assumptions Eq. (66) which was derived for $N_\nu = 3$ becomes

$$N_{\rm eff} = 3\left(\frac{z_\nu z^{\rm stand}}{z}\right)^4 + (N_\nu - 3)\left(\frac{z^{\rm stand}}{z}\right)^4, \quad (166)$$

from which we deduce in particular that $\mathrm{d}N_{\rm eff}/\mathrm{d}N_\nu = \left(z^{\rm stand}/z\right)^4 \simeq 1.0090$. In fact, this relation is unchanged as long as the energy exchange between the plasma and the neutrino sector remains identical to Eq. (60), that is if the function $\mathcal{N}(T)$ is unchanged. More generally the effective number of neutrinos is insensitive to any type of neutrino spectral distortions which leaves the total neutrino energy density unchanged. Hence, as long as the energy transfer with the plasma is the same, we can also assume that the new neutrino degrees of freedom share a part of the energy transfer during the incomplete decoupling phase, and still use Eq. (166). This relation allows to convert the distribution $P(\Omega_{\rm b}h^2, N_{\rm eff}|{\rm CMB})$ into $P(\Omega_{\rm b}h^2, N_\nu|{\rm CMB})$. This approach is different from the one chosen by Cyburt *et al.* (2016) where Eq. (66) is assumed to hold even for $N_\nu \neq 3$. However, given the rather large observational bounds on N_ν obtained, and the smallness of z_ν^4, this difference in the conversion of neutrino numbers is not crucial.

The posteriors obtained are depicted in Fig. 29. They are to be compared with the plots of Cyburt *et al.* (2016, Fig. 10). Furthermore, it presents a significant improvement compared to Cooke *et al.* (2018, Fig. 7) thanks to the inclusion of the measured $Y_{\rm P}$ in the BBN constraint. We used the full results of the chains for the CMB prior, but it can be very well represented by a two-dimensional Gaussian distribution with $\Omega_{\rm b}h^2 = 0.022197 \pm 0.000245$, $N_\nu = 2.945 \pm 0.203$ and a rather strong correlation coefficient $r = 0.7699$, since this approximation affects only marginally the posteriors obtained. Once marginalized over baryon abundance, the constraints on the numbers of neutrinos are

$$N_\nu = \begin{cases} 2.95 \pm 0.20 & {\rm CMB} \\ 2.88 \pm 0.27 & {\rm BBN} \\ 3.01 \pm 0.15 & {\rm BBN + CMB.} \end{cases} \quad (167)$$

As for the marginalized baryon abundances we get

$$100 \times \Omega_{\rm b}h^2 = \begin{cases} 2.220 \pm 0.025 & {\rm CMB} \\ 2.168 \pm 0.055 & {\rm BBN} \\ 2.216 \pm 0.022 & {\rm BBN + CMB.} \end{cases} \quad (168)$$

Note that if we had used a code which predicts D/H $\simeq 2.61 \times 10^{-5}$ instead of D/H $\simeq 2.46 \times 10^{-5}$ for the Planck

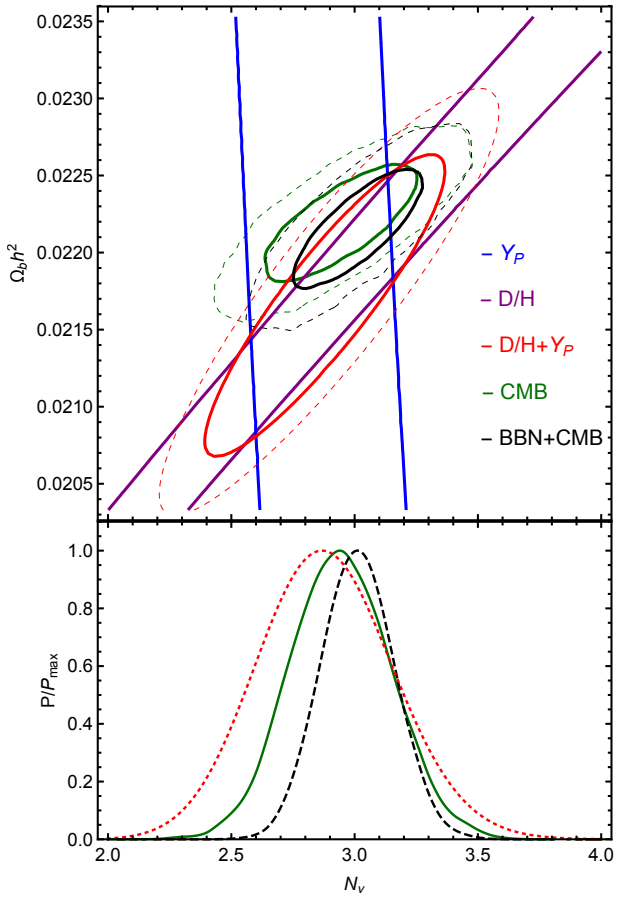

FIG. 29 Top : $P(\Omega_b h^2, N_\nu)$. with 68.27% and 95.45% contours for different combinations of data. Bottom : $P(N_\nu)$ from marginalization. Continuous green is from CMB only, dotted red from BBN only, and dashed black is the combination of BBN and CMB. Note that the average value of N_ν for the combination of BBN and CMB is not between the corresponding averages obtained from CMB and BBN considered separately. There is no contradiction since the nearly elliptic preferred regions in the $(\Omega_b h^2, N_\nu)$ space for BBN and CMB taken separately overlap away from the line defined by their respective average points.

parameters, we would have obtained $N_\nu = 2.84 \pm 0.27$ from BBN alone, corresponding to $N_{\rm eff} = 2.88 \pm 0.27$, whose central value is similar to the one obtained in Consiglio *et al.* (2017, Eq. 26). Since we use consistently the CMB prior $P(\Omega_b h^2, N_\nu|{\rm CMB})$ when obtaining constraints from BBN and CMB, we cannot compare our results with those of Consiglio *et al.* (2017) in that case, since they use only a CMB prior on $\Omega_b h^2$.

Conclusion

It is widely acknowledged that Cosmology has entered in the "precision era"; this should also apply to big bang nucleosynthesis. For both D and ^{4}He isotopes the precision on the abundances deduced from observations have reached the percent level. The precision on primordial D abundance prediction by BBN codes is now limited to a few percents because of the uncertainties on the D(p,γ)^{3}He, D(d,n)^{3}He and D(d,p)^{3}H thermonuclear reaction rates (Coc *et al.*, 2015; Di Valentino *et al.*, 2014). Ongoing experiments (Gustavino, 2017) from LUNA at the Gran Sasso underground facility, supplemented by theoretical works (Marcucci *et al.*, 2016) are expected to improve the situation. Here, we concentrated on the prediction of ^{4}He primordial abundance. Uncertainties on $Y_{\rm P}$ related to experimental data come from the neutron lifetime 879.5 ($\pm$0.8) s (but that may be affected by systematic uncertainties (Patrignani and Particle Data Group, 2016 and 2017 update)), leading to a $\Delta Y_{\rm P}^{(4)} = 1.7$ (Eq. 7) uncertainties and from the ^{1}H(n,γ)^{2}H, D(d,n)^{3}He and D(d,p)^{3}H reaction rates ($\sim$1% factor uncertainty (Ando *et al.*, 2006; Gómez Iñesta *et al.*, 2017)) leading to $\Delta Y_{\rm P}^{(4)} \lesssim 0.5$ in total (Eq. 143). These uncertainties are small, compared with the observational uncertainty of $\Delta Y_{\rm P}^{(4)} = 40$ (Eq. 4). However, the predicted ^{4}He primordial abundance includes corrections to the "bare" weak rates: zero–temperature radiative corrections, finite nucleon mass corrections, finite temperature radiative corrections, weak-magnetism, QED plasma effects and incomplete neutrino decoupling that, in total, shift the abundance by $\delta Y_{\rm P}^{(4)} = 44.7$ (Table V), i.e. larger than the uncertainties.

It is thus of the utmost importance to precisely calculate all these corrections, in order to limit theoretical uncertainties. Here, they are for the first time all included and calculated in a self consistent way allowing to take into account the correlations between them. In addition, it was verified that all satisfy detailed balance, a crucial point since it directly affects the neutron/proton number ratio, and hence the ^{4}He abundance. Table V details the contributions of these corrections to the ^{4}He, D, ^{3}He and ^{7}Li primordial abundance. We did not calculate the effect of incomplete neutrino decoupling, but use the results of Pisanti *et al.* (2008). This amounts to ignoring the spectral distortions, but this affects $Y_{\rm P}^{(4)}$ by approximately less than one unit. However we find results for incomplete neutrino decoupling effects which are very similar to Grohs *et al.* (2016), and most notably we find a coherence on the sign of light element abundances variations which is different from Mangano *et al.* (2005). Given the coupling we find with finite nucleon mass effect, this is the very last correction which requires careful evaluation to fully settle the weak rates corrections.

In this work, we have been using a network of $\approx$400 nuclear reactions (and their reverse), from neutron to sodium to encompass the light element big bang nucleosynthesis up to the CNO isotopes (Coc *et al.*, 2012). We used the most up to date reaction rates, and in particular those involved in deuterium production (Gómez Iñesta *et al.*, 2017; Iliadis *et al.*, 2016), but even more impor-

tant, the weak rates with their carefully calculated corrections. Hence, we claim that our predicted abundances (Table VII) are the most accurate to date, not only for D, ^{3}He, ^{7}Li and CNO isotopes but also for ^{4}He. Our predicted deuterium and ^{4}He primordial abundances are in agreement with observations, within error bars (Fig. 26 and Table VIII), and in particular, there is no need for extra relativistic degrees of freedom (i.e. $N_\nu > 3$). Our predicted lithium abundance remains a factor of $\approx$3 above the Spite plateau. The solution of this problem probably involves several mechanisms including stellar depletion and possibly some physics beyond the standard model. Finally, our prediction of CNO abundance (Table VII) does not completely rule out the possibility that they may influence the evolution of some of the first, Population III, stars (Ekström *et al.*, 2008).

Last, but not least, we provide at `http://www2.iap.fr/users/pitrou/primat.htm`, a freely available *Mathematica* code that includes all the physics discussed in this work. We expect that it will be used and hopefully modified in order to include new physics (see e.g. Iocco *et al.* (2009); Mathews and Kusakabe (2017)), or just to update some reaction rates [20].

Acknowledgments

We are indebted to our collaborators on these topics: Pierre Descouvemont, Brian Fields, Stéphane Goriely, Faïrouz Hammache, Christian Iliadis, Keith Olive, Patrick Petitjean. C.P. thanks A. Sirlin and W. J. Marciano for discussions on radiative corrections and neutron lifetime, D. Seckel for comments on (Seckel, 1993), and G. Lavaux for discussions on Bayesian inference. We also thank warmly Monique and François Spite for their kind help regarding the Lithium data, and Maxim Pospelov for discussions on radiative corrections.

Appendix A: Thermodynamics

1. Thermodynamical quantities

From the distribution function of a given species, it is possible to define macroscopic quantities such as number density n, energy density ρ, and pressure P. Due to the isotropy of the FL spacetime, the distribution function depends only on the magnitude of spatial momenta, that is it is of the form $f(t,p)$. Furthermore isotropy implies that there is no anisotropic stress. Omitting the time dependence to alleviate the notation, we define

$$n = g\int f(p)\frac{4\pi p^2 \mathrm{d}p}{(2\pi)^3} \tag{A1a}$$

$$\rho = g\int f(p)E\frac{4\pi p^2 \mathrm{d}p}{(2\pi)^3} \tag{A1b}$$

$$P = g\int f(p)\frac{p^2}{3E}\frac{4\pi p^2 \mathrm{d}p}{(2\pi)^3} \tag{A1c}$$

with $E=\sqrt{p^2+m^2}$ and g the number of spin degrees of freedom of the species considered ($g=1$ for neutrinos and $g=2$ for all other species). Using $E\mathrm{d}E = p\mathrm{d}p$, and given that both Fermi-Dirac and Bose-Einstein distributions are given as functions of E and not p, it is often more convenient to rewrite these expressions as

$$n = \frac{g}{2\pi^2}\int f(E)pE\mathrm{d}E \tag{A2a}$$

$$\rho = \frac{g}{2\pi^2}\int f(E)pE^2\mathrm{d}E \tag{A2b}$$

$$P = \frac{g}{6\pi^2}\int f(E)p^3\mathrm{d}E \tag{A2c}$$

with $p=\sqrt{E^2-m^2}$.

Bose-Einstein and Fermi-Dirac with statistical physics convention for chemical potential are defined as

$$g^{\pm}_{T,\mu}(E) \equiv \frac{1}{\mathrm{e}^{\frac{E-\mu}{T}}\pm 1} \tag{A3}$$

with upper (lower) sign for fermions (bosons). For these distributions we find from Eqs. (A2)

$$n(t) = \frac{gT^3}{2\pi^2}I^{(1,1)}_{\pm}(x,\xi) \tag{A4a}$$

$$\rho(t) = \frac{gT^4}{2\pi^2}I^{(2,1)}_{\pm}(x,\xi) \tag{A4b}$$

$$P(t) = \frac{gT^4}{6\pi^2}I^{(0,3)}_{\pm}(x,\xi) \tag{A4c}$$

with $x\equiv m/T$ and $\xi\equiv\mu/T$ and the integrals

$$I^{(m,n)}_{\pm}(x,y) = \int_x^\infty \frac{u^m(u^2-x^2)^{n/2}}{\mathrm{e}^{u-y}\pm 1}\mathrm{d}u\,, \tag{A5a}$$

$$= \int_0^\infty \frac{(v^2+x^2)^{(m-1)/2}v^{n+1}}{\mathrm{e}^{\sqrt{v^2+x^2}-y}\pm 1}\mathrm{d}v\,. \tag{A5b}$$

When the chemical potential can be neglected ($\xi \ll 1$) we also use the notation

$$I^{(m,n)}_{\pm}(x) \equiv I^{(m,n)}_{\pm}(x,0)\,. \tag{A6}$$

Finally when the mass can also be neglected ($x \ll 1$) we define

$$I^{(m,n)}_{\pm} \equiv I^{(m,n)}_{\pm}(0,0)\,, \tag{A7}$$

whose most useful values are reported in table IX. When

[20] They can be provided in tabular form, in a format similar to the Starlib one (Sallaska *et al.*, 2013) at `https://starlib.github.io/Rate-Library/`, or as (possibly parameter dependent) analytical formulae.

TABLE IX Integrals involved in the expressions of thermodynamical quantities when $x \ll 1$ and $\xi \ll 1$.

	Bosons (−)	Fermions (+)
$I_{\pm}^{(0,1)}$	$\pi^2/6$	$\pi^2/12$
$I_{\pm}^{(1,1)}$	$2\zeta(3)$	$3\zeta(3)/2$
$I_{\pm}^{(2,1)}$	$\pi^4/15$	$7\pi^4/120$
$I_{\pm}^{(0,3)}$	$\pi^4/15$	$7\pi^4/120$

the temperature is much smaller than the mass of the particles, that is for $x = m/T \gg 1$, we find the approximate relations

$$n \simeq gT^3 \left(\frac{x}{2\pi}\right)^{3/2} \mathrm{e}^{\xi - x} \tag{A8a}$$

$$\rho \simeq \left(m + \frac{3}{2}T\right) n\,. \tag{A8b}$$

2. Chemical potential of electrons

In chemical equilibrium $\mu_{e^-} = -\mu_{e^+} \equiv \mu_e$ because of reactions $2\gamma \leftrightarrow e^+ + e^-$. Hence the net negative charge density in electrons and positrons is

$$n_{e^-} - n_{e^+} = \frac{2T^3}{2\pi^2}\left[I_+^{(1,1)}(x,\xi) - I_+^{(1,1)}(x,-\xi)\right] \tag{A9}$$

with $x \equiv m_e/T$ and $\xi \equiv \mu_e/T$. The chemical potential of electrons and positrons must adapt to ensure the electric neutrality of the Universe, hence it is constrained by

$$n_{e^-} - n_{e^+} = n_p\,. \tag{A10}$$

Let us estimate the chemical potential at the end of BBN for simplicity. Indeed, since ξ increases with time, it is enough to check that its final value at the end of BBN is small. We use therefore the final value of baryon-to-photon ratio η [defined in Eq. (36)] and use that the baryonic matter is essentially in protons and ^{4}He nuclei. We find

$$n_{e^-} - n_{e^+} = (1 - Y_{\mathrm{P}}/2)\eta_0\, \bar{n}_\gamma T^3\,. \tag{A11}$$

In that limit, the electric charge density of electrons and positrons is given by

$$n_{e^-} - n_{e^+} \simeq 4T^3 \left(\frac{x}{2\pi}\right)^{3/2} \mathrm{e}^{-x} \sinh\xi\,. \tag{A12}$$

Combining these two equations we obtain

$$\xi \simeq \mathrm{Arcinsh}\left(\frac{\eta(1 - Y_{\mathrm{P}}/2)\mathrm{e}^x\sqrt{2}\zeta(3)}{\sqrt{\pi}x^{3/2}}\right). \tag{A13}$$

The evolution of the electrons chemical potential is depicted in Fig. 30. $\xi = \mu_e/T$ stays much below 10^{-5} whenever $T > 5\times10^8$K. For lower temperatures, ξ rises but it is only because electron-positron annihilations are nearly complete and the chemical potential adapts so that the relic density of electrons is equal to the number of protons. That is, whenever the chemical potential of electrons rises at low temperature, the amount of electrons is insignificant due to the low value of the baryon to photon ratio. Hence for all practical purposes, from Eq. (20) we deduce that whenever there is no heat exchange with the neutrinos, the total entropy of the plasma is conserved, that is $\dot{S}_{\mathrm{pl}} = \mathrm{d}(s_{\mathrm{pl}}a^3)/\mathrm{d}t = 0$.

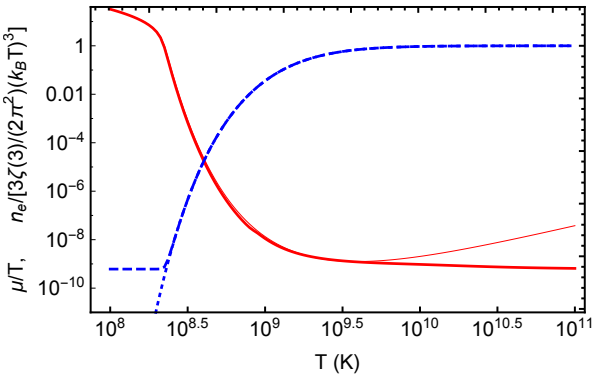

FIG. 30 *Continuous red lines* : Thick line is μ_e/T computed exactly from Eq. (A10), thin line is the approximation (A13). *Dashed blue line* : $2\pi^2/[3\zeta(3)]\, n_e/(k_BT)^3$ with the chemical potential taken into account. *Dotted blue line* : $2\pi^2/[3\zeta(3)]\, n_e/(k_BT)^3$ with vanishing chemical potential.

3. Nucleons at thermodynamical equilibrium

The chemical potential of neutrons and protons are not negligible individually, and they are constrained to give the number density in the low temperature limit (A8a). However the difference $\mu_n - \mu_p$ is negligible with respect to T. Indeed we can neglect $\xi_e \equiv \mu_e/T$ (see § A.2) and assuming it is also the case for neutrinos (see §VI.C for degenerate neutrinos), and given that at equilibrium we have necessarily

$$\mu_n + \mu_\nu = \mu_p + \mu_e \quad \Rightarrow \quad \mu_n - \mu_p = \mu_e - \mu_\nu\,, \tag{A14}$$

then we deduce $\mu_n - \mu_p \ll 1$.

Hence from (A8a) we obtain that the neutron to proton ratio is

$$\frac{n_n}{n_p} = \left(\frac{m_n}{m_p}\right)^{3/2} \mathrm{e}^{-\frac{\Delta}{T}} \simeq \mathrm{e}^{-\frac{\Delta}{T}}\left(1 + \frac{3\Delta}{2m_N}\right). \tag{A15}$$

It is possible to determine the chemical potential of neutrons and protons from the expression (A8a) and the baryon-to-photon number ratio η. For instance for protons, we must have

$$\bar{n}_p \equiv \frac{n_p}{T^3} = 2\left(\frac{x_p}{2\pi}\right)^{3/2} \mathrm{e}^{\xi_p - x_p} = \eta\frac{n_p}{n_{\mathrm{b}}}\bar{n}_\gamma = Y_p\eta\bar{n}_\gamma \tag{A16}$$

with $x_p \equiv m_p/T$ and $\xi_p = \mu_p/T$, which can be used to solve for ξ_p. In particular the distribution function of protons is approximately given by

$$f_p(p) \simeq \mathrm{e}^{\frac{\mu_p - E}{T}} \simeq \exp\left(\xi_p - x_p - \frac{p^2}{2m_pT}\right) \tag{A17}$$

and thus it is approximated by the Maxwellian distribution

$$\begin{aligned} f_p(p) &\simeq \frac{n_p}{2}\left(\frac{2\pi}{m_pT}\right)^{3/2} \exp\left(-\frac{p^2}{2m_pT}\right) \\ &\simeq Y_p \frac{\eta\zeta(3)\sqrt{8}}{\sqrt{\pi}}\left(\frac{T}{m_p}\right)^{3/2} \exp\left(-\frac{p^2}{2m_pT}\right). \end{aligned} \tag{A18}$$

From this last equation we deduce that $f_p(p) \ll 1$, justifying that we neglect Pauli-blocking effects in reactions rates for protons (and similarly for neutrons).

The distribution function for an isotope i is exactly similar with the obvious replacement $Y_p \to Y_i$, $n_p \to n_i$ and $m_p \to m_i$. The distribution of velocities is defined as (omitting the i index of the isotope considered)

$$\phi_{\rm MB}(v)\mathrm{d}v \equiv \frac{1}{n}\frac{\mathrm{d}n}{\mathrm{d}p}\mathrm{d}p = \frac{2}{n}f(p)\frac{4\pi p^2 \mathrm{d}p}{(2\pi)^3}, \tag{A19}$$

where $mv = p$, and using the kinetic energy $E \equiv \frac{1}{2}mv^2 \Rightarrow \mathrm{d}E = mv\mathrm{d}v$, it takes the form given in Eq. (123).

4. Abundances at nuclear statistical equilibrium

At nuclear statistical equilibrium (NSE), a given isotope i is at chemical equilibrium with its nucleons, hence the relation between chemical potentials

$$\mu_i = Z_i\mu_p + (A_i - Z_i)\mu_n\,. \tag{A20}$$

From Eq. (A8a)

$$n_i = g_i\left(\frac{m_iT}{2\pi}\right)^{3/2}\mathrm{e}^{\xi_i - x_i}, \quad g_i \equiv 2s_i + 1\,, \tag{A21}$$

where s_i is the spin of species i. Using Eq. (A20) and (A21), we get

$$\begin{aligned} n_i^{\rm NSE} &= \frac{g_i m_i^{3/2}}{2^{A_i}}\left(\frac{n_p}{m_p^{3/2}}\right)^{Z_i}\left(\frac{n_n}{m_n^{3/2}}\right)^{A_i - Z_i} \\ &\times \left(\frac{2\pi}{T}\right)^{\frac{3(A_i-1)}{2}} \mathrm{e}^{B_i/T} \end{aligned} \tag{A22}$$

where we defined the binding energy

$$B_i \equiv Z_i m_p + (A_i - Z_i)m_n - m_i\,. \tag{A23}$$

Using (36), the abundances are then given at NSE by

$$\begin{aligned} Y_i^{\rm NSE} &= g_i\zeta(3)^{A_i-1}2^{\frac{3A_i-5}{2}}\pi^{\frac{1-A_i}{2}}\left(\frac{m_iT^{A_i-1}}{m_p^{Z_i}m_n^{A_i-Z_i}}\right)^{3/2} \\ &\times \eta^{A_i-1}Y_p^{Z_i}Y_n^{A_i-Z_i}\mathrm{e}^{B_i/T}\,. \end{aligned} \tag{A24}$$

We check in particular that for neutrons and protons $B_n = B_p = 0$ and $A_n = A_p = 1$, so we get the tautological relation $Y_n^{\rm NSE} = Y_n$ and $Y_p^{\rm NSE} = Y_p$. In order to obtain the NSE values from (A24), we use Audi *et al.* (2017) for the masses and spins of nuclear elements. In Fig. 31, we plot jointly the abundances of the main isotopes together with their NSE values to check that they are equal at high temperatures.

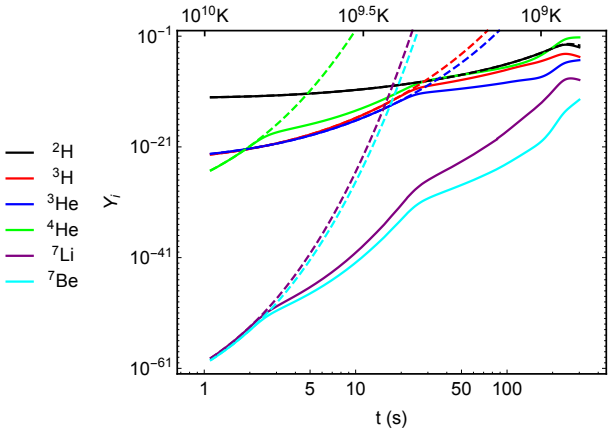

FIG. 31 Evolution of the first elements abundances in solid lines, together with the nuclear statistical equilibrium values in dashed lines. The deuterium abundance stays very close to its NSE value until the time it is more efficiently destroyed than formed around $t \simeq 200\,$s.

Appendix B: Weak reactions rates

In this section, we gather all the technicalities required to obtain the theoretical forms of the weak-rates including the most relevant corrections.

1. General expressions

Let us consider first the reactions with neutrons in the initial state. Throughout this section we use the mostly minus metric signature since it is the most common in particle physics. The general expression for each of the three reactions involved is of the form (Fidler and Pitrou, 2017; Lopez *et al.*, 1997)

$$\begin{aligned} n_n\Gamma = \int \Pi_i[\mathrm{d}^3\mathbf{p}_i](2\pi)^4\delta^4\left(\underline{p}_n - \underline{p}_p + \alpha_\nu\underline{p}_\nu + \alpha_e\underline{p}_e\right) \\ \times |M|^2 f_n(E_n)[1 - f_p(E_p)]f_\nu(\alpha_\nu E_\nu)f_e(\alpha_e E_e) \end{aligned} \tag{B1}$$

where the $\underline{p}_i$ with $i = n, p, e, \nu$ are the four-momenta of particles, and we used the compact notation for the relativistic volume element

$$[\mathrm{d}^3\mathbf{p}] \equiv \frac{\mathrm{d}^3\mathbf{p}}{2E(2\pi)^3} = \frac{4\pi p^2\mathrm{d}p}{2E(2\pi^3)}\,. \tag{B2}$$

The factor α_ν is $+1$ if the neutrino is in the initial state and -1 otherwise with a similar definition for α_e and the electron or positron. In (B1), it is apparent that the Dirac function ensures energy and momentum conservation. For a Fermi-Dirac distribution

$$g(-E) = 1 - g(E)\,, \tag{B3}$$

implying that the coefficients α_e, α_ν also ensure that either it is the distribution function which appears if the lepton is in the initial state, or the Pauli-blocking factor if it is in the final state.

A first simplification consists in neglecting the Pauli-blocking factor of the final state proton due to the very low value of the baryon-to-photon ratio [see Eq. (A18)]. Having no dependence on the distribution function of the final protons, we can simplify Eq. (B1) further by performing the integral on spatial momenta of protons, using the spatial part of the Dirac function. The reaction rates reduces to

$$\begin{aligned} n_n\Gamma \;=\; & \int \frac{\mathrm{d}^3\mathbf{p}_n \mathrm{d}^3\mathbf{p}_e \mathrm{d}^3\mathbf{p}_\nu}{2^4(2\pi)^8}\delta\left(E_n - E_p + \alpha_e E_e + \alpha_\nu E_\nu\right) \\ & \times \frac{|M|^2}{E_n E_p E_e E_\nu} f_n(E_n) f_\nu(\alpha_\nu E_\nu) f_e(\alpha_e E_e) \end{aligned} \tag{B4}$$

where the proton momentum and energies are related by

$$\mathbf{p}_p = \mathbf{p}_n + \alpha_\nu \mathbf{p}_\nu + \alpha_e \mathbf{p}_e\,, \quad E_p = \sqrt{\mathbf{p}_p \cdot \mathbf{p}_p + m_p^2}\,. \tag{B5}$$

For a given reaction, $|M|^2$ is the corresponding matrix-element of the weak interaction summed over all initial and final states, computed from the interaction Hamiltonian. For the reactions (68), the relevant part of the interaction Hamiltonian is a coupling of weak currents in the form

$$\mathcal{H}_I = \frac{G_F}{\sqrt{2}} J^\mu_{e\nu} J_{pn,\,\mu} \tag{B6}$$

where G_F is the Fermi constant. The electron-neutron weak current is purely left chiral, and of the form

$$J^\mu_{e\nu} = \bar{\boldsymbol{\nu}}\gamma^\mu(1-\gamma^5)\mathbf{e}\,. \tag{B7}$$

$\mathbf{e}$ and $\boldsymbol{\nu}$ are the fermionic quantum fields of electrons and neutrinos, and the γ^μ are the matrices of the Clifford algebra [we use the conventions of (Fidler and Pitrou, 2017)]. The proton-neutron current is of the form (Ivanov *et al.*, 2013, Eqs. 1 and A2)

$$J^\mu_{pn} = \cos\theta_{\mathrm{C}} \bar{\mathbf{p}} \left(\gamma^\mu(1 - g_A\gamma^5) + \mathrm{i}\frac{f_{\mathrm{wm}}}{m_N} 2\Sigma^{\mu\nu} q_\nu \right) \mathbf{n} \tag{B8}$$

where $\mathbf{p}$ and $\boldsymbol{n}$ are the Fermionic quantum fields of protons and neutrons and $2\Sigma^{\mu\nu} \equiv \mathrm{i}/2(\gamma^\mu\gamma^\nu - \gamma^\nu\gamma^\mu)$. g_A is the axial current constant for nucleons (also sometimes written C_A/C_V or λ in the literature), and f_{wm} is the weak magnetism constant whose numerical value is given by (Horowitz, 2002; Horowitz and Li, 2000; Ivanov *et al.*, 2013)

$$f_{\mathrm{wm}} = \frac{\mu_p - \mu_n}{2} \simeq \frac{1.793 - (-1.913)}{2} \simeq 1.853\,. \tag{B9}$$

θ_{C} is the Cabbibo-Kobayashi-Maskawa (CKM) angle ($\cos\theta_{\mathrm{C}}$ also noted V_{ud} in the literature), q^μ is the nucleon four-momentum transfer, that is the difference between the final nucleon four-momentum and the initial one. The most recent numerical values for the constants in weak interactions are gathered in appendix D.

It is possible to show that from Eqs. (B6)-(B8) the matrix element is of the form [see e.g. (Fidler and Pitrou, 2017)]

$$\frac{|M|^2}{2^7 G_F^2} = c_{LL}\mathcal{M}_{LL} + c_{RR}\mathcal{M}_{RR} + c_{LR}\mathcal{M}_{LR} \tag{B10}$$

with the coupling factors

$$c_{LL} \;\equiv\; \frac{(1+g_A)^2}{4} \tag{B11a}$$

$$c_{RR} \;\equiv\; \frac{(1-g_A)^2}{4} \tag{B11b}$$

$$c_{LR} \;\equiv\; \frac{g_A^2 - 1}{4}\,. \tag{B11c}$$

If weak interactions for nucleons were purely left-chiral, that is with $g_A = 1$, only the $\mathcal{M}_{LL}$ would contribute. $\mathcal{M}_{RR}$ contains the contribution of the right-chiral part of the interaction, and $\mathcal{M}_{LR}$ is an interference between left and right chiral contributions.

Let us ignore first the contribution from weak-magnetism that are investigated further in § B.4. We then find

$$\mathcal{M}_{LL} \;=\; (\underline{p}_n \cdot \underline{p}_\nu)(\underline{p}_p \cdot \underline{p}_e) \tag{B12a}$$

$$\mathcal{M}_{RR} \;=\; (\underline{p}_n \cdot \underline{p}_e)(\underline{p}_p \cdot \underline{p}_\nu) \tag{B12b}$$

$$\mathcal{M}_{LR} \;=\; m_p m_n (\underline{p}_\nu \cdot \underline{p}_e)\,. \tag{B12c}$$

It is worth noting that all weak reactions (68) have in fact the same matrix element. First the three reactions with a neutron in the initial state are obtained by crossing symmetry. Crossing symmetry for the electron amounts for instance to the formal replacement $\underline{p}_e \to -\underline{p}_e$ with an overall minus sign (Fidler and Pitrou, 2017) and it is straightforward to check that this leaves the matrix element invariant. The same property arises obviously for neutrinos. Second, the three reverse reactions (with an initial proton and a final neutron) are obtained by time reversal, and since there is no CP violation at this level, there is also a time-reversal symmetry so as to ensure the CPT symmetry. Hence all reverse rates have exactly the same matrix element.

2. Fokker-Planck expansion

The integral in (B4) is 8-dimensional when one removes the Dirac function. Due to the isotropy of all distribu-

tions, this can be reduced to a 5-dimensional integral. This is the method followed by Lopez *et al.* (1997). Here we follow a much simpler route by performing a Fokker-planck expansion in the energy transferred in reactions. Even though our method is different from Seckel (1993), it follows a method which is similar in spirit. As we shall see, this results in one-dimensional integrals which are much faster to evaluate.

At low temperature, it is enough to assume that nucleons follow an isotropic Maxwellian distribution of velocities at the plasma temperature T given by Eq. (A18). Hence the following integrals are obtained

$$2\int f_N(\mathbf{p})\frac{\mathrm{d}^3\mathbf{p}}{(2\pi)^3} = n_N\,, \tag{B13a}$$

$$2\int f_N(\mathbf{p})\frac{p^i}{m_N}\frac{\mathrm{d}^3\mathbf{p}}{(2\pi)^3} = 0\,, \tag{B13b}$$

$$2\int f_N(\mathbf{p})\frac{p^ip^j}{m_N^2}\frac{\mathrm{d}^3\mathbf{p}}{(2\pi)^3} = \frac{T}{m_N}\delta^{ij}n_N\,. \tag{B13c}$$

In particular contracting with δ_{ij} we recover the expression for the pressure of nucleons in the low temperature limit

$$P_N = 2\int f_N(\mathbf{p})\frac{p^2}{3m_N}\frac{\mathrm{d}^3\mathbf{p}}{(2\pi)^3} = Tn_N\,. \tag{B14}$$

For electron or neutrino distributions, since we have assumed isotropy, we deduce the property

$$\int g(E)p^\alpha E^\beta p^ip^j\frac{\mathrm{d}^3\mathbf{p}}{(2\pi)^3} = \frac{\delta^{ij}}{3}\int g(E)p^{\alpha+2}E^\beta\frac{\mathrm{d}^3\mathbf{p}}{(2\pi)^3} \tag{B15}$$

where α and β are some numbers. From isotropy we also find that

$$\int g(E)p^\alpha E^\beta p^i\frac{\mathrm{d}^3\mathbf{p}}{(2\pi)^3} = 0\,. \tag{B16}$$

Hence for all practical purposes, we can perform the replacements

$$p^ip^j \to p^2\delta^{ij}/3\,,\qquad p^i\to 0\,. \tag{B17}$$

on all species, resulting in great simplifications.

We assess the importance of corrections to the Born approximations as explained in § III.G, that is in powers of $\epsilon \equiv T/m_N$. To evaluate the order of each term, we consider that the momentum or energies of neutrinos are of order $T\sim\Delta$, that is factors of the type E_e/m_N or E_ν/m_N are of order ϵ. Furthermore, from (B13) a factor $\mathbf{p}_n/m_n$ is of order $\sqrt{T/M}\sim\sqrt{\Delta/M}$ and thus $\sqrt{\epsilon}$. However since only even powers of the spatial momentum of nucleons must appear [see Eqs. (B13)], we shall encounter terms of the type $|\mathbf{p}_p/m_n^2|$ which are of order ϵ.

The Fokker-Planck expansion consists in expanding the energy difference between the nucleons, $E_n - E_p$ around the lowest order value $\Delta = m_n - m_p$. Keeping only the lowest corrections this expansion reads

$$E_n - E_p = \Delta + \delta Q_1 + \delta Q_2 + \delta Q_3 \tag{B18}$$

$$\delta Q_1 \equiv -\frac{\mathbf{p}_n\cdot\mathbf{q}}{m_N} \tag{B19a}$$

$$\delta Q_2 \equiv -\frac{|\mathbf{q}|^2}{2m_N} \tag{B19b}$$

$$\delta Q_3 \equiv \frac{|\mathbf{p}_n|^2}{2}\left(\frac{1}{m_n}-\frac{1}{m_p}\right) \simeq -\frac{|\mathbf{p}_n|^2\Delta}{2m_N^2}\,. \tag{B19c}$$

where $\mathbf{q}\equiv\mathbf{p}_p-\mathbf{p}_n = \alpha_\nu\mathbf{p}_\nu+\alpha_e\mathbf{p}_e$ is the spatial momentum transferred. The first term in (B18) is the lowest order, or Born approximation, that is the only appearing when considering the infinite nucleon mass approximation. The second term is an order $\sqrt{\epsilon}$ correction, and the third term is an order ϵ correction. Finally the last term is of order $T\Delta/m_N$ so it is an order ϵ correction as well. It is the only corrective term for which it is crucial to take into account the difference of mass between neutrons and protons. Using Eq. (B18), we expand the Dirac delta function on energies as

$$\delta\left(E_n-E_p+\alpha_eE_e+\alpha_\nu E_\nu\right)\simeq \tag{B20}$$
$$\delta(\Sigma)+\delta'(\Sigma)\left(\sum_{i=1}^{3}\delta Q_i\right)+\frac{1}{2}\delta''(\Sigma)(\delta Q_1)^2\,,$$

where $\Sigma\equiv\Delta+\alpha_eE_e+\alpha_\nu E_\nu$.

We must then expand the matrix element and the energies appearing in Eq. (B4). It proves much easier to expand all these contributions together. Furthermore, whenever a term is already of order ϵ, we know that it should multiply only the Born term of the expansion (B20), so we can apply the simplification rule (B17). With this method we find

$$\frac{\mathcal{M}_{LL}}{\Pi_iE_i} \to 1-\frac{\mathbf{p}_n}{m_N}\cdot\left(\frac{\mathbf{p}_e}{E_e}+\frac{\mathbf{p}_\nu}{E_\nu}\right)-\frac{\alpha_\nu|\mathbf{p}_\nu|^2}{m_NE_\nu} \tag{B21a}$$

$$\frac{\mathcal{M}_{RR}}{\Pi_iE_i} \to 1-\frac{\mathbf{p}_n}{m_N}\cdot\left(\frac{\mathbf{p}_e}{E_e}+\frac{\mathbf{p}_\nu}{E_\nu}\right)-\frac{\alpha_e|\mathbf{p}_e|^2}{m_NE_e} \tag{B21b}$$

$$\frac{\mathcal{M}_{LR}}{\Pi_iE_i} \to \left(1-\frac{|\mathbf{p}_n|^2}{m_N^2}\right)\left(1-\frac{\mathbf{p}_e\cdot\mathbf{p}_\nu}{E_eE_\nu}\right)\,. \tag{B21c}$$

The second term in Eqs. (B21a) and (B21b) is of order $\sqrt{\epsilon}$ and the last term in these equations is of order ϵ. Hence the second term needs to be coupled with the order $\sqrt{\epsilon}$ term in the Dirac delta expansion (B20) which is $\delta'(\Sigma)\delta Q_1$, and simplified with the rules (B17).

There are four steps to complete this Fokker-Planck expansion.

1. First, using Eqs. (B21) and (B20) in the reaction rates (B4) we perform the integral on the initial neutron momentum with the rules (B13).

2. Second, we can replace the differential elements for the integral on electron and neutrino momenta with $\mathrm{d}^3p \to 4\pi p^2 \mathrm{d}p$ because we have already performed all angular averages.

3. We are left with a two dimensional integral on the electron and neutrino momentum magnitudes $p_e = |\mathbf{p}_e|$ and $p_\nu = |\mathbf{p}_\nu|$. Let us note $E_\nu = p_\nu$ in order to write the result in a easily readable form. Third, we perform the integral on E_ν using the Dirac delta and their derivatives. Whenever a Dirac delta derivative appears, it means that we have to perform integration by parts to convert it into a normal Dirac delta. This will introduce derivatives with respect to the E_ν applied on the neutrino distribution function or Pauli-blocking factor. Also for a given reaction it might appear that the value of E_ν constrained by the Dirac delta is not physical for that reaction if $\alpha_\nu = 1$ and physical if $\alpha_\nu = -1$, or vice-versa. This is the reason why we consider the total reaction rate of the reactions (68a) and (68b). Once their rates are added, the Dirac delta automatically selects either the neutrino in the initial state, with the corresponding distribution function, or the neutrino in the final state, with the associated Pauli-blocking factor. Eventually once the rates (68a) and (68b) are added, we might forget about α_ν, that is about the position of the neutrino. We need only to compute two rates, one where the electrons is in the initial state [reaction (68c)], and one where it is a positron which is in the final state [the sum of reactions (68a) and (68b)].

4. Finally, we need to determine the procedure to convert the rate with a neutron in the initial state into the reverse rate with a proton in the initial state. Even if the matrix element is the same for all reactions, as explained in § B.1, the method to perform a finite mass expansion is not symmetric under the interchange $p \leftrightarrow n$. Indeed we chose to expand the momentum of the final nucleon around the initial one, and we remove the integral on the final nucleon momenta. It is apparent on Eqs. (B12) that the electron (resp. neutrino) momentum is contracted with the neutron (resp. proton) in the LL term but this is the opposite in the RR term. Since the coupling factors of these terms are interchanged by the replacement $g_A \to -g_A$, we can deduce the rates with an initial proton from those with an initial neutron using the rule $g_A \to -g_A$. Obviously the argument of the Dirac delta contains now $E_p - E_n = -\Delta + \dots$ instead of $E_n - E_p = \Delta + \dots$ so we must also apply the rule $\Delta \to -\Delta$. Finally when considering a reverse reaction, the electron in the initial state turns into a positron in the final state so we must also apply the rule $E_e \to -E_e$, that is change the electron distribution function to a Pauli-blocking factor or vice-versa. These are the rules used extensively in § III to deduce the reverse rates.

Having sketched the details of the procedure, we are in position to give the results. The Born approximation results are obvious under this expansion. From Eqs. (B21) we obtain in the limit

$$\frac{\mathcal{M}_{LL}}{\Pi_i E_i} \simeq \frac{\mathcal{M}_{RR}}{\Pi_i E_i} \simeq 1\,, \tag{B22a}$$

$$\frac{\mathcal{M}_{LR}}{\Pi_i E_i} \simeq \left(1 - \frac{\mathbf{p}_e \cdot \mathbf{p}_\nu}{E_e E_\nu}\right). \tag{B22b}$$

Furthermore in the Dirac expansion (B20) we keep only $\delta(\Sigma)$, and the average over electrons and neutrino spatial momenta removes the momentum dependent part of Eq. (B22b). The Born rates are gathered and commented in § III.B.

The first corrections in this Fokker-Planck expansion, and which are due to finite nucleon mass, are reported in the next section.

3. Finite nucleon mass corrections

The finite nucleon mass corrections take the form (114) [or (115) if radiative corrections are added]. The function $\chi_\pm^{\mathrm{FM}}$ is

$$\chi_{\pm}^{\rm FM}(E,g_A) \;=\; \tilde{c}_{LL}\frac{p^2}{m_N E}g_\nu(E_\nu^{\mp})g(-E) - \tilde{c}_{RR}\frac{E_\nu^{\mp}}{m_N}g_\nu^{(2,0)}(E_\nu^{\mp})g(-E) \tag{B23}$$
$$+\,(\tilde{c}_{LL}+\tilde{c}_{RR})\,\frac{T}{m_N}\left(g_\nu^{(2,1)}(E_\nu^{\mp})g(-E)\frac{p^2}{E} - g_\nu^{(3,1)}(E_\nu^{\mp})g(-E)\right)$$
$$+\,(\tilde{c}_{LL}+\tilde{c}_{RR}+\tilde{c}_{LR})\left[\frac{T}{2m_N}\left(g_\nu^{(4,2)}(E_\nu^{\mp})g(-E)+g_\nu^{(2,2)}(E_\nu^{\mp})g(-E)p^2\right)\right.$$
$$\left.+\frac{1}{2m_N}\left(g_\nu^{(4,1)}(E_\nu^{\mp})g(-E)+g_\nu^{(2,1)}(E_\nu^{\mp})g(-E)p^2\right)\right]$$
$$-\,(\tilde{c}_{LL}+\tilde{c}_{RR}+\tilde{c}_{LR})\,\frac{3T}{2}\left(1-\frac{m_n}{m_p}\right)g_\nu^{(2,1)}(E_\nu^{\mp})g(-E)$$
$$+\tilde{c}_{LR}\left[-\frac{3T}{m_N}g_\nu^{(2,0)}(E_\nu^{\mp})g(-E)+\frac{p^2}{3m_N E}g_\nu^{(3,1)}(E_\nu^{\mp})g(-E)+\frac{p^2T}{3m_N E}g_\nu^{(3,2)}(E_\nu^{\mp})g(-E)\right]$$

where $p=\sqrt{E^2-m_e^2}$, $E_\nu^{\mp}=E\mp\Delta$. We defined the reduced couplings

$$\tilde{c}_{LL} \;\equiv\; \frac{4}{1+3g_A^2}c_{LL} \tag{B24a}$$
$$\tilde{c}_{RR} \;\equiv\; \frac{4}{1+3g_A^2}c_{RR} \tag{B24b}$$
$$\tilde{c}_{LR} \;\equiv\; \frac{4}{1+3g_A^2}c_{LR}\,, \tag{B24c}$$

and the functions [with the notation (75)]

$$g_\nu^{(n,p)}(E_\nu) \equiv \frac{\partial^p[(E_\nu)^n g_\nu(E_\nu)]}{\partial E_\nu^p}\,. \tag{B25}$$

For the neutron beta decay, the expression (B23) for $T=0$ gives (with $E_\nu\equiv\Delta-E$ here)

$$\chi_{+}^{\rm FM}(E,g_A)\big|_{T=0} = \tilde{c}_{LL}\frac{p^2E_\nu^2}{m_N E}+\tilde{c}_{RR}\frac{E_\nu^3}{m_N} \tag{B26}$$
$$-\,(\tilde{c}_{LL}+\tilde{c}_{RR}+\tilde{c}_{LR})\,\frac{\left(2E_\nu^3+E_\nu p^2\right)}{m_N}+\tilde{c}_{LR}\frac{p^2E_\nu^2}{m_N E}\,.$$

4. Weak-magnetism corrections

Because the weak-magnetic term enters in the current (B8) with a factor q_ν/m_N, with the momentum transfer to nucleon being of the order of T, it is an order ϵ correction and thus vanishes at the Born approximation level. The matrix element is corrected by the addition of

$$\frac{|M|^2}{2^7G_F^2} \;\supset\; f_{\rm wm}g_A\frac{m_n+m_p}{2}\left(\mathcal{M}_{LL}-\mathcal{M}_{RR}\right) \tag{B27}$$
$$+\;\frac{f_{\rm wm}}{2}\left[\frac{m_n+m_p}{2}\left(\mathcal{M}_{LR}-\mathcal{M}_{LL}-\mathcal{M}_{RR}-(\underline{p}_n\cdot\underline{p}_p)(\underline{p}_\nu\cdot\underline{p}_e)\right)+m_p(\underline{p}_n\cdot\underline{p}_e)(\underline{p}_n\cdot\underline{p}_\nu)+m_n(\underline{p}_p\cdot\underline{p}_e)(\underline{p}_p\cdot\underline{p}_\nu)\right]$$

where we used the expressions (B12). It is possible to show, although rather tedious, that the contributions of the second line vanish at first order in ϵ. This remarkable simplification has been noticed earlier by Seckel (1993). Hence the weak-magnetism contributes exactly as the axial vector current coupled to the vector current. It is taken into account by changing the coupling constants (B11) to the values (119), modifying accordingly the constants (B24) appearing in the finite nucleon mass corrections.

Only the first two terms of Eq. (B23) can in principle contribute to λ_0 since weak-magnetism does no affect the

sum $c_{LL}+c_{RR}$ nor c_{LR}. However, it is straightforward to show that they result in a vanishing contribution since

$$\begin{aligned}\lambda_0^{\rm wm} &\propto \int_0^{\sqrt{\Delta^2-1}} {\rm d}pp^2(E-\Delta)^2\left(\frac{p^2}{E}+(E-\Delta)\right)\\ &= \tfrac{1}{3}\int_m^{\Delta}{\rm d}E\partial_E\left[(E-\Delta)^3(E^2-m^2)^{3/2}\right]\\ &= 0\,. \end{aligned} \tag{B28}$$

Note that when the weak-magnetism contribution is coupled with radiative corrections, this result is no longer valid and there is a small change in λ_0 that we give in § III.H.

5. Mandelstam variables

Let us define the Mandelstam variables for $\nu+n\to e+p$.

$$s \equiv (\underline{p}_\nu+\underline{p}_n)^2=(\underline{p}_e+\underline{p}_p)^2 \tag{B29a}$$

$$t \equiv (\underline{p}_\nu-\underline{p}_e)^2=(\underline{p}_n-\underline{p}_p)^2 \tag{B29b}$$

$$u \equiv (\underline{p}_\nu-\underline{p}_p)^2=(\underline{p}_n-\underline{p}_e)^2\,. \tag{B29c}$$

The total matrix element $|M|^2$ deduced from Eqs. (B6)-(B8), is the sum of Eqs. (B10) and (B27), where we use the definitions (B12). Once expressed with the Mandelstam variables, we checked that it takes the form given in Lopez *et al.* (1997, App. A) (published version and with $m_1=m_\nu$, $m_2=m_n$, $m_3=m_e$ and $m_4=m_p$), except for a few differences. First, we do not include their term t_3 because this is second order in finite nucleon mass effects. Hence, we kept only contributions which are linear in $f_{\rm wm}$. Second, we find that there is a typo in t_5 of Lopez *et al.* (1997), since there should be a factor g_A instead of g_A^2.

We also performed a comparison with Seckel (1993) and found that it matches our result and the one of Lopez *et al.* (1997) if we replace its f_2 by $2f_{\rm wm}$ (again ignoring terms which are quadratic in f_2 and the parameter f_{ps} in Seckel (1993)).

6. Radiative corrections and Sirlin's universal function

When considering the effect of radiative corrections, the function $\mathcal{C}$ defined in Eq. (103) is given by

$$\mathcal{C}(E,k_{\rm max})=4\ln\frac{m_Z}{m_p}+\ln\frac{m_p}{m_A}+2C+A_g+g(E,k_{\rm max}) \tag{B30}$$

with

$$C\simeq 0.891\,,\qquad A_g\simeq -0.34\,,\qquad m_A\simeq 1.2\,{\rm GeV}\,. \tag{B31}$$

$g(E,k_{\rm max})$ is Sirlin's universal function

$$\begin{aligned} g(E,k_{\rm max}) &= 3\ln\frac{m_p}{m_e}-\frac{3}{4}+\frac{4}{\beta}L\left(\frac{2\beta}{1+\beta}\right)\\ &+ 4[R(\beta)-1]\left[\frac{k_{\rm max}}{3E}-\frac{3}{2}+\ln\left(2\frac{k_{\rm max}}{m_e}\right)\right]\\ &+ R(\beta)\left[2(1+\beta^2)+\frac{k_{\rm max}^2}{6E^2}-4\beta R(\beta)\right], \end{aligned} \tag{B32}$$

with $\beta=p/E=\sqrt{E^2-m_e^2}/E$ and

$$R(\beta)\equiv\frac{E}{p}\ln\left(\frac{p+E}{m}\right)=\frac{1}{2\beta}\ln\left(\frac{1+\beta}{1-\beta}\right)=\frac{\arctan(\beta)}{\beta}$$

and where the Spence function is defined as

$$L[x]=\int_0^x\frac{\ln(1-t)}{t}{\rm d}t\,. \tag{B33}$$

It is possible to use an expansion of the Spence function. We report it here to correct typos in Dicus *et al.* (1982) and subsequently in Lopez and Turner (1999); Smith and Fuller (2010)

$$\begin{aligned}&\frac{1}{\beta}L\left(\frac{2\beta}{1+\beta}\right)\simeq-\frac{1}{(1+\beta)^6}\times\\ &\left(2+11\beta+\tfrac{224}{9}\beta^2+\tfrac{89}{3}\beta^3+\tfrac{1496}{75}\beta^4+\tfrac{596}{75}\beta^5+\tfrac{128}{49}\beta^6\right).\end{aligned} \tag{B34}$$

Finally in order to obtain even more accurate results, it is also possible to refine the expression for the radiative corrections by using Czarnecki *et al.* (2004, Eq. 15) which is a resummation of higher order corrections. Unless specified, this is the radiative correction that we use so we report it here.

$$\begin{aligned} R(E,k_{\rm max}) &= \left[1+\frac{\alpha_{\rm FS}}{2\pi}\left(g(E,k_{\rm max})-3\ln\frac{m_p}{2\Delta}\right)\right]\\ &\times\left(L+\frac{\alpha_{\rm FS}}{\pi}C+\frac{\alpha_{\rm FS}}{2\pi}\delta\right)\\ &\times\left[S+\frac{\alpha_{\rm FS}(m_p)}{2\pi}\left(\ln\frac{m_p}{m_A}+A_g\right)+{\rm NLL}\right] \end{aligned} \tag{B35}$$

$$\alpha_{\rm FS}(m_p)\simeq\frac{1}{134}\,,\quad \frac{\alpha_{\rm FS}}{2\pi}\delta\simeq-0.00043\,,\quad {\rm NLL}\simeq-10^{-4}$$

$$L\simeq 1.02094\,,\qquad S\simeq 1.02248 \tag{B36}$$

7. Bremsstrahlung

We review in the next section the bremsstrahlung correction to the neutron decay, also called radiative neutron decay when the photon is detected (Cooper *et al.*, 2010). We then extend it to the other weak processes during BBN. This allows to find the difference between the correct treatment of bremsstrahlung and how it was partially included in the radiative correction factor detailed above in § B.6. We report subsequently the detailed expression of this bremsstrahlung correction.

a. Neutron decay

Let us consider first the bremsstrahlung for the decay of neutron. We note the emitted photon momentum $\underline{k}$. Its spatial part is $\mathbf{k}$, that we decompose into energy k and direction $\hat{\mathbf{k}}$ as $\mathbf{k} = k\hat{\mathbf{k}}$. We note the electron energy E and its spatial momentum p for simplicity. In the infinite nucleon mass approximation, the bremsstrahlung differential decay rate is of the form [see e.g. Ivanov *et al.* (2013, Eq. B12), Cooper *et al.* (2010, Eq. 4), Abers *et al.* (1968, Eq. 6.6) or Ivanov *et al.* (2017, Eq. A40)]

$$\begin{aligned}\frac{\mathrm{d}\Gamma^{\mathrm{BS}}_{n\to}}{\mathrm{d}E\mathrm{d}k\mathrm{d}\mu} &= \frac{\alpha_{\mathrm{FS}}K}{2\pi}\frac{\beta E_\nu^2}{k} \\ &\times \left[\frac{\beta^2(1-\mu^2)}{(1-\beta\mu)^2}\left(1+\frac{k}{E}\right)+\frac{k^2}{E^2}\frac{1}{1-\beta\mu}\right]\end{aligned} \tag{B37}$$

where

$$\mu \equiv \mathbf{p}_e\cdot\hat{\mathbf{k}} \tag{B38}$$

is the (cosinus) of the angle between the photon momentum and the electron momentum. The neutrino energy is constrained from energy conservation to be

$$E_\nu = \Delta - E - k\,. \tag{B39}$$

Performing the integral on μ leads to

$$\frac{\mathrm{d}\Gamma^{\mathrm{BS}}_{n\to}}{\mathrm{d}k\mathrm{d}E} = \frac{\alpha_{\mathrm{FS}}K}{2\pi k}E_\nu^2 F_+(E,k)\,. \tag{B40}$$

with

$$\begin{aligned}F_\pm(E,k) &\equiv A(E,k)\pm kB(E,k) \\ A(E,k) &\equiv (2E^2+k^2)\ln\left(\frac{E+p}{E-p}\right)-4pE \\ B(E,k) &\equiv 2E\ln\left(\frac{E+p}{E-p}\right)-4p\,.\end{aligned} \tag{B41}$$

The total decay rate cannot be obtained from a simple integration of the form

$$\Gamma^{\mathrm{BS}}_{n\to} = \int_{m_e}^{E_{\max}}\mathrm{d}E\int_0^{\Delta-E}\mathrm{d}k\frac{\mathrm{d}\Gamma^{\mathrm{BS}}}{\mathrm{d}k\mathrm{d}E}\,. \tag{B42}$$

since there is an infrared divergence. However this divergence cancels a corresponding divergence in the pure radiative corrections. The usual procedure consists in letting the photon having a mass and taking the limit $m_\gamma \to 0$ [see e.g. Ivanov *et al.* (2013) or Abers *et al.* (1968)].

b. Bremsstrahlung for other reactions

The other rates of bremsstrahlung can be deduced from crossing symmetry. Indeed, if one considers the process $n + e^+ \to p + \bar{\nu}$ it is obtained from crossing symmetry of beta decay. A crossing symmetry is performed by inverting the four-momentum of the corresponding particle. Hence changing the position of the final electron to an initial positron amounts to $E \to -E$ and $p \to -p$. This leads to $F_+ \to F_-$ in (B40). In fact it is simple to check that if the electron (or positron) and the photon are on the same side, one should use F_+ and if they are on opposite sides, we should use F_-. The contributions of bremsstrahlung to the reaction rates is then straightforward, provided it is clear that we should take the infrared regularized contribution, and they read

$$\begin{aligned}\Gamma_{n\to p\gamma} &= \frac{\alpha_{\mathrm{FS}}K}{2\pi}\int_{m_e}^{\infty}\mathrm{d}E \\ &\times \left[g(-E)\widetilde{\chi}^+_+(E)+g(E)\widetilde{\chi}^-_+(-E)\right]\end{aligned} \tag{B43a}$$

$$\Gamma_{p\to n\gamma} = \Gamma_{n\to p\gamma}\big|_{\widetilde{\chi}^s_+\to\widetilde{\chi}^s_-} \tag{B43b}$$

with the definitions

$$\widetilde{\chi}^s_\pm(E) \equiv \int_0^\infty\frac{\mathrm{d}k}{k}F_s(E,k)\widetilde{\chi}_\pm(k+E) \tag{B44}$$

$$\widetilde{\chi}_\pm(E) \equiv (E_\nu^\mp)^2 g_\nu^\mp(E_\nu)\,,\quad E_\nu^\mp = E\mp\Delta\,. \tag{B45}$$

c. Correction for bremsstrahlung

However, the bremsstrahlung radiative corrections included in § III.E, that is in the factor (103), are those of neutron beta decay. Indeed the radiative correction function R in Eqs. (101) and (104) is the sum of a pure radiative correction and a bremsstrahlung correction. It is decomposed as

$$R(E,k_{\max}) = R^{\mathrm{pure}}(E) + R^{\mathrm{BS}}(E,k_{\max}) \tag{B46}$$

with the BS part being

$$R^{\mathrm{BS}}(E,k_{\max}) \equiv \frac{\alpha_{\mathrm{FS}}}{2\pi}\int_0^{k_{\max}}\frac{\mathrm{d}k}{k}\frac{(k_{\max}-k)^2}{k_{\max}^2}\frac{F_+(E,k)}{Ep}\,. \tag{B47}$$

In Eqs. (101) and (104) the choice was made to take $k_{\max}$ as being the energy of the neutrino because this is the case for neutron beta decay. However the maximum energy of the photon emitted is not the neutrino energy in the other reactions. Furthermore, the distribution function for the neutrino appearing in Eqs. (101) and (104) is incorrectly taken in the limit in which the photon energy is so soft that it does not affect the neutrino energy. These are the two shortcomings that we need to correct for by adding the difference between the correct correction [Eqs. (B43)] and the approximate contribution [it is formally Eqs. (101) and (104) with $R \to R^{\mathrm{BS}}$]. We write this bremsstrahlung correction in a form which contains explicitly no infrared divergence and this is given by Eqs. (107) with the definitions

$$\begin{aligned}
\delta\Gamma^{\rm BS}_{n\to p+e} &= \int_0^{|\Delta-E|}\frac{\mathrm{d}k}{k}F_+(E,k)\left[\widetilde{\chi}_+(E+k)-(|\Delta-E|-k)^2 g_\nu(E-\Delta)\right]+\int_{|\Delta-E|}^{\infty}\frac{\mathrm{d}k}{k}F_+(E,k)\widetilde{\chi}_+(E+k)\\
\delta\Gamma^{\rm BS}_{n+e\to p} &= \int_0^{\Delta+E}\frac{\mathrm{d}k}{k}\left[F_-(E,k)\widetilde{\chi}_+(k-E)-F_+(E,k)(|\Delta+E|-k)^2 g_\nu(-E-\Delta)\right]\\
&+ \int_{\Delta+E}^{\infty}\frac{\mathrm{d}k}{k}F_-(E,k)\widetilde{\chi}_+(k-E)
\end{aligned}\tag{B48}$$

$$\begin{aligned}
\delta\Gamma^{\rm BS}_{p\to n+e} &= \int_0^{\Delta+E}\frac{\mathrm{d}k}{k}F_+(E,k)\left[\widetilde{\chi}_-(E+k)-(|E+\Delta|-k)^2 g_\nu(E+\Delta)\right]+\int_{\Delta+E}^{\infty}\frac{\mathrm{d}k}{k}F_+(E,k)\widetilde{\chi}_-(E+k)\\
\delta\Gamma^{\rm BS}_{p+e\to n} &= \int_0^{|\Delta-E|}\frac{\mathrm{d}k}{k}\left[F_-(E,k)\widetilde{\chi}_-(k-E)-F_+(E,k)(|E-\Delta|-k)^2 g_\nu(-E+\Delta)\right]\\
&+ \int_{|\Delta-E|}^{\infty}\frac{\mathrm{d}k}{k}F_-(E,k)\widetilde{\chi}_-(k-E)\,.
\end{aligned}\tag{B49}$$

With these corrections added to Eqs. (101) and (104), the total effect of bremsstrahlung is taken into account. However, with this new contribution the rates no longer satisfy the detailed balance relation (86). Indeed the emission of a final photon needs to be compensated by the absorption of photons from the thermal bath to lead to a thermodynamical equilibrium. It is only when the finite temperature radiative corrections are taken into account, with stimulated emission and absorption, that the total rates can satisfy detailed balance. This is shown explicitly in Fig. 18.

Note that by construction the bremsstrahlung corrections do not modify the radiative corrections for $\lambda_0^{\rm RC0}$ because the neutron beta decay in vacuum, is the only reaction for which bremsstrahlung is fully taken into account already.

Finally note that there was some intuition in Brown and Sawyer (2001) about the incorrect treatment of real-photon processes. Indeed in this reference, the authors advocate that one should add the process $n+\bar{\nu}+e^+\to p+\gamma$, that they call the *five-body process*, since it cannot be a correction to $n+\bar{\nu}+e^+\to p$ which is forbidden energetically. This is indeed correct and it corresponds to the last term in $\delta\Gamma^{\rm BS}_{n+e\to p}$, where the photon emitted must have an energy larger than $\Delta+E$. What we find is that not only this process needs to be added, but *all other processes need to be corrected* except for the neutron beta decay.

8. Finite temperature radiative corrections

The finite temperature radiative corrections are made of Eqs. (109), (112) and (113). These last two contributions involve implicitly principal parts in the apparently divergent part of the integrals. After rearrangement, they can be put in the form (Brown and Sawyer, 2001, Eq. (5.15))

$$\Gamma^{\Delta E,T}_{n\to p}+\Gamma^{ep+ee,T}_{n\to p} = \frac{\alpha_{\rm FS}K}{2\pi}\int_{m_e}^{\infty}\mathrm{d}E[\chi_+(E)+\chi_+(-E)]\left[-\frac{2\pi^2T^2E}{3p}+\int_{m_e}^{\infty}\mathrm{d}E' F^T(E,E')\right]\tag{B50a}$$

$$\Gamma^{\Delta E,T}_{p\to n}+\Gamma^{ep+ee,T}_{p\to n} = \left(\Gamma^{\Delta E,T}_{n\to p}+\Gamma^{ep+ee,T}_{n\to p}\right)\Big|_{\chi_+\to\chi_-}\tag{B50b}$$

$$\begin{aligned}
F^T(E,E') \equiv\ & -\frac{1}{4}\ln^2\left(\frac{p+p'}{p-p'}\right)^2\left\{g'(E')\frac{p'E^2}{pE'}(E+E')+g(E')\frac{E^2}{pp'}\left[E'+\frac{m_e^2E}{E'^2}\right]\right\}-g(E')\left[4E\frac{p'}{p}+2E'L(E,E')\right]\\
&+\ln\left(\frac{p+p'}{p-p'}\right)^2\left\{g'(E')\left[p'^2\frac{E}{E'}\left(\frac{m_e^2}{p^2}+2\right)-E^2\frac{p'}{p}L[E,E']\right]\right.\\
&\left.+g(E')\left[\frac{Em_e^2}{p^2E'^2}(E'^2+2p^2+m_e^2)-\frac{E^2+E'^2}{E+E'}-\frac{E^2E'}{pp'}L(E,E')\right]\right\}
\end{aligned}\tag{B51a}$$

$$L(E,E') \equiv \ln\left(\frac{EE'+pp'+m_e^2}{EE'-pp'+m_e^2}\right),\tag{B51b}$$

where $g'(E) \equiv \partial_E g(E)$.

This form is simpler numerically if the double integration on E and E' is performed on the variables $E_\Sigma \equiv E + E'$ and $E_\Delta \equiv E - E'$ using $2\int\int \mathrm{d}E\mathrm{d}E' = \int\int \mathrm{d}E_\Sigma \mathrm{d}E_\Delta$.

The first contribution (109) is made of real photon processes, such as absorption and stimulated emission, see Fig. 14, but not simple emission which has been already accounted for as bremsstrahlung (see appendix B.7). To obtain it we start from the real photons processes (Brown and Sawyer, 2001, Eq. B28)

$$\Gamma^{\gamma}_{n\to p} = \frac{\alpha_{\rm FS} K}{2\pi}\int_{m_e}^{\infty}\mathrm{d}E \quad \text{(B52a)}$$
$$\times \left[g(-E)\widetilde{\chi}_+^{\gamma,+}(E) + g(E)\widetilde{\chi}_+^{\gamma,-}(-E)\right]$$
$$\Gamma^{\gamma}_{p\to n} = \Gamma^{\gamma}_{n\to p}\big|_{\widetilde{\chi}_+^{\gamma,s}\to\widetilde{\chi}_-^{\gamma,s}} \quad \text{(B52b)}$$

where we defined

$$\widetilde{\chi}_\pm^{\gamma,s}(E) \equiv \int_0^\infty \frac{\mathrm{d}k}{k}\left[(1+f(k))F_s(E,k)\widetilde{\chi}_\pm(E+k) + f(k)F_{-s}(E,k)\widetilde{\chi}_\pm(E-k)\right], \quad \text{(B53)}$$

and $f(k) \equiv g^-(k/T) = 1/[\exp(k/T)-1]$. Note that from the property

$$1 + f(k) = -f(-k) = \mathrm{e}^{\frac{k}{T}} f(k) \quad \text{(B54)}$$

combined with the property (84), the detailed balance relation (86) for the real photon processes (B52) is automatically satisfied[21].

Then we replace the factor $[1 + f(k)]$ by $f(k)$ so as to keep only stimulated emission, since bremsstrahlung processes (B43) which are taken into account separately are obtained by $f(k) \to 0$. A consequence is that the real photon processes without bremsstrahlung do no satisfy formally the detailed balance relation. It is only when all real photon processes are added that it is recovered, as illustrated in Fig. (18).

Finally, in order to obtain the form (109) for which it is apparent that there is no infrared divergence, it is necessary to add an infrared diverging contribution (Brown and Sawyer, 2001, Eq. (B53)) that can be considered as part of the wave-function radiative correction (it is partially coming from the diagram 17a) and which is

$$\Gamma^{\gamma,Z}_{n\to p} = \frac{\alpha_{\rm FS} K}{2\pi}\int_{m_e}^{\infty}\mathrm{d}E \quad \text{(B55a)}$$
$$\times \left[g(-E)\widetilde{\chi}_+^{\gamma,Z}(E) + g(E)\widetilde{\chi}_+^{\gamma,Z}(-E)\right]$$
$$\Gamma^{\gamma,Z}_{p\to n} = \Gamma^{\gamma,Z}_{n\to p}\big|_{\widetilde{\chi}_+^{\gamma,Z}\to\widetilde{\chi}_-^{\gamma,Z}} \quad \text{(B55b)}$$

$$\widetilde{\chi}_\pm^{\gamma,Z}(E) \equiv -2\int_0^\infty \frac{\mathrm{d}k}{k} f(k) A(E,k)\widetilde{\chi}_\pm(E). \quad \text{(B56)}$$

Again on Eqs. (B55) it is apparent using the property (84) that these extra terms formally satisfy the detailed balance relation (86).

[21] At this stage this is only formal since this presents infrared divergences.

Appendix C: Nuclear reactions

1. Conventions for nuclear reaction rates

Let us consider for simplicity a two-body reaction of the type $k + l \to i + j$ and its reverse reaction $i + j \to k + l$. From Eqs. (136) and (137) their contributions to the evolution of the abundance Y_i take the form

$$\dot{Y}_i \supset Y_k Y_l \rho_n N_A \langle\sigma v\rangle_{kl\to ij} - Y_i Y_j \rho_n N_A \langle\sigma v\rangle_{ij\to kl}, \quad \text{(C1)}$$

with

$$\rho_{\rm n} \equiv \frac{n_{\rm b}}{N_A} \equiv n_{\rm b}{\cdot}u \ \ (\mathrm{g/cm^3}). \quad \text{(C2)}$$

We see that $\rho_{\rm n}$ has the dimension of a mass density since u is the atomic mass unit, that, by definition is related to Avogadro's number by $N_A.u$=1g. By convention, N_A has been introduced in the definition of the reaction rate, hence what is tabulated for a given reaction is $N_A\langle\sigma v\rangle$ and one must multiply by $\rho_{\rm n}$ in order to build the rates (e.g. $\Gamma_{kl\to ij}$) which appear in the general form Eq. (138). More generally for a reaction of the type $i_1 + \cdots + i_p \to j_1 + \ldots j_q$, the contribution to the evolution of the species i_1 is

$$\dot{Y}_{i_1} \supset -Y_{i_1}\ldots Y_{i_p}\rho_{\rm n}^{p-1} N_A^{p-1}\gamma_{i_1\ldots i_p\to j_1\ldots j_q}. \quad \text{(C3)}$$

Conventionally what is tabulated is $N_A^{p-1}\gamma_{i_1\ldots i_p\to j_1\ldots j_q}$ [22] and one must multiply by $\rho_{\rm n}^{p-1}$ to build the reaction rate $\Gamma_{i_1\ldots i_p\to j_1\ldots j_q}$ appearing in Eq. (138). The method is similar for a reaction of the type $j_1 + \ldots j_q \to i_1 + \cdots + i_p$ which creates species i_1. See also appendix E of Serpico *et al.* (2004) on this topic.

To summarize, in nucleosynthesis calculations (as in chemistry) we are concerned with number densities. However, it is convenient to normalize them to Avogadro's number whose dimension can be considered[23] to be the inverse of a mass. The form (C1) is purely conventional and $\rho_{\rm n}$ is just another manner to define a number density even though it has the dimension of a mass density.

[22] More precisely, from (139) the factor is $N_A^{(N_{i_1}+\cdots+N_{i_p})-1}$ if the stoichiometric coefficients are not unity.

[23] A subject of controversy, but irrelevant as soon as it is consistent with the definition of the reaction rate units.

2. Baryonic density and nucleonic density

In practice, except for BBN, the nucleonic density of Eq. (C2) is usually identified with the atomic matter density, and the nuclear energy source is calculated independently as nuclear flow × Q This corresponds to the approximation

$$A{\cdot}u \approx Zm_p + (A-Z)m_n - B(A,Z) + Zm_e\,, \qquad \text{(C4)}$$

i.e. an error of ≈1%, completely negligible in stellar modeling. For BBN where D/H observations reach the percent level of uncertainty, it is worth considering the difference between nucleonic density and baryonic density.

The baryonic density $\Omega_{\rm b}{\cdot}h^2$ deduced from CMB observations is the atomic density i.e. taking into account the ^{4}He binding energy and the mass of the electrons. Given that the fraction of baryons in the form of helium is $Y_{\rm P} \equiv 4\,Y_{^4{\rm He}}$ and the rest is in the form of hydrogen, the average mass of baryons is (Steigman, 2006)

$$m_{\rm b} \equiv \xi u \qquad \text{(C5)}$$

$$\xi \equiv \frac{Y_{\rm P}}{4}\frac{m_{^4{\rm He}}}{u} + (1-Y_{\rm P})\frac{m_{^1{\rm H}}}{u} \qquad \text{(C6)}$$

$$= \frac{m_{^1{\rm H}}}{u}\left(1 - 1.75891\times10^{-3}\frac{Y_{\rm P}}{0.24709}\right)$$

where $m_{^4{\rm He}}$ and $m_{^1{\rm H}}$ are the *atomic* masses (see appendix D). Using $Y_{\rm P} \simeq 0.24709$ for the final BBN Helium abundance (it is the most relevant abundance for CMB since stellar formation has not started during CMB formation) we get

$$\xi \simeq 1.006052\,, \quad \xi^{-1} \simeq 0.993984\,. \qquad \text{(C7)}$$

Hence, from Eqs. (35) and (C2), one should use in Eq. (C1)

$$\rho_{\rm n} = \xi^{-1}\rho_{\rm b}\,, \qquad \text{(C8)}$$

where $\rho_{\rm b}$ is obtained from Eq. (34). One can estimate the error introduced if we ignore this subtlety and use $\xi = 1$ in nuclear reaction. Numerically we found

$$\Delta Y_{\rm P} = 5.6\times10^{-4} \qquad \text{(C9a)}$$

$$\Delta\left(\frac{\rm D}{\rm H}\right) = -2.4\times10^{-7} \qquad \text{(C9b)}$$

$$\Delta\left(\frac{^3{\rm He}}{\rm H}\right) = 3.7\times10^{-8} \qquad \text{(C9c)}$$

$$\Delta\left(\frac{^7{\rm Li}}{\rm H}\right) = 7.1\times10^{-12}\,. \qquad \text{(C9d)}$$

Finally, since the abundances deduced from observations, other than ^{4}He, are expressed as number ratios, hence, e.g. the observed D/H can be directly compared to the BBN $Y_{\rm D}/Y_{^1{\rm H}}$ calculated ratio. The ^{4}He (pseudo-)mass fraction, $Y_{\rm P}$ deduced from spectroscopic observations is defined as (Izotov *et al.*, 1994; Pagel *et al.*, 1992)

$$Y_{\rm P} \equiv \frac{4y}{4y+1} \qquad \text{(C10)}$$

with $y{\equiv}n_{^4{\rm He}}/n_{^1{\rm H}}{\equiv}Y_{^4{\rm He}}/Y_{^1{\rm H}}$ being the *number* ratio, resulting in a definition of $Y_{\rm P}$ identical to the BBN one.

Appendix D: Numerical values

The values of $\cos\theta_C = V_{\rm ud}$ and $g_A = C_A/C_V$ are taken from the Particle Data Group (PDG) (Patrignani and Particle Data Group, 2016 and 2017 update). The neutron decay rate $\tau_n = 879.5(\pm0.8)$ s is from Serebrov *et al.* (2017, Fig. 22) and includes only experiments after 2000. This value is slightly lower and with less experimental error than the previously admitted value $\tau_n = 880.2(1.1)$ s of the PDG. We report errors on numerical parameters only if they are meaningful for BBN. Cosmological parameters are taken from Ade *et al.* (2016).

TABLE X Numerical values used for the BBN code.

u	931.494061 MeV
m_n	939.565360 MeV
m_p	938.272029 MeV
m_Z	91.1876 GeV
m_W	80.385 GeV
$m_{^4{\rm He}}$ (atomic)	4.00260325413 u
$m_{^1{\rm H}}$ (atomic)	1.00782503223 u
g_A	1.2723(23)
$\cos\theta_C$	0.97420(20)
$f_{\rm WM}$	1.853
G_F	1.1663787×10^{-5} GeV^{-2}
τ_n	879.5(8) s
r_p	0.841×10^{-15} m
$\alpha_{\rm FS}$	1/137.03599911
T_0	2.7255 (±0.0006) K
$h = H/H_{100}$	0.6727 (±0.0066)
$h^2\Omega_b$	0.022250 (±0.00016)
$h^2\Omega_c$	0.1198 (±0.0015)
$\rho_{100}^{\rm crit} \equiv 3H_{100}^2/(8\pi G)$	1.87847×10^{-29} g/cm^3

References

Abers, E. S., D. A. Dicus, R. E. Norton, and H. R. Quinn, 1968, Phys. Rev. **167**, 1461.

Ade, P. A. R., *et al.* (Planck), 2016, Astron. Astrophys. **594**, A13.

Adelberger, E. G., A. García, R. G. H. Robertson, K. A. Snover, A. B. Balantekin, K. Heeger, M. J. Ramsey-Musolf, D. Bemmerer, A. Junghans, C. A. Bertulani, J.-W. Chen, H. Costantini, *et al.*, 2011, Rev. Mod. Phys. **83**, 195.

Aliotta, M., F. Raiola, G. Gyürky, A. Formicola, R. Bonetti, C. Broggini, L. Campajola, P. Corvisiero, H. Costantini, A. D'Onofrio, Z. Fülöp, G. Gervino, *et al.*, 2001, Nuclear Physics A **690**, 790.

Amsler, C., M. Doser, M. Antonelli, D. M. Asner, K. S. Babu, H. Baer, H. R. Band, R. M. Barnett, E. Bergren,

J. Beringer, G. Bernardi, W. Bertl, *et al.*, 2008, Physics Letters B **667**, 1.
Anders, M., D. Trezzi, R. Menegazzo, M. Aliotta, A. Bellini, D. Bemmerer, C. Broggini, A. Caciolli, P. Corvisiero, H. Costantini, T. Davinson, Z. Elekes, *et al.*, 2014, Phys, Rev. Lett. **113**, 042501.
Ando, S., R. H. Cyburt, S. W. Hong, and C. H. Hyun, 2006, Phys. Rev. **C74**, 025809.
Angulo, C., M. Arnould, M. Rayet, P. Descouvemont, D. Baye, C. Leclercq-Willain, A. Coc, S. Barhoumi, P. Aguer, C. Rolfs, R. Kunz, J. W. Hammer, *et al.*, 1999, Nuclear Physics A **656**, 3.
Angulo, C., E. Casarejos, M. Couder, P. Demaret, P. Leleux, F. Vanderbist, A. Coc, J. Kiener, V. Tatischeff, T. Davinson, A. S. Murphy, N. L. Achouri, *et al.*, 2005, Astrophys. J. Lett. **630**, L105.
Aoki, W., P. S. Barklem, T. C. Beers, N. Christlieb, S. Inoue, A. E. García Pérez, J. E. Norris, and D. Carollo, 2009, Astrophys. J. **698**, 1803.
Arai, K., S. Aoyama, Y. Suzuki, P. Descouvemont, and D. Baye, 2011, Phys. Rev. Lett. **107**, 132502.
Arbey, A., 2012, Comput. Phys. Commun. **183**, 1822.
Asplund, M., D. L. Lambert, P. E. Nissen, F. Primas, and V. V. Smith, 2006, Astrophys. J. **644**, 229.
Audi, G., F. G. Kondev, M. Wang, W. J. Huang, and S. Naimi, 2017, Chinese Physics C **41**, 030001.
Aver, E., K. A. Olive, and E. D. Skillman, 2015, "JCAP" **7**, 011.
Balashev, S. A., E. O. Zavarygin, A. V. Ivanchik, K. N. Telikova, and D. A. Varshalovich, 2016, MNRAS **458**, 2188.
Bania, T. M., R. T. Rood, and D. S. Balser, 2002, Nature **415**, 54.
Barbagallo, M., A. Musumarra, L. Cosentino, E. Maugeri, S. Heinitz, A. Mengoni, R. Dressler, D. Schumann, F. Käppeler, N. Colonna, P. Finocchiaro, M. Ayranov, *et al.*, 2016, Phys. Rev. Lett. **117**, 152701.
Becchetti, F. D., J. A. Brown, W. Z. Liu, J. W. Jänecke, D. A. Roberts, J. J. Kolata, R. J. Smith, K. Lamkin, A. Morsad, R. E. Warner, R. N. Boyd, and J. D. Kalen, 1992, Nucl. Phys. A **550**, 507.
Bernstein, J., L. S. Brown, and G. Feinberg, 1989, Rev. Mod. Phys. **61**, 25.
Birrell, J., C.-T. Yang, and J. Rafelski, 2014, Nucl. Phys. **B890**, 481.
Blas, D., J. Lesgourgues, and T. Tram, 2011, JCAP **7**, 034.
Bonifacio, P., P. Molaro, T. Sivarani, R. Cayrel, M. Spite, F. Spite, B. Plez, J. Andersen, B. Barbuy, T. C. Beers, E. Depagne, V. Hill, *et al.*, 2007, Astron. Astrophys. **462**, 851.
Broggini, C., L. Canton, G. Fiorentini, and F. L. Villante, 2012, JCAP **6**, 030.
Brown, L. S., and R. F. Sawyer, 2001, Phys. Rev. **D63**, 083503.
Bystritsky, V. M., V. V. Gerasimov, A. R. Krylov, S. S. Parzhitskii, G. N. Dudkin, V. L. Kaminskii, B. A. Nechaev, V. N. Padalko, A. V. Petrov, G. A. Mesyats, M. Filipowicz, J. Wozniak, *et al.*, 2008, Nuclear Instruments and Methods in Physics Research A **595**, 543.
Cambier, J.-L., J. R. Primack, and M. Sher, 1982, Nucl. Phys. **B209**, 372.
Casella, C., H. Costantini, A. Lemut, B. Limata, R. Bonetti, C. Broggini, L. Campajola, P. Corvisiero, J. Cruz, A. D'Onofrio, A. Formicola, Z. Fülöp, *et al.*, 2002, Nucl. Phys. A **706**, 203.
Cassisi, S., and V. Castellani, 1993, Astrophys. J. Supp. **88**, 509.
Chakraborty, N., B. D. Fields, and K. A. Olive, 2011, Phys. Rev. **D83**, 063006.
Chapman, I. A., 1997, Phys. Rev. **D55**, 6287.
Charbonnel, C., and F. Primas, 2005, Astron. Astrophys. **442**, 961.
Clayton, D. D., 1983, *Principles of stellar evolution and nucleosynthesis* (Chicago: University of Chicago Press).
Coc, A., 2013, Acta Physica Polonica B **44**, 521.
Coc, A., S. Goriely, Y. Xu, M. Saimpert, and E. Vangioni, 2012, Astrophys. J. **744**, 158.
Coc, A., F. Hammache, and J. Kiener, 2015, European Physical Journal A **51**, 34.
Coc, A., K. A. Olive, J.-P. Uzan, and E. Vangioni, 2009, Phys. Rev. **D79**, 103512.
Coc, A., P. Petitjean, J.-P. Uzan, E. Vangioni, P. Descouvemont, C. Iliadis, and R. Longland, 2015, Phys. Rev. **D92**, 123526.
Coc, A., J.-P. Uzan, and E. Vangioni, 2014, JCAP **1410**, 050.
Coc, A., and E. Vangioni, 2010, in *Big-Bang nucleosynthesis with updated nuclear data*, volume 202 of *Journal of Physics Conference Series*, p. 012001.
Coc, A., and E. Vangioni, 2014, in *Proceedings, XIII Nuclei in the Cosmos, Debrecen, Hungary, July 7-11, 2014, PoS (NIC XIII)*, p. 22.
Coc, A., and E. Vangioni, 2017, International Journal of Modern Physics E **26**, 1741002.
Coc, A., E. Vangioni-Flam, M. Cassé, and M. Rabiet, 2002, Phys. Rev. **D65**, 043510.
Coc, A., E. Vangioni-Flam, P. Descouvemont, A. Adahchour, and C. Angulo, 2004, Astrophys. J. **600**, 544.
Consiglio, R., P. F. de Salas, G. Mangano, G. Miele, S. Pastor, and O. Pisanti, 2017, eprint 1712.04378.
Cooke, R. J., 2015, Astrophys. J. Lett. **812**, L12.
Cooke, R. J., M. Pettini, R. A. Jorgenson, M. T. Murphy, and C. C. Steidel, 2014, Astrophys. J. **781**, 31.
Cooke, R. J., M. Pettini, K. M. Nollett, and R. Jorgenson, 2016, Astrophys. J. **830**, 148.
Cooke, R. J., M. Pettini, and C. C. Steidel, 2018, Astrophys. J. **855**, 102.
Cooper, R. L., T. E. Chupp, M. S. Dewey, T. R. Gentile, H. P. Mumm, J. S. Nico, A. K. Thompson, B. M. Fisher, I. Kremsky, F. E. Wietfeldt, E. J. Beise, K. G. Kiriluk, *et al.*, 2010, Phys. Rev. **C81**, 035503.
Creminelli, P., C. Pitrou, and F. Vernizzi, 2011, JCAP **1111**, 025.
Cyburt, R. H., 2004, Phys. Rev. **D70**, 023505.
Cyburt, R. H., and B. Davids, 2008, Phys. Rev. **C78**, 064614.
Cyburt, R. H., B. D. Fields, and K. A. Olive, 2008, JCAP **11**, 012.
Cyburt, R. H., B. D. Fields, K. A. Olive, and T.-H. Yeh, 2016, Rev. Mod. Phys. **88**, 015004.
Cyburt, R. H., and M. Pospelov, 2012, International Journal of Modern Physics E **21**, 1250004-1-1250004-13.
Czarnecki, A., W. J. Marciano, and A. Sirlin, 2004, Phys. Rev. **D70**, 093006.
Czarnecki, A., W. J. Marciano, and A. Sirlin, 2018, Phys. Rev. Lett. **120**, 202002.
deBoer, R. J., J. Görres, K. Smith, E. Uberseder, M. Wiescher, A. Kontos, G. Imbriani, A. Di Leva, and F. Strieder, 2014, Phys. Rev. **C90**, 035804.
Descouvemont, P., A. Adahchour, C. Angulo, A. Coc, and E. Vangioni-Flam, 2004, Atomic Data and Nuclear Data

Tables **88**, 203.
Di Valentino, E., C. Gustavino, J. Lesgourgues, G. Mangano, A. Melchiorri, G. Miele, and O. Pisanti, 2014, Phys. Rev. **D90**(2), 023543.
Dicus, D. A., E. W. Kolb, A. M. Gleeson, E. C. G. Sudarshan, V. L. Teplitz, and M. S. Turner, 1982, Phys. Rev. **D26**, 2694.
Dodelson, S., and M. S. Turner, 1992, PHys. Rev. **D46**, 3372.
Dolgov, A. D., S. H. Hansen, S. Pastor, S. T. Petcov, G. G. Raffelt, and D. V. Semikoz, 2002, Nucl. Phys. **B632**, 363.
Dolgov, A. D., S. H. Hansen, and D. V. Semikoz, 1997, Nucl. Phys. **B503**, 426.
Dolgov, A. D., S. H. Hansen, and D. V. Semikoz, 1999, Nucl. Phys. **B543**, 269.
Dvorkin, I., E. Vangioni, J. Silk, P. Petitjean, and K. A. Olive, 2016, MNRAS **458**, L104.
Ekström, S., G. Meynet, C. Chiappini, R. Hirschi, and A. Maeder, 2008, Astron. Astrophys. **489**, 685.
Esposito, S., G. Mangano, G. Miele, and O. Pisanti, 1999, Nucl. Phys. **B540**, 3.
Esposito, S., G. Mangano, G. Miele, and O. Pisanti, 2000a, Nucl. Phys. **B568**, 421.
Esposito, S., G. Miele, S. Pastor, M. Peloso, and O. Pisanti, 2000b, Nucl. Phys. **B590**, 539.
Famiano, M. A., A. B. Balantekin, and T. Kajino, 2016, Phys. Rev. **C93**, 045804.
Fidler, C., and C. Pitrou, 2017, JCAP **1706**(06), 013.
Fields, B. D., 2011, Annual Review of Nuclear and Particle Science **61**, 47.
Fields, B. D., S. Dodelson, and M. S. Turner, 1993, Phys. Rev. **D47**, 4309.
Fornal, B., and B. Grinstein, 2018, ArXiv e-prints eprint 1801.01124.
Fornengo, N., C. W. Kim, and J. Song, 1997, Phys. Rev. **D56**, 5123.
Fowler, W. A., G. R. Caughlan, and B. A. Zimmerman, 1967, Ann. Rev. of Astron. and Astrophys. **5**, 525.
Fröberg, C.-E., 1955, Reviews of Modern Physics **27**, 399.
Fu, X., A. Bressan, P. Molaro, and P. Marigo, 2015, MNRAS **452**, 3256.
Fu, X., D. Romano, A. Bragaglia, A. Mucciarelli, K. Lind, E. Delgado Mena, S. G. Sousa, S. Randich, A. Bressan, L. Sbordone, S. Martell, A. J. Korn, *et al.*, 2018, Astron. Astrophys. **610**, A38.
Gnedin, N. Y., and O. Y. Gnedin, 1998, Astrophys. J. **509**, 11.
Gómez Iñesta, Á., C. Iliadis, and A. Coc, 2017, ArXiv e-prints eprint 1710.01647.
Goriely, S., S. Hilaire, and A. J. Koning, 2008, Astron. Astrophys. **487**, 767.
Goudelis, A., M. Pospelov, and J. Pradler, 2016, Phys. Rev. Lett. **116**, 211303.
Greife, U., F. Gorris, M. Junker, C. Rolfs, and D. Zahnow, 1995, Zeitschrift fur Physik A Hadrons and Nuclei **351**, 107.
Grohs, E., G. M. Fuller, C. T. Kishimoto, and M. W. Paris, 2017, Phys. Rev. **D95**, 063503.
Grohs, E., G. M. Fuller, C. T. Kishimoto, M. W. Paris, and A. Vlasenko, 2016, Phys. Rev. **D93**, 083522.
Gruyters, P., K. Lind, O. Richard, F. Grundahl, M. Asplund, L. Casagrande, C. Charbonnel, A. Milone, F. Primas, and A. J. Korn, 2016, Astron. Astrophys. **589**, A61.
Gustavino, C., 2017, in *European Physical Journal Web of Conferences*, volume 136, p. 01009.
Hammache, F., A. Coc, N. de Séréville, I. Stefan, P. Roussel, S. Ancelin, M. Assié, L. Audouin, D. Beaumel, S. Franchoo, B. Fernandez-Dominguez, S. Fox, *et al.*, 2013, Phys. Rev. **C88**, 062802.
Hammache, F., M. Heil, S. Typel, D. Galaviz, K. Sümmerer, A. Coc, F. Uhlig, F. Attallah, M. Caamano, D. Cortina, H. Geissel, M. Hellström, *et al.*, 2010, Phys. Rev. **C82**, 065803.
Hannestad, S., 2002, Phys. Rev. **D65**, 083006.
Hannestad, S., and J. Madsen, 1995, Phys. Rev. **D52**, 1764.
Heckler, A. F., 1994, Phys. Rev. **D49**, 611.
Hernanz, M., J. Jose, A. Coc, and J. Isern, 1996, Astrophys. J. Lett. **465**, L27.
Horowitz, C. J., 2002, Phys. Rev. **D65**, 043001.
Horowitz, C. J., and G. Li, 2000, Phys. Rev. **D61**, 063002.
Hosford, A., S. G. Ryan, A. E. García Pérez, J. E. Norris, and K. A. Olive, 2009, Astron. Astrophys. **493**, 601.
Hou, S. Q., J. J. He, S. Kubono, and Y. S. Chen, 2015, Phys. Rev. **C91**, 055802.
Howk, J. C., N. Lehner, B. D. Fields, and G. J. Mathews, 2012, Nature **489**, 121.
Iliadis, C., 2007, *Nuclear Physics of Stars* (Wiley-VCH Verlag).
Iliadis, C., K. S. Anderson, A. Coc, F. X. Timmes, and S. Starrfield, 2016, Astrophys. J. **831**, 107.
Iliadis, C., R. Longland, A. E. Champagne, A. Coc, and R. Fitzgerald, 2010, Nucl. Phys. **A841**, 31.
Iocco, F., G. Mangano, G. Miele, O. Pisanti, and P. D. Serpico, 2007, Phys. Rev. **D75**, 087304.
Iocco, F., G. Mangano, G. Miele, O. Pisanti, and P. D. Serpico, 2009, Phys. Rep. **472**, 1.
Ivanov, A. N., R. Höllwieser, N. I. Troitskaya, M. Wellenzohn, and Ya. A. Berdnikov, 2017, Phys. Rev. **D95**, 033007.
Ivanov, A. N., M. Pitschmann, and N. I. Troitskaya, 2013, Phys. Rev. **D88**, 073002.
Izotov, Y. I., T. X. Thuan, and N. G. Guseva, 2014, MNRAS **445**, 778.
Izotov, Y. I., T. X. Thuan, and V. A. Lipovetsky, 1994, Astrophys. J. **435**, 647.
Izzo, L., M. Della Valle, E. Mason, F. Matteucci, D. Romano, L. Pasquini, L. Vanzi, A. Jordan, J. M. Fernandez, P. Bluhm, R. Brahm, N. Espinoza, *et al.*, 2015, Astrophys. J. Lett. **808**, L14.
Kawabata, T., Y. Fujikawa, T. Furuno, T. Goto, T. Hashimoto, M. Ichikawa, M. Itoh, N. Iwasa, Y. Kanada-En'yo, A. Koshikawa, S. Kubono, E. Miyawaki, *et al.*, 2017, Phys. Rev. Lett. **118**, 052701.
Kawano, L., 1992, Let's go: Early universe. 2. Primordial nucleosynthesis: The Computer way.
Kernan, P. J., 1993, *Two astroparticle physics problems: Solar neutrinos and primordial He-4*, Ph.D. thesis, Ohio State University.
Kirsebom, O. S., and B. Davids, 2011, Phys. Rev. **C84**, 058801.
Korn, A. J., F. Grundahl, O. Richard, P. S. Barklem, L. Mashonkina, R. Collet, N. Piskunov, and B. Gustafsson, 2006, Nature **442**, 657.
Kusakabe, M., M.-K. Cheoun, and K. S. Kim, 2014, Phys. Rev. **D90**, 045009.
Lesgourgues, J., 2011, CLASS, `http://class-code.net/`.
Lewis, A., and A. Challinor, 1999, CAMB, `http://camb.info`.
Lewis, A., A. Challinor, and A. Lasenby, 2000, Astrophys. J. **538**, 473.

Lind, K., J. Melendez, M. Asplund, R. Collet, and Z. Magic, 2013, Astron. Astrophys. **554**, A96.

Longland, R., C. Iliadis, A. E. Champagne, J. R. Newton, C. Ugalde, A. Coc, and R. Fitzgerald, 2010, Nucl. Phys. **A841**, 1.

Lopez, R. E., and M. S. Turner, 1999, Phys. Rev. **D59**, 103502.

Lopez, R. E., M. S. Turner, and G. Gyuk, 1997, Phys. Rev. **D56**, 3191.

Ma, L., H. J. Karwowski, C. R. Brune, Z. Ayer, T. C. Black, J. C. Blackmon, E. J. Ludwig, M. Viviani, A. Kievsky, and R. Schiavilla, 1997, Phys. Rev. **C55**, 588.

Mangano, G., G. Miele, S. Pastor, and M. Peloso, 2002, Phys. Lett. **B534**, 8.

Mangano, G., G. Miele, S. Pastor, T. Pinto, O. Pisanti, and P. D. Serpico, 2005, Nucl. Phys. **B729**, 221.

Mangano, G., G. Miele, S. Pastor, T. Pinto, O. Pisanti, and P. D. Serpico, 2006, Nucl. Phys. **B756**, 100.

Marciano, W. J., and A. Sirlin, 2006, Phys. Rev. Lett. **96**, 032002.

Marcucci, L. E., G. Mangano, A. Kievsky, and M. Viviani, 2016, Phys. Rev. Lett. **116**, 102501.

Marcucci, L. E., M. Viviani, R. Schiavilla, A. Kievsky, and S. Rosati, 2005, Phys. Rev. **C72**, 014001.

Mathews, G. J., and M. Kusakabe, 2017, International Journal of Modern Physics E **26**, 1702006.

Mathews, G. J., M. Kusakabe, and T. Kajino, 2017, International Journal of Modern Physics E **26**, 1741001.

Meléndez, J., L. Casagrande, I. Ramírez, M. Asplund, and W. J. Schuster, 2010, Astron. Astrophys. **515**, L3.

Mendes, D. R., Jr., A. Lépine-Szily, P. Descouvemont, R. Lichtenthäler, V. Guimarães, P. N. de Faria, A. Barioni, K. C. C. Pires, V. Morcelle, R. Pampa Condori, M. C. Morais, E. Leistenschneider, *et al.*, 2012, Phys. Rev. **C86**, 064321.

Michaud, G., G. Fontaine, and G. Beaudet, 1984, Astrophys. J. **282**, 206.

Mirbabayi, M., and M. Zaldarriaga, 2015, JCAP **1503**(03), 056.

Mukhamedzhanov, A. M., Shubhchintak, and C. A. Bertulani, 2016, Phys. Rev. **C93**, 045805.

Nakamura, R., M.-a. Hasahimoto, R. Ichimasa, and K. Arai, 2017, Int. J. Mod. Phys. **E26**(08), 1741003.

Neff, T., 2011, Phys. Rev. Lett. **106**, 042502.

Nollett, K. M., and S. Burles, 2000, PHys. Rev. **D61**, 123505.

Oldengott, I. M., and D. J. Schwarz, 2017, Europhys. Lett. **119**(2), 29001.

Olive, K. A., 2010, ArXiv e-prints eprint 1005.3955.

Olive, K. A., P. Petitjean, E. Vangioni, and J. Silk, 2012, MNRAS **426**, 1427.

O'Malley, P. D., D. W. Bardayan, A. S. Adekola, S. Ahn, K. Y. Chae, J. A. Cizewski, S. Graves, M. E. Howard, K. L. Jones, R. L. Kozub, L. Lindhardt, M. Matos, *et al.*, 2011, Phys. Rev. **C84**, 042801.

Pagel, B. E. J., E. A. Simonson, R. J. Terlevich, and M. G. Edmunds, 1992, Mon. Not. R. Astron. Soc. **255**, 325.

Patrignani, C., and Particle Data Group, 2016 and 2017 update, Chinese Physics C **40**, 100001.

Pettini, M., and R. Cooke, 2012, MNRAS **425**, 2477.

Pisanti, O., A. Cirillo, S. Esposito, F. Iocco, G. Mangano, G. Miele, and P. D. Serpico, 2008, Comput. Phys. Commun. **178**, 956.

Pitrou, C., and A. Stebbins, 2014, Gen. Rel. Grav. **46**(11), 1806.

Pospelov, M., and J. Pradler, 2010, Annual Review of Nuclear and Particle Science **60**, 539.

Reggiani, H., J. Meléndez, C. Kobayashi, A. Karakas, and V. Placco, 2017, Astron. Astrophys. **608**, A46.

Richard, O., G. Michaud, and J. Richer, 2005, Astrophys. J. **619**, 538.

Riemer-Sørensen, S., S. Kotuš, J. K. Webb, K. Ali, V. Dumont, M. T. Murphy, and R. F. Carswell, 2017, MNRAS **468**, 3239.

de Salas, P. F., and S. Pastor, 2016, JCAP **1607**(07), 051.

Sallaska, A. L., C. Iliadis, A. E. Champange, S. Goriely, S. Starrfield, and F. X. Timmes, 2013, Astrophys. J. **207**, 18.

Sawyer, R. F., 1996, Phys. Rev. **D53**, 4232.

Sbordone, L., P. Bonifacio, E. Caffau, H.-G. Ludwig, N. T. Behara, J. I. González Hernández, M. Steffen, R. Cayrel, B. Freytag, C. van't Veer, P. Molaro, B. Plez, *et al.*, 2010, Astron. Astrophys. **522**, A26.

Schaeuble, M., and J. R. King, 2012, PASP **124**, 164.

Schmid, G. J., B. J. Rice, R. M. Chasteler, M. A. Godwin, G. C. Kiang, L. L. Kiang, C. M. Laymon, R. M. Prior, D. R. Tilley, and H. R. Weller, 1997, Phys. Rev. **C56**, 2565.

Scholl, C., Y. Fujita, T. Adachi, P. von Brentano, H. Fujita, M. Górska, H. Hashimoto, K. Hatanaka, H. Matsubara, K. Nakanishi, T. Ohta, Y. Sakemi, *et al.*, 2011, Phys. Rev. **C84**, 014308.

Scholz, R.-D., U. Heber, C. Heuser, E. Ziegerer, S. Geier, and F. Niederhofer, 2015, Astron. Astrophys. **574**, A96.

Seckel, D., 1993, eprint hep-ph/9305311.

Serebrov, A. P., *et al.*, 2017, eprint 1712.05663.

Serpico, P. D., S. Esposito, F. Iocco, G. Mangano, G. Miele, and O. Pisanti, 2004, JCAP **0412**, 010.

Serpico, P. D., and G. G. Raffelt, 2005, Phys. Rev. **D71**, 127301.

Simha, V., and G. Steigman, 2008, JCAP **0808**, 011.

Simonucci, S., S. Taioli, S. Palmerini, and M. Busso, 2013, Astrophys. J. **764**, 118.

Sirlin, A., 1967, Phys. Rev. **164**, 1767.

Smith, C. J., and G. M. Fuller, 2010, Phys. Rev. **D81**, 065027.

Spite, F., and M. Spite, 1982, Astron. Astrophys. **115**, 357.

Spite, M., F. Spite, and P. Bonifacio, 2012, Memorie della Societa Astronomica Italiana Supplementi **22**, 9.

Spite, M., F. Spite, E. Caffau, and P. Bonifacio, 2015, Astron. Astrophys. **582**, A74.

Steigman, G., 2006, JCAP **0610**, 016.

Steigman, G., 2007, Annual Review of Nuclear and Particle Science **57**, 463.

Tajitsu, A., K. Sadakane, H. Naito, A. Arai, H. Kawakita, and W. Aoki, 2016, Astrophys. J. **818**, 191.

Vangioni-Flam, E., A. Coc, and M. Cassé, 2000, Astron. Astrophys. **360**, 15.

Vangioni-Flam, E., K. A. Olive, B. D. Fields, and M. Cassé, 2003, Astrophys. J. **585**, 611.

Vernizzi, F., 2005, Phys. Rev. **D71**, 061301.

Wagoner, R. V., 1969, Astrophys. J. Supp. **18**, 247.

Wagoner, R. V., 1973, Astrophys. J. **179**, 343.

Wagoner, R. V., W. A. Fowler, and F. Hoyle, 1967, Astrophys. J. Supp. **148**, 3.

Wang, B., C. A. Bertulani, and A. B. Balantekin, 2011, Phys. Rev. **C83**, 018801.

Weinberg, S., 1972, *Gravitation and Cosmology: Principles and Applications of the General Theory of Relativity* (Wiley).

Weinberg, S., 2003, Phys. Rev. **D67**, 123504.

Wietfeldt, F. E., and G. L. Greene, 2011, Rev. Mod. Phys. **83**, 1173.
Wilkinson, D. H., 1982, Nucl. Phys. **A377**, 474.
Wong, Y. Y. Y., 2002, Phys. Rev. **D66**, 025015.
Xu, Y., K. Takahashi, S. Goriely, M. Arnould, M. Ohta, and H. Utsunomiya, 2013, Nucl. Phys. **A918**, 61.
Yamazaki, D. G., M. Kusakabe, T. Kajino, G. J. Mathews, and M.-K. Cheoun, 2014, Phys. Rev. **D90**, 023001.
Young, A. R., S. Clayton, B. W. Filippone, P. Geltenbort, T. M. Ito, C.-Y. Liu, M. Makela, C. L. Morris, B. Plaster, A. Saunders, S. J. Seestrom, and R. B. Vogelaar, 2014, Journal of Physics G Nuclear Physics **41**, 114007.
Zavarygin, E. O., J. K. Webb, V. Dumont, and S. Riemer-Sørensen, 2017, ArXiv e-prints eprint 1706.09512.
Zavarygin, E. O., J. K. Webb, S. Riemer-Sørensen, and V. Dumont, 2018, ArXiv e-prints eprint 1801.04704.